FIELD INSTRUMENTATION AND ANALYSIS OF THE TUTTLE CREEK BRIDGE

Br. No. 16-81-2.24 (017)

Nathan Marshall, E.I.T.
Guillermo Ramirez, Ph.D., P.E.
W. M. Kim Roddis, Ph.D., P.E.
Stanley T. Rolfe, Ph.D., P.E.
Adolfo B. Matamoros, Ph.D., E.I.T.

KDOT PROJECT NUMBER: KTRAN, KU-04-5
KUCR PROJECT NUMBER: KAN 35730
Final Report

Department of Civil, Environmental,
and Architectural Engineering
The University of Kansas
Lawrence, Kansas 66045

ABSTRACT

Fatigue cracking has been an extensive problem for many steel bridges designed prior to the identification of fatigue-prone details. Distortion in bridges coupled with stress concentrations within bridge components can eventually lead to crack initiation. The Tuttle Creek Bridge, built in 1962, has developed fatigue cracks like many older steel bridges. The structure is a 5,350 ft. long, plate-girder bridge with two girders supporting a non-composite concrete deck.

The majority of the cracks on the bridge are found in the upper web-gap region, which lies between the vertical connection stiffener and the upper flange. Cracks also have occurred in the transverse welds attaching the lateral gusset plates to the lower flange. Both these crack types are believed to be caused by differential deflection of the two girders.

In 1986, the bridge was retrofitted to prevent further cracking. Cracking, however, continued after the 1986 retrofit. In 2000, the Kansas Department of Transportation retained the services of the University of Kansas to investigate the fatigue cracking. Finite element models were created to estimate the stresses in the upper web-gap regions in order to determine a proper repair plan. The recommended repair scheme was to positively attach the connection stiffener to the upper flange, which was also successfully performed in similar web-gap repairs.

The University of Kansas also was retained to perform two load tests on the bridge to investigate the effectiveness of the repair. The first load test, which this report entails, examined the stresses within the fatigued regions prior to retrofit. A second test will be conducted after the repairs have been performed. Measurements taken during both tests will be compared to determine the fatigue improvement within the structure. Also, information gathered during the first test will also provide insight to improving the finite element models.

This report includes information about the Tuttle Creek Bridge and a summary of its structural deficiencies. Details of the gage installation and load

testing are provided. Stresses induced by the truck loadings are presented in addition to the inferences from the measurements taken.

ACKNOWLEDGEMENTS

The completion of this project would not be possible without the contributions of the following people:

First, I would like to thank Dr. Guillermo Ramirez for bringing me to the University of Kansas to work on such a neat project. Dr. W. M. Kim Roddis must be acknowledged for educating me about the project and making beneficial suggestions on my testing setup. Thanks to Dr. Stanley Rolfe for his guidance and for making the advisor transition as smooth as possible.

Special thanks are due to the personnel at the Kansas Department of Transportation. Thanks to John Jones for providing all the information on the bridge and for setting up the test. Thanks to the KDOT fracture-critical inspection team of Clem Boos and Raymond Boller. They were very helpful and entertaining people. Appreciation must be shown to the KDOT district workers for keeping the traffic away from me.

Thanks to Kaise Haris for his long hours teetering above the Tuttle Creek waters. The success of this project would not have been possible without his valuable input. Thanks also to Jim Weaver for his suggestions on the testing. My office buddies also must be thanked for keeping me on the right track and for occasionally leading me off it.

Finally, I would like to thank my family for their love and kindness. Your encouragement was greatly appreciated and essential for succeeding in graduate school. Also, thanks for listening while I rambled on about my exciting project.

TABLE OF CONTENTS

LIST OF FIGURES

LIST OF TABLES

CHAPTER 1 INTRODUCTION

The Tuttle Creek Bridge was constructed in 1962 to cross the Tuttle Creek Reservoir, which is located in north-central Kansas. The bridge, as shown in Figure 1-1, is a two-girder, pin and hanger system with 30 spans totaling a length of 5,350 ft. The non-composite deck is composed of two – 12 ft. lanes with two – 2 ft. shoulders. A cross-sectional view of the bridge can be found in Figure 1-2, while profile and plan views can be seen in Figure 1-3 and 1-4, respectively. The two haunched girders directly support the weight of the deck. The bridge is located in a relatively low traffic area, with a daily traffic count of 520 vehicles per day and 13% truck traffic. The bridge lies in a very flat region, where it is exposed to high winds from the Kansas plains.

The Tuttle Creek Bridge has developed many fatigue cracks due to distortion-induced stresses. These fatigue cracks pose a safety concern to the public, since the bridge is considered fracture-critical. With only two girders supporting the deck, the bridge is a non-redundant structure. Failure of any structural component would lead to complete destruction of the bridge.

The web-gap region, found at each diaphragm, was the primary site of crack initiation. The web-gap region is between the girder flange/web fillet weld and the top of the connection stiffener weld. Crack prevention repairs were performed in 1986, however, recent inspection reports have shown continuing crack initiation and propagation. Cracks also have occurred in the weld attaching the lateral gusset plate to the lower flange. Successful repairs were performed on the plates adjacent to the piers, however the remaining unrepaired plates have developed new cracks.

Two fracture-critical inspection reports were made available for the University of Kansas research staff. Both reports dealt exclusively with the steel superstructure. The first report, dated August 28, 2000, consisted of tables detailing crack type and location. This report put most of its emphasis on the web-gap cracking, with no mention of the gusset plate fatigue problem. The second report,

dated September 9, 2002, also included gusset plate crack locations. The amount of information found in these reports offered researchers an opportunity to survey each span and determine any patterns of the fatigue cracks.

In 2000, the University of Kansas was retained by the Kansas Department of Transportation to perform a finite element model of the web-gap regions on the bridge. Yuan Zhao, a former KU graduate student, investigated the theoretical effectiveness of different retrofit measures.

Two field investigations were recommended by KU to check the accuracy of the finite element model and to measure the effects of the repair. The first investigation, performed prior to retrofit, would provide a standard to compare against the finite element model. This study would also investigate other fatigue-prone details, such as the gusset plates and the longitudinal stiffeners. Information gathered from these areas will be used to improve future theoretical models. The second investigation will be performed after the retrofit measures have been accomplished. The results of this study will be compared with results from the first one in order to examine the structural improvement due to the retrofits.

This report addresses the results of the first field investigation only. The fatigue history of the bridge is examined with both the location and patterns of cracks displayed. For the web-gap region, a comparison of stress values predicted by the finite element model and actual field-tested values are presented. Results of other components investigated, including gusset plate cracking, longitudinal stiffener retrofitting, and vibration testing also are provided. The data obtained from this report is organized to provide helpful information when creating finite element models and for comparison with post-retrofit results.

Figure 1-1 Tuttle Creek Bridge

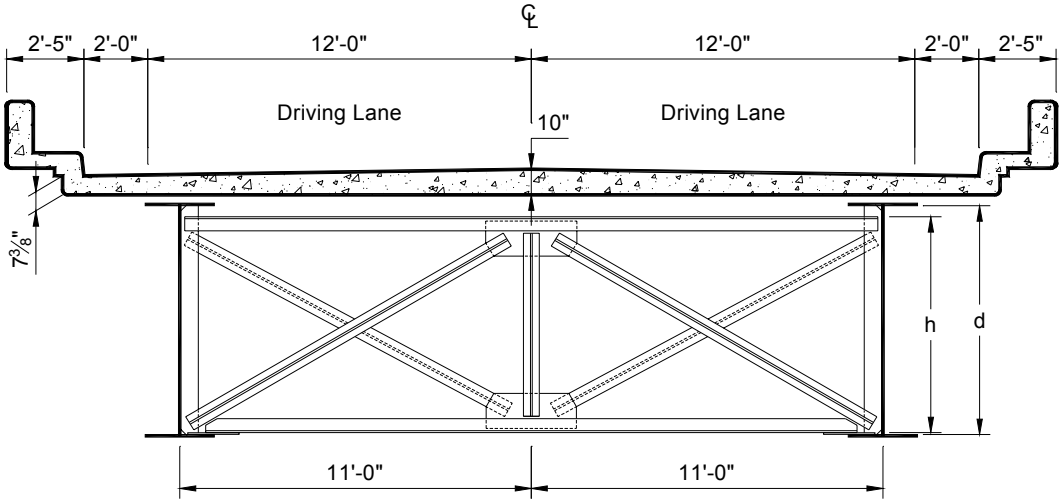

Figure 1-2 Bridge Cross-section

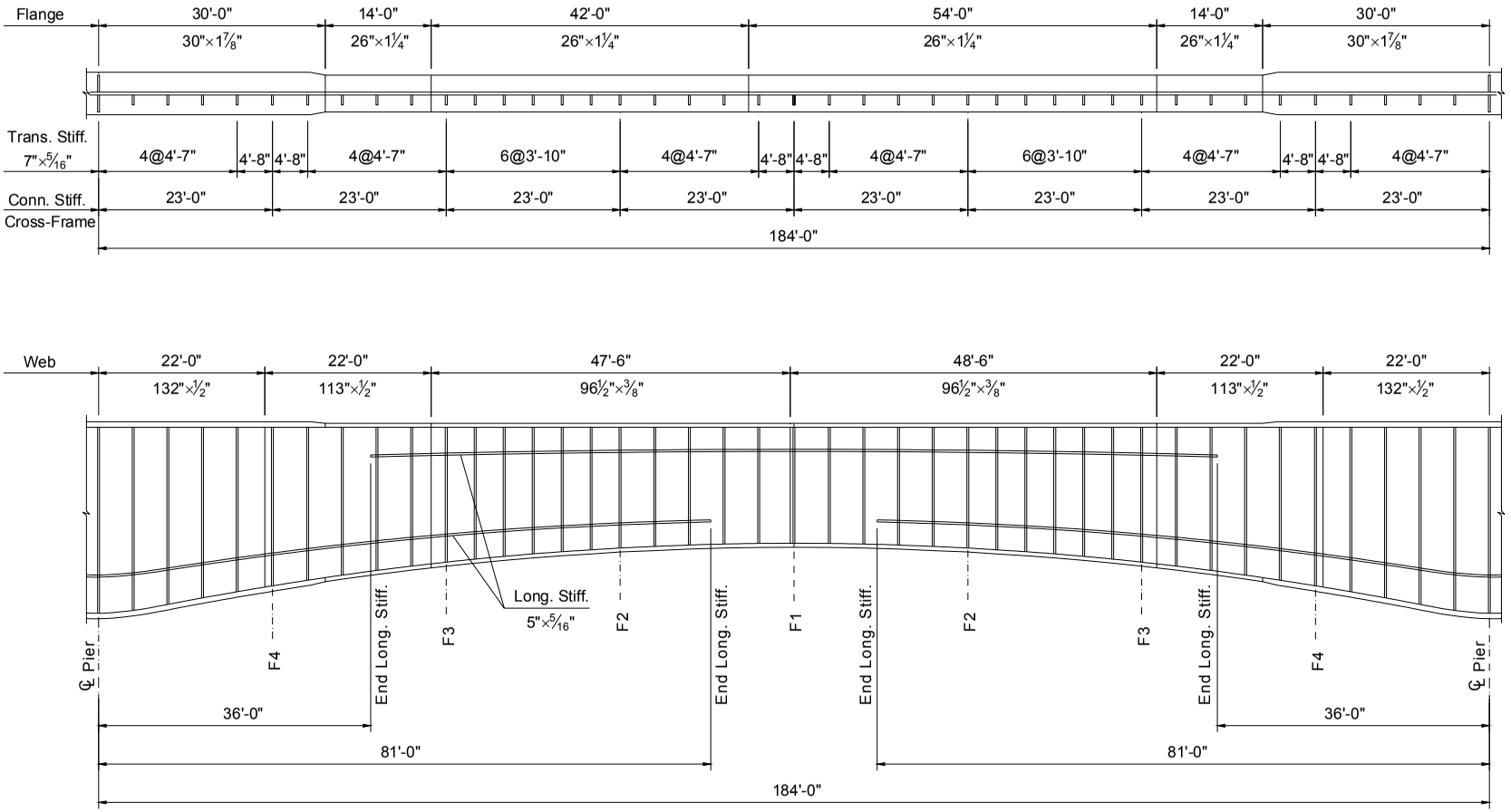

Figure 1-3 Girder Details of Typical Intermediate Spans

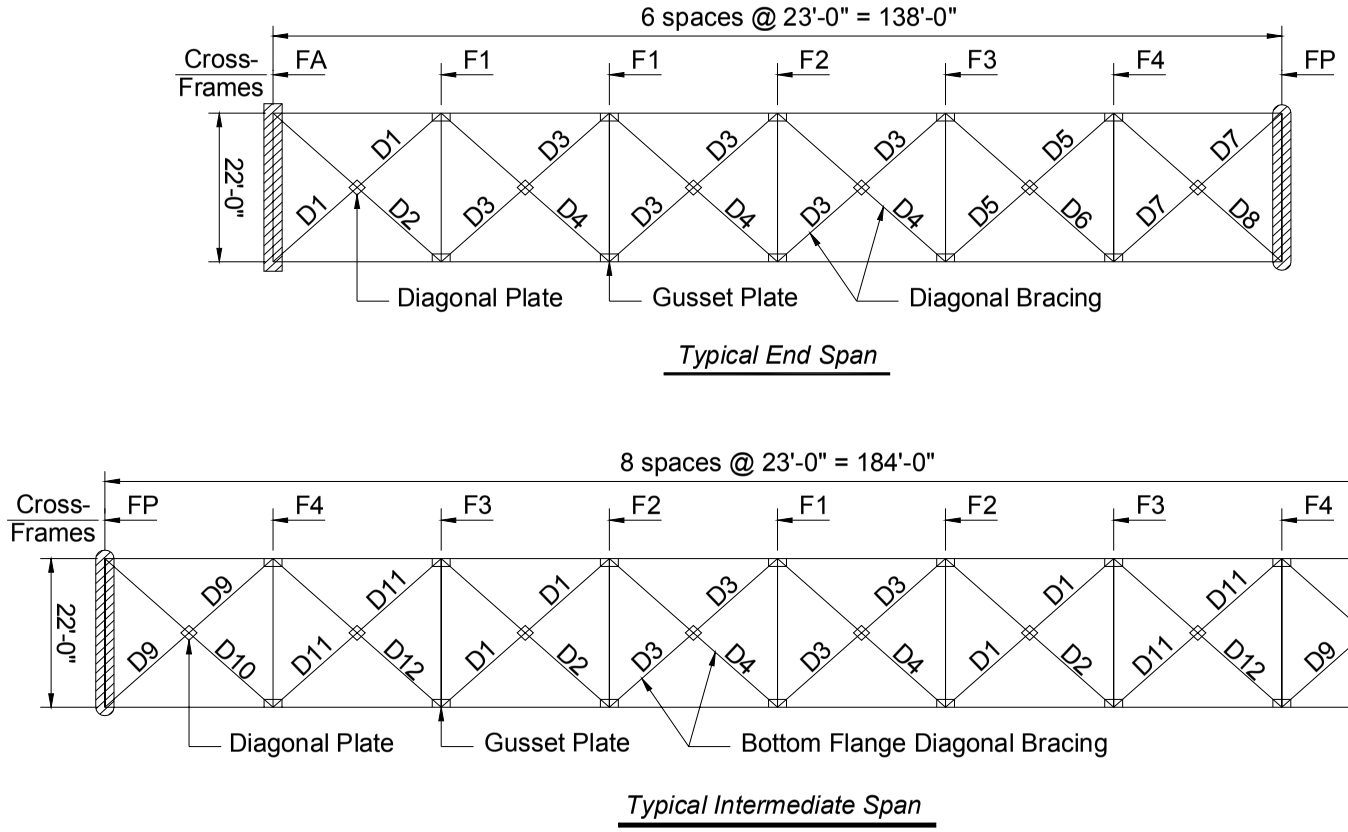

Figure 1-4 Framing Plan

CHAPTER 2 FATIGUE HISTORY

The Tuttle Creek Bridge was designed before fatigue-prone details were properly identified. The most common oversight was distortion-induced fatigue cracking. The deflection of certain elements of a structure can cause high secondary stresses, which can lead to crack initiation. The primary cause of fatigue cracking in the Tuttle Creek Bridge is due to differential deflection of the two primary girders. The differential deflection causes secondary stresses at the diaphragm locations. Locations investigated due to high stress concentrations are located in the web-gap region, along the lateral gusset plates, and the ends of the longitudinal stiffeners.

Additional repairs to the Tuttle Creek Bridge, including replacement of the pin and hangers and repair of web field splices, are also planned, but they are beyond the scope of this study.

2.1 Web-Gap Cracking

The majority of cracking in the Tuttle Creek Bridge is within the web-gap region of the girders. The web-gap region is a 1 x 1 in. diagonal clip from the top and bottom of the connection stiffener to allow for the fillet weld of the primary member to be continuous, as seen in Figures 2-1 and 2-2. Unfortunately, this cope creates high stress concentrations in the web that can initiate fatigue cracking. Two types of cracks have been observed in the upper web-gap: weld tears and horizontal cracks.

2.1.1 Cracking Patterns

Two distinct cracking patterns are found in the web-gap region. Figure 2-3 shows a drawing of the cracking patterns, while Figure 2-4 shows an actual picture of the cracking. The most common cracking pattern is a weld tear. The weld tears begin at the weld connecting the stiffener to the girder web. The stiffener is welded to the primary girder web with 4 in. fillet welds at each end and 6 in. welds spaced at 12 in. between the end welds. The cracks propagate down the top 4 in. weld

connecting the upper portion of the stiffener to the web. Some weld tears have tapered off from the fillet weld and into the web of the girder. Many of the 4 in. top intermittent welds on the stiffener have been broken completely by the weld tears. A total of 379 weld tears have been found in the bridge.

Another frequent cracking pattern is horizontal cracking. The horizontal cracks are found at the bottom of the fillet weld connecting the upper flange to the web of the girder. The cracks are located on both the interior and exterior sides of the girders. Exterior horizontal cracks are found less frequently than the similar interior horizontal cracks. Only 13 exterior, horizontal cracks have been found, as opposed to 291 interior, horizontal cracks.

2.1.2 Cracking Locations

The inspection reports revealed helpful information concerning the web-gap cracking problem. Surveys of each span indicated that web-gap cracks were not more or less abundant for any particular span. Full spans compared to hinged spans did not show any recognizable patterns. However, the comparison of diaphragm locations did indicate patterns for the cracking. Interior horizontal cracks showed a bell-shaped curve distribution, with larger number of cracks appearing in the middle diaphragms, as shown in Figures 2-5 and 2-7. Weld tears displayed a rather constant development regardless of diaphragm location, as shown in Figures 2-6 and 2-8.

2.1.3 Source of Cracking

The primary fatigue design problem with the Tuttle Creek Bridge is the lack of attachment of the connection stiffener to the tension flange, as shown in Figure 2-9. Past engineers believed that having transverse welds on the tension girder would initiate cracking. Unknowingly, they produced a region of high stress concentration in the web-gap region. Experience has shown that the web-gap region is much more fatigue-prone than the proposed tension flange welds. As a result, many older steel bridges have experienced web-gap cracking. New bridges, with the exception of heavily skewed bridges, do not have this problem since current design practice

requires positive attachment of the connection stiffener to the flange (AASHTO LRFD, 2004). Due to the abundance of this type of cracking, retrofitting of the web-gap has been a focal point of steel bridge research. Details of experiments focusing on the web-gap region of steel bridges can be found in Appendix A.

Web-gap cracking is a result of differential deflection of girders. When the braces in the diaphragms "pull" on the connection stiffener due to the varying deflections, the web-gap undergoes double-curvature bending. Figure 2-10 demonstrates the pulling of the diaphragm braces due to loading from a vehicle. Because this detail can quickly lead to crack initiation, AASHTO has labeled this design detail a fatigue category C (AASHTO LFRD, 2004).

Since the diaphragms cause the web-gap cracking, these cracks only occur at diaphragm locations along the girder. Two web-gap regions, an upper and lower, are located on each diaphragm connection. For the Tuttle Creek Bridge, only upper web-gap cracks have been found. The absence of lower web-gap cracks can be accounted for by the relative flexibility of the lower flange. While the concrete decking rigidly holds the upper flange, the bottom flange is free to rotate when loaded by the diaphragm bracing. The freedom to rotate of the lower flange prevents higher stresses from being developed in the lower web-gap. This difference explains why web-gap cracks have only developed in the upper gap region, while no cracking of the bottom flange web-gap has been located to date.

2.1.4 Crack Repairs

In 1986, a retrofit strategy of increasing the web-gap was performed. For the 1986 repair, the connection stiffeners were cut 1 in. below the termination of the existing weld tears. A 0.5 in. radius was placed at the end of the cut. The radial cut was supposed to reduce stress concentrations from initiating a new crack, however, cracks continued to grow in this region.

In addition to increasing the web-gap length during the 1986 retrofit, 0.75 in. diameter stop holes were drilled at the tips of the horizontal cracks. Ideally, the holes

would stop crack propagation, however, the horizontal cracks reinitiated after the retrofit.

KDOT recognized this problem and requested a study of the web-gap region. Yuan Zhao, a former KU graduate student, created finite element models of the web-gap region for the Tuttle Creek Bridge. She investigated various retrofit strategies, as summarized in Appendix B. Her predictions were compared with results of this load test.

2.2 Gusset Plate Cracking

In addition to web-gap cracking, the Tuttle Creek Bridge also has fatigue cracks within the gusset plate connection. The gusset plates, which are fillet welded to the lower flange, connect the lateral bracing of the girders. As shown in Figure 2-11, three structural tees enter the connection: two members cross diagonally, while one spans perpendicular to the girders. The lateral bracing is believed to have caused cracking of the gusset plate connection.

Tack welds were placed on the underside of the gusset plate where it overhangs the girder lower flange. Many of these tack welds have broken. The broken tack welds due not pose a structural danger to the bridge, unless cracks extend into the lower flange. Defects in the tension flange could initiate significant crack growth.

2.2.1 Cracking Patterns

Two types of gusset plate cracks have developed: cracking of the fillet weld perpendicular with the girder and tack welds parallel with the girder. Figure 2-11 shows a drawing of the cracking patterns, while Figure 2-12 displays an actual fillet weld crack.

The most problematic gusset plate crack found on the Tuttle Creek Bridge is cracking of the fillet weld connecting the gusset plate with the primary girders. The fillet welds extend symmetrically across the back and extend six inches along the

sides of the gusset plate. The cracks are found at the termination of the weld along the sides of the plate. The cracks are assumed to be only in the weld material, however, their continued propagation could enter into the lower tension flange. A total of 20 cracks have been found in this AASHTO Category E detail.

2.2.2 Crack Locations

The gusset plate cracks are found throughout the bridge, without any concentration on any particular spans. A survey of the diaphragm locations revealed that most of the gusset plate cracking was confined to the second diaphragm, labeled F3 in Figure 1-4. The distribution of the cracks between the diaphragms is displayed in Figure 2-13. The first diaphragm from the pier, labeled F4, displayed no evidence of fillet weld cracking, since these locations had been retrofitted in 1986. The cracks are equally dispersed on each side of the gusset plates. In other words, the sides closer to the pier were not more or less likely to crack than the opposite side.

2.2.3 Sources of Cracking

As opposed to the web-gap cracking, the source of the gusset plate cracks is in debate. One theory is the cracks have developed from the bending stress of the girder, a solely load-based fatigue. Figure 2-14 shows a diagram of this type of fatigue source. Another possibility is due to distortion of the girder causing high compressive stresses in the diagonal bracing. The lateral bracing buckles upward along its weak axis causing a prying action on the gusset plate. A drawing of this theory is presented in Figure 2-15. Another theory is racking of the gusset plate due to loads from the diagonal bracing. The twisting of the gusset plate would cause cracking to develop at the ends of the fillet weld. Figure 2-16 shows this theory of plate distortion.

2.3 Longitudinal Stiffener Cracking

The Tuttle Creek Bridge utilizes longitudinal web stiffeners in regions of high compressive stress. Stiffeners are located in the compressive region of both the positive and negative moment regions. The negative moment stiffeners extend symmetrically 81 ft from each pier, while the positive moment stiffeners extend 56 ft symmetrically about the centerline of typical spans.

2.3.1 Cracking Pattern

Longitudinal stiffeners have developed cracking in the butt welds of the stiffener splices. The cracks are found only in the weld material. Figure 2-17 shows a crack in the longitudinal stiffener. Details of the longitudinal stiffener cracks were not described in the inspection reports. The inspectors mentioned these cracks, but did not detail the exact locations of the cracking. Therefore, a survey similar to those in the web-gap and gusset plate regions could not be performed.

2.3.2 Source of Cracking

A defect in the weld was the probable source of crack initiation in the stiffener. Stress cycles in the stiffener due to bending of the girder propagated the crack. Even during compression stress cycles, residual stresses would transform the stress cycles from compressive to tensile. The resulting tensile cycles would quickly propagate a crack.

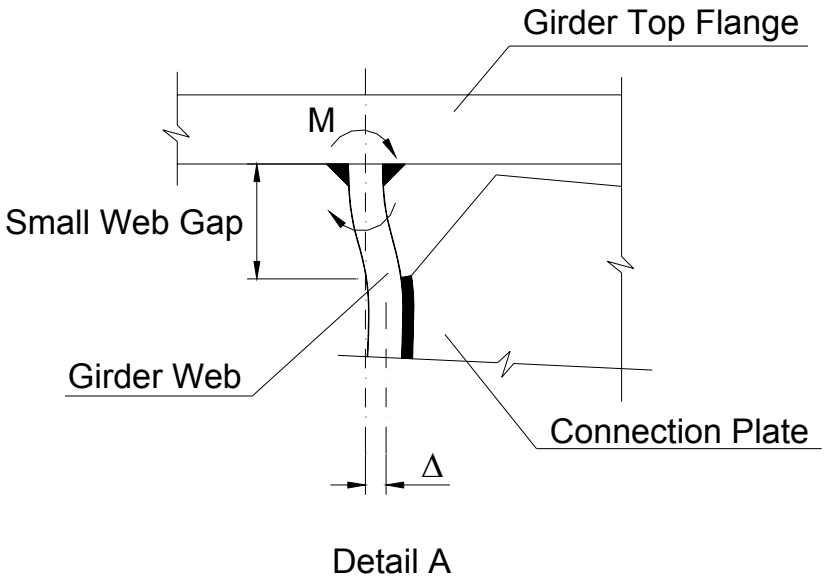

Figure 2-1 Web-Gap Region

Figure 2-2 Web-Gap Region (Picture)

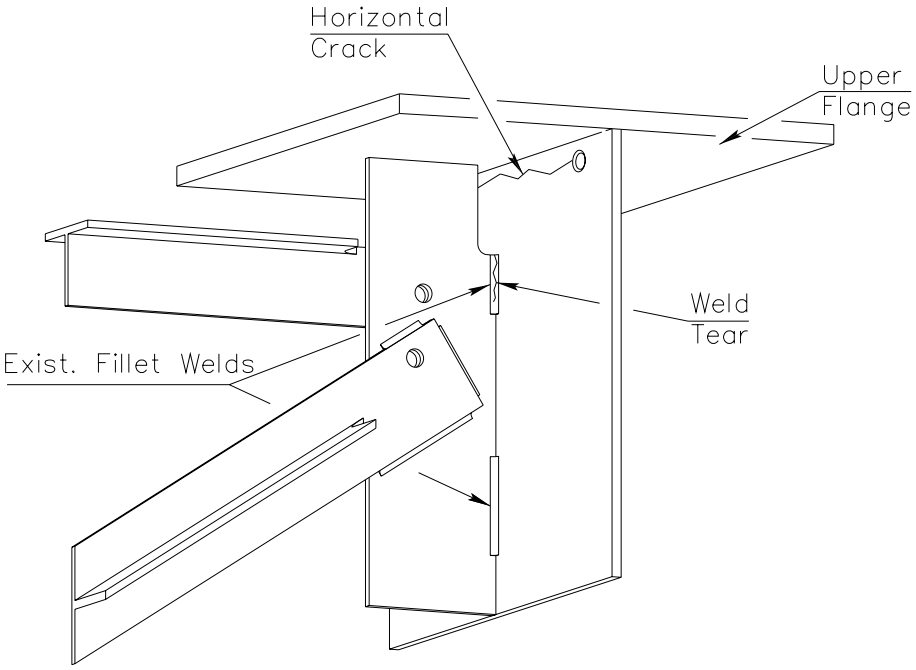

Figure 2-3 Web-Gap Cracking Patterns

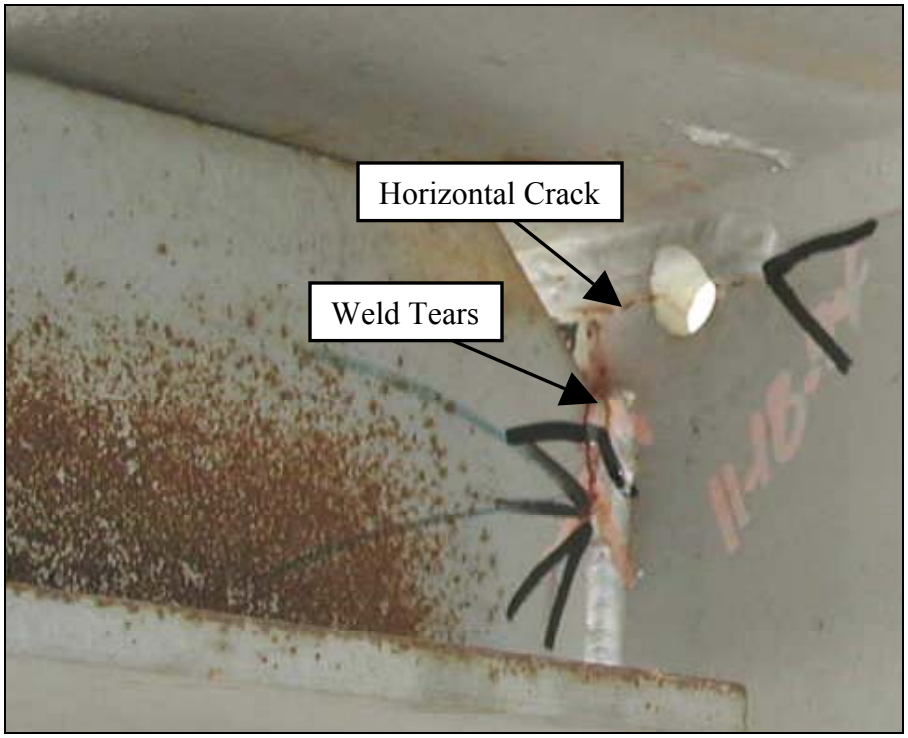

Figure 2-4 Web-Gap Cracking Patterns (Picture)

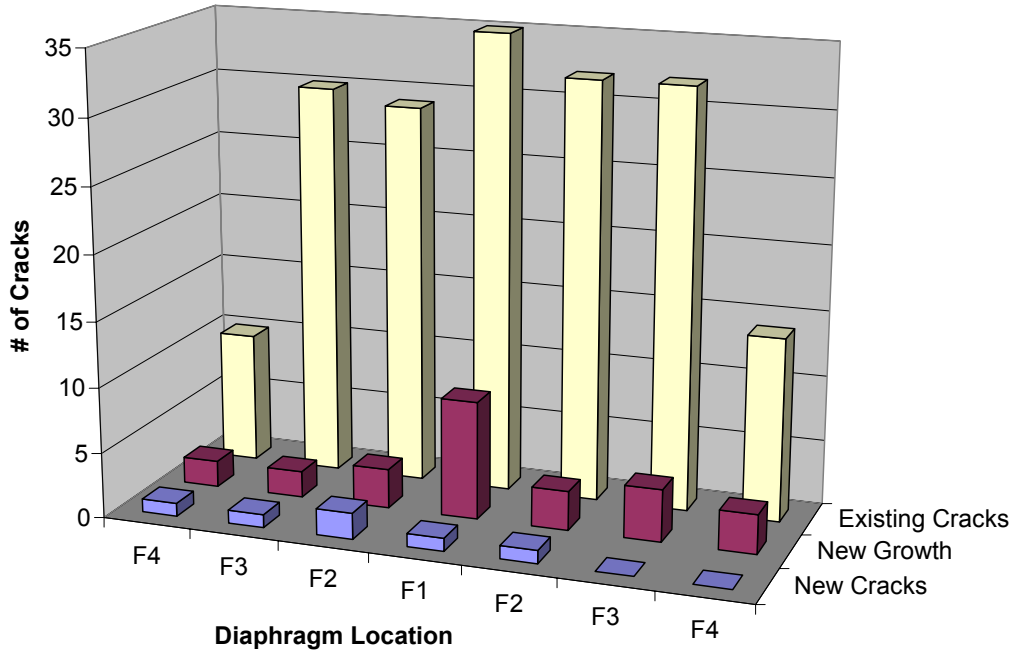

Figure 2-5 Horizontal Cracking Survey (Full Spans)

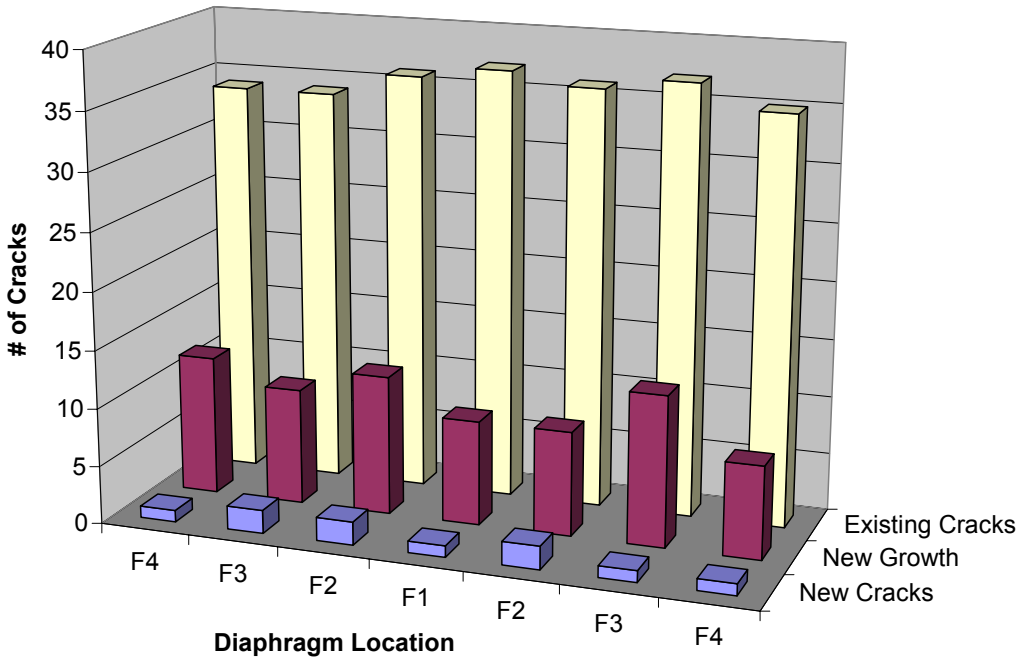

Figure 2-6 Weld Tear Survey (Full Spans)

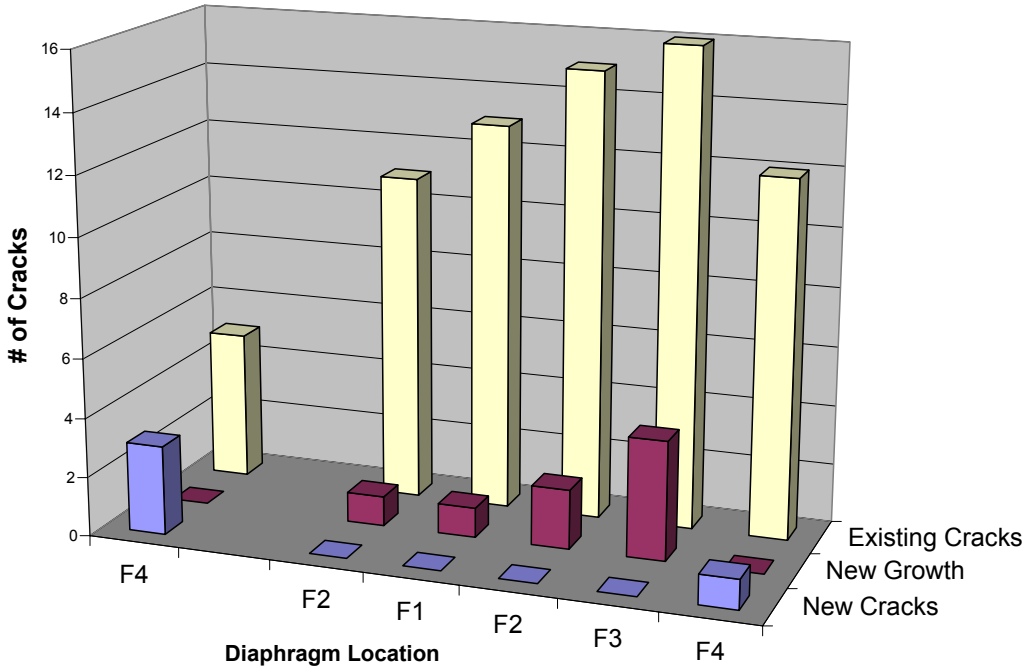

Figure 2-7 Horizontal Cracking Survey (Hinged Spans)

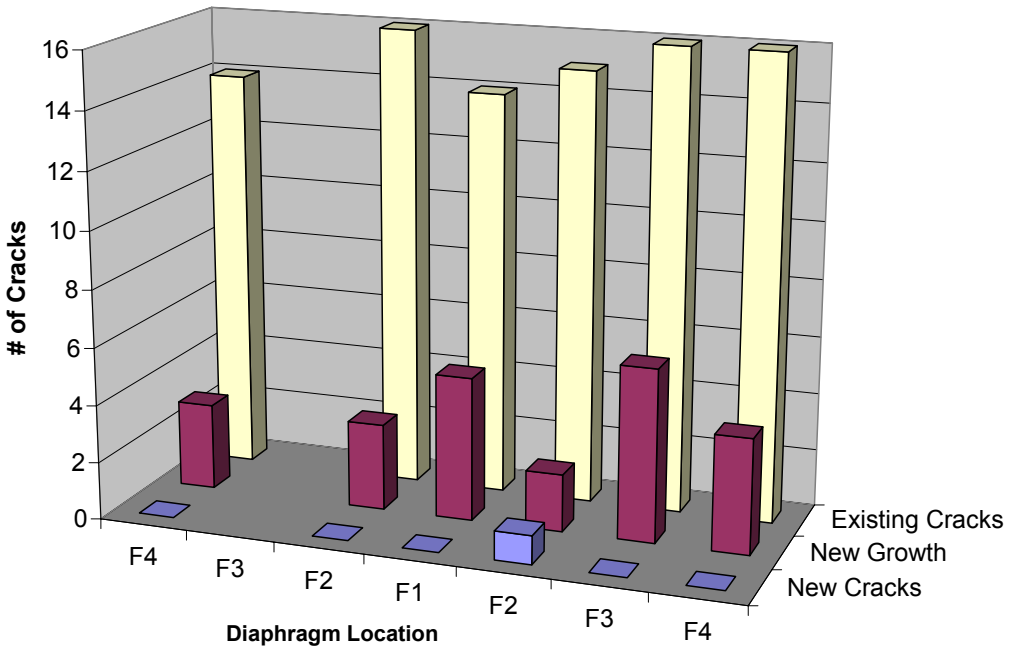

Figure 2-8 Weld Tear Survey (Hinged Spans)

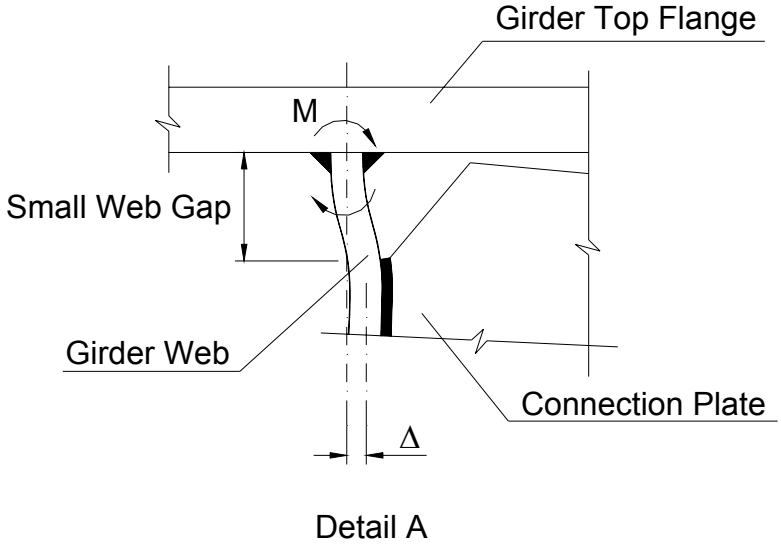

Figure 2-9 Distortion in the Web-Gap Region

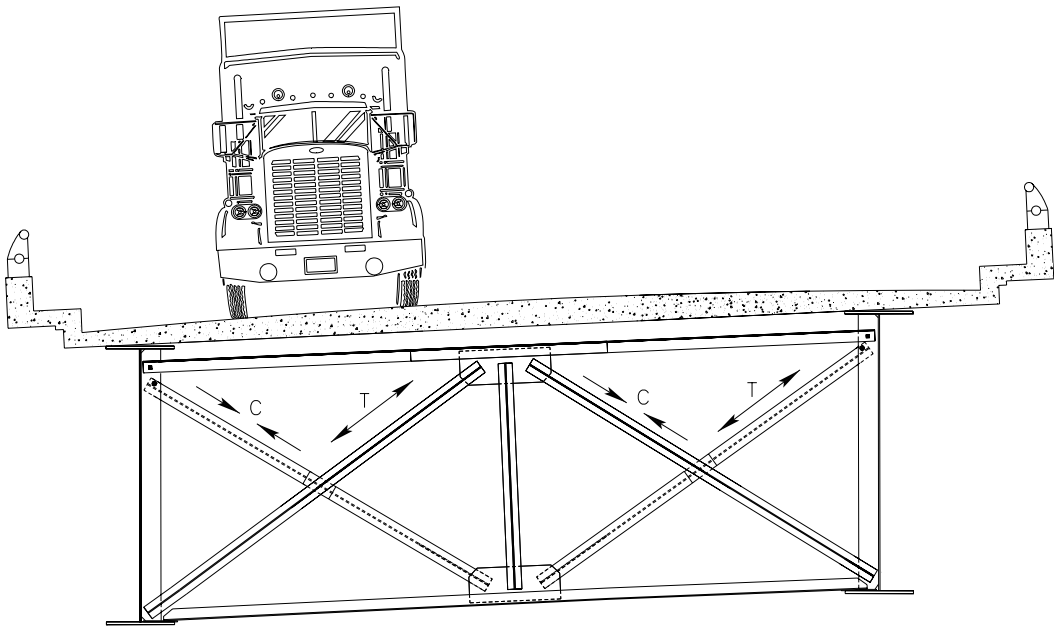

Figure 2-10 Differential Deflection of Girders

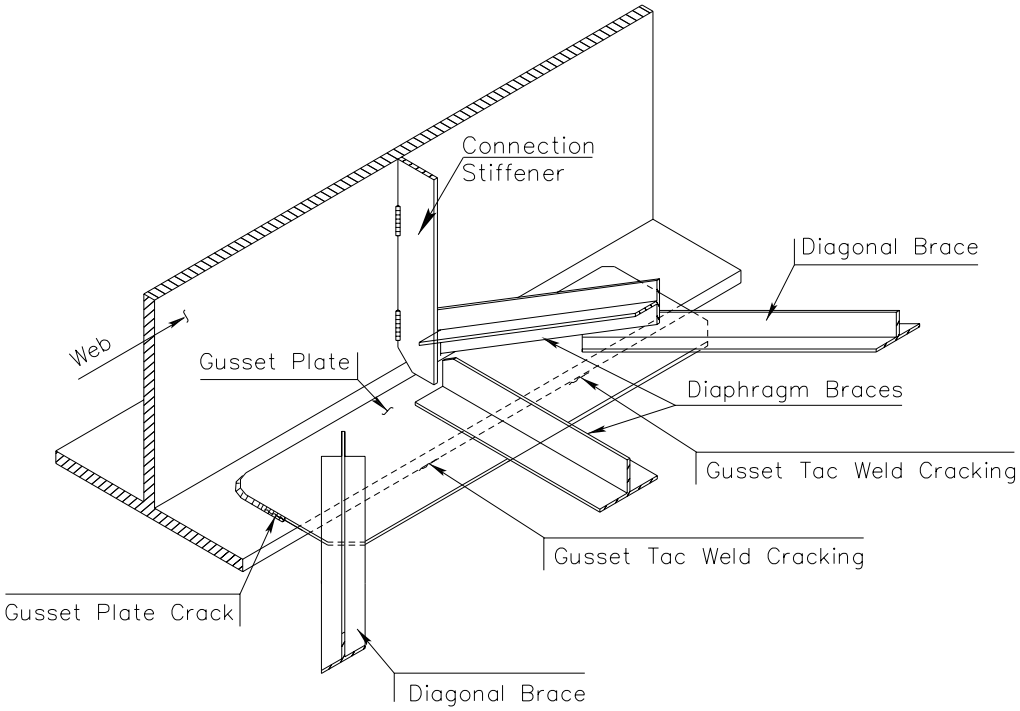

Figure 2-11 Gusset Plate Cracking Patterns

Figure 2-12 Gusset Plate Cracking Patterns (Picture)

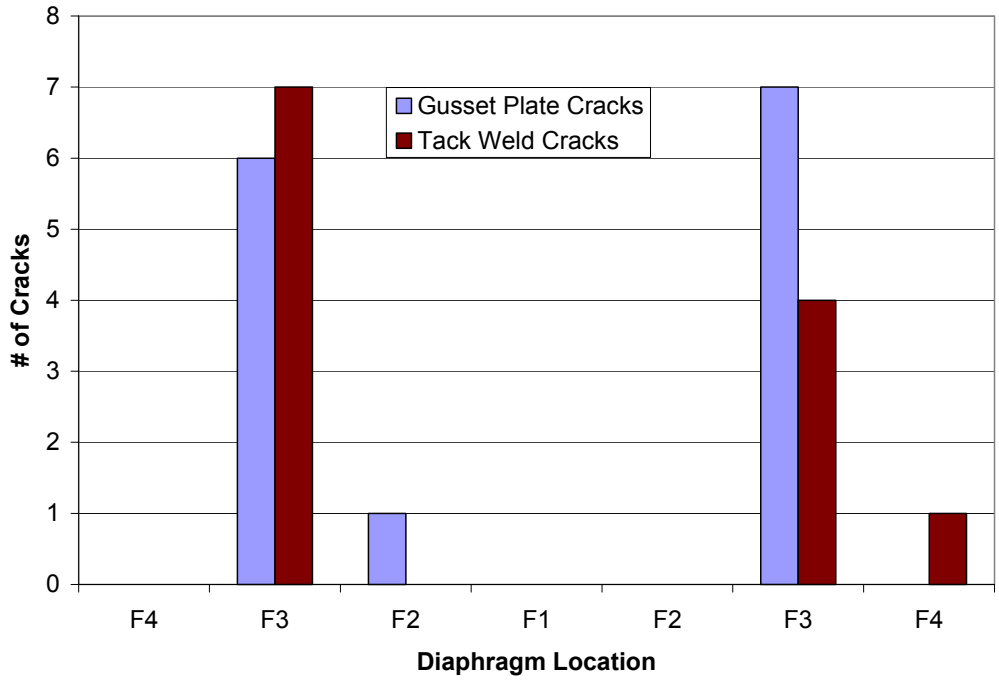

Figure 2-13 Gusset Plate Cracking (Full Spans)

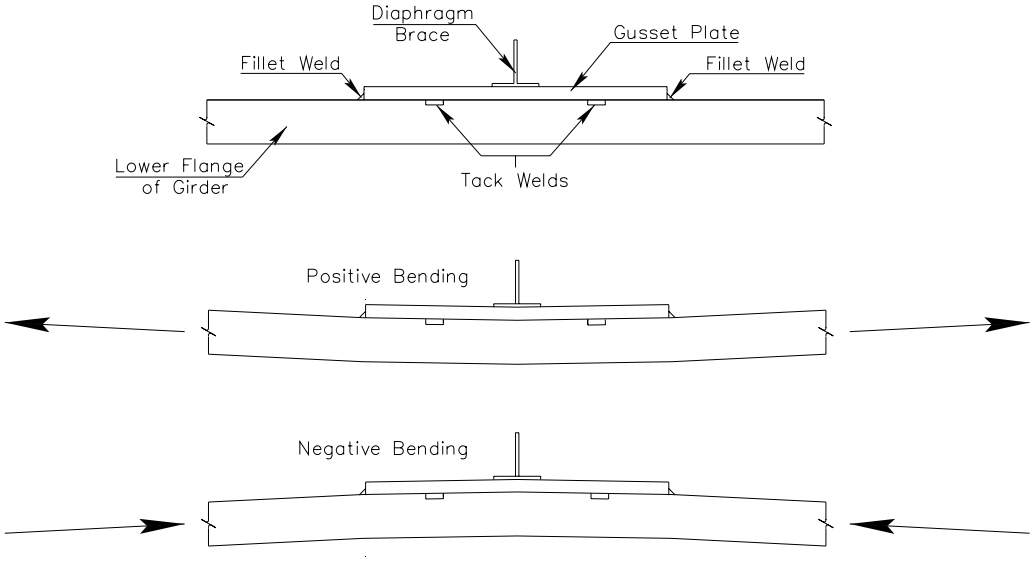

Figure 2-14 Gusset Plate Cracking Source (Bending Stresses)

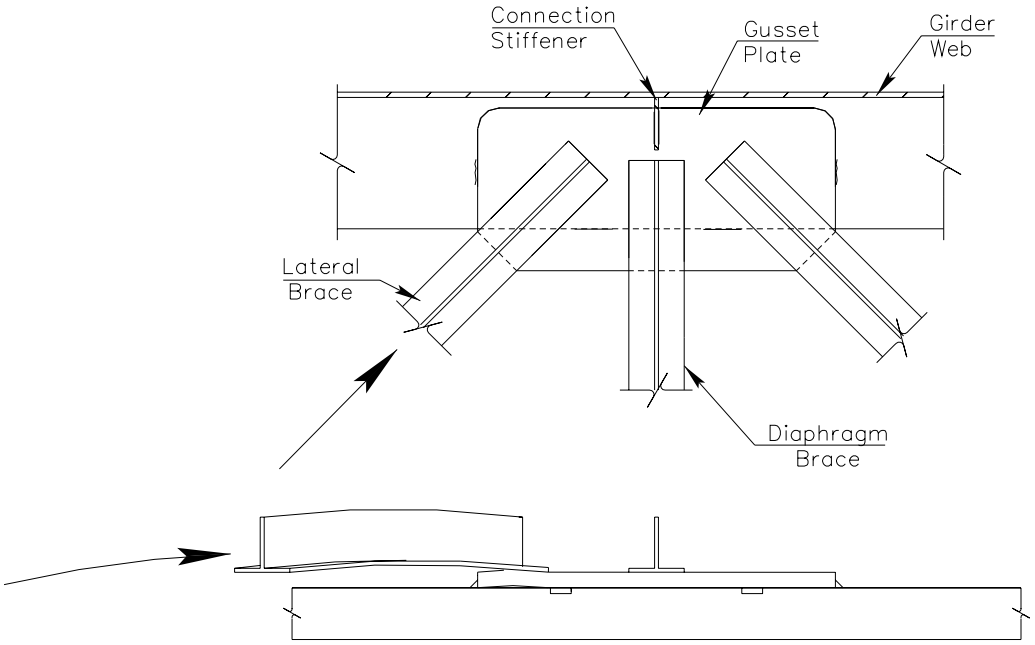

Figure 2-15 Gusset Plate Cracking Source (Distortion of Lateral Brace)

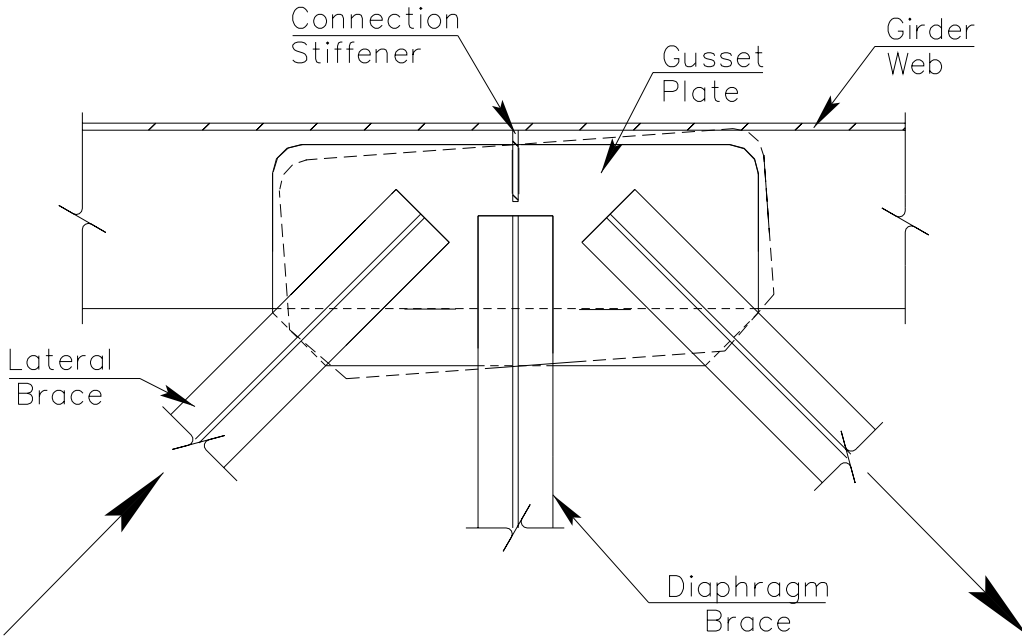

Figure 2-16 Gusset Plate Cracking Source (Racking of Gusset Plate)

Figure 2-17 Longitudinal Stiffener Crack

CHAPTER 3 INSTALLATION & TESTING

In order to estimate the stresses prior to retrofit, strain gages were installed on the Tuttle Creek Bridge. Strain gages have commonly been used to experimentally determine the stresses in various regions of steel bridges. Details of previous load tests performed on in-service structures can be found in Appendix A.

The positions of the gages were chosen after reviewing other researchers' work. For this test, only 23 gages could be used, since that was the maximum number of channels available on the data acquisition system. Gages were installed in the web-gap region to measure vertical bending stresses. Additional gages were placed on the diaphragm bracing that is loading the web-gap region. The degree of composite action in the bridge was measured by two gages. Gages were also used to investigate the gusset plate cracking problem. One gage measured the strain prior to a longitudinal stiffener retrofit.

Vibration testing, though use of accelerometers, was also a component of the field-testing. Accelerometers were placed on the midspan and quarterspan of both girders. Results from the vibration testing can be found in Appendix D. Previous work in bridge vibration studies, in addition to strain gage research, can be found in Appendix A.

After reviewing the inspection reports and discussing logistics of the test with KDOT workers, span 29 was chosen to be tested. Span 29 was the first full span away from the easternmost abutment. The proximity to the abutment allowed a generator, which powered the data acquisition equipment, to be placed on the ground, thus reducing vibrations on the bridge. All gages were placed on girder A, the southernmost girder. This girder had an average number of fatigue cracks as compared to the others. The effects of traffic loading were assumed to be symmetrical. In other words, the effects of the eastbound traffic on girder A would be the same as the effects of westbound traffic on girder B.

3.1 Test Preparation

In addition to reviewing previous test methods, test setup began with two visits to the bridge. The underside of the bridge was studied at the abutments from a maintenance road. Key points to the testing strategy, such as the traffic control procedures and the location of the data acquisition system, were determined. The visitations prevented any surprises when actual testing occurred.

Data collection equipment was checked prior to the load test. The instrument wires were cut to length and soldered appropriately. The gages were taped to a rigid, plastic sheet for easy installation. All supplies and equipment were neatly organized in advance of the installation. Further details of test preparation can be referenced in Appendix C.

3.2 Instrument Installation

Installation of the instruments was accomplished by using a Mark IV snooper provided by KDOT. The snooper, which was operated by KDOT personnel, was able to maneuver through the bracing and reach remote areas on the bridge. The snooper boom, shown in Figure 3-1, was composed of two baskets, one for the operator and one for the gage installer.

Along with providing the snooper, KDOT also provided traffic control for the installation. Two trucks were stationed at opposite ends of the snooper. Personnel for the gage installation included: two snooper operators, two gage installers, and four traffic control experts.

Installation of the gages lasted three days, with work performed from 8:00 AM to 4:30 PM. In addition to installing gages, work performed also included setting up the data acquisition system on top of pier 29 and running of wires under the bridge. Figure 3-2 displays the testing station mounted under the bridge. Further details of instrument installation and data acquisition setup can be found in Appendix C of this report. When the gages and accelerometers were fully installed, a test run was performed to ensure all gages were working properly.

3.3 Test Setup

After installation of the gages, field-testing was performed. Testing was accomplished by using the following personnel: four traffic controllers, a data collector, a truck driver, and a radio operator. The radio operator communicated to the data collector, who was under the bridge as shown in Figure 3-3, when to start and stop the data acquisition system. Maintenance workers stationed at opposite ends of the bridge controlled ambient traffic. The bridge was first closed to allow for calibration of the system. The truck driver was instructed to maintain the proper speeds by the radio operator. Ambient traffic was stopped during data collection, but released after each truck passing.

3.4 Data Collection

The length for data collection extended from the bridge abutment to the first expansion joint, a total of 552 ft. The radio operator recorded the time of the truck to travel from the abutment to the first joint to check the speed of the truck. A ten second pre-trigger was created to ensure recording of important data. Strain gages readings were taken at a frequency of 200 Hz. After each truck pass, the collected data was checked for any errors by using macros in Microsoft Excel. The macros automatically graphed each gage output and allowed toggling between each gage. This system ensured that all gages were working properly after each loading.

A tandem-axle dump truck, as shown in Figure 3-4, was used to load the structure. The truck weight totaled 54 kips, with 17.2 kips on the front axle and 36.8 kips on the rear axles. The vehicle completed two passes at speeds of 0, 25, 45, and 65 mph for each direction of travel. A total of 16 loadings were recorded for the strain gage data. Six additional loadings were recorded with only the accelerometers collecting data. The collection frequency was increased to 5000 Hz for the accelerometers readings. The truck completed one pass in each direction at speeds of 25, 45, and 65 mph. All the data was stored in the laptop and transported back to the University of Kansas for analysis.

Figure 3-1 Mark IV Snooper

Figure 3-2 Data Acquisition System

Figure 3-3 Acquiring Data

Figure 3-4 Loading Vehicle

CHAPTER 4 BRIDGE BEHAVIOR

The purpose of many of the gages used during testing was to assist in the analysis of future finite element models. The degree of composite action and the forces within the bracing were both investigated during the load test in order to obtain information about the structural system. The bracing stresses were measured at two locations: Diaphragms F2 and F3, as shown in Figure 4-1. Diaphragm F2 gages were used to investigate web-gap cracking, while Diaphragm F3 gages were used to measure stresses related to cracking of the gusset plates.

4.1 Composite Action

When designed in the 1960's, the girders were assumed to act non-compositely. However, since the girder flanges are so wide, large amounts of friction could create some composite action. This phenomenon can be related to the current fatigue problems on the bridge. Web-gap distortion is created by uneven deflection of the primary girders, as detailed in Chapter 2. If one of the girders does not deflect as far as predicted due to some composite action, the web-gap strains would be lower than predicted. Therefore, the percentage of composite action would drastically affect the amount of web-gap strain measured, since the strain values are a function of the deflection of the girders.

4.1.1 Gage Locations

If the girders were acting completely non-compositely, gages placed symmetrically about the centroid should read identical strains. However, if the symmetric girders were acting compositely with the deck, higher strains would be found in the lower flange than in the upper flange in the positive moment region. Therefore, single element gages, labeled G9 and G10, were placed on each of the flanges of Girder A, as shown in Figures 4-2 through 4-5. The gages were used to measure the neutral axis of the girder under loading. The neutral axis can be used to

measure the amount of composite action within the girders, and thus, the increased moment of inertia of the girders.

4.1.2 Results

The degree of composite action was determined by comparing strain values of the upper flange with the lower flange. Maximum and minimum values measured by the gages are summarized in Tables 4-1 through 4-4. Since the girders are symmetric about the neutral axis, equal strain values would indicate complete non-composite action. This test indicated a higher strain in the bottom flange (Gage 10), than the top flange (Gage 9), thus showing that the bridge is acting semi-compositely. The ratios of the two strain values were determined to estimate the degree of composite action.

After analyzing all load cases, an average ratio of the lower and upper flange gages was 3.5. This number indicates that the lower flange is undergoing over three and a half times the amount of stress as the upper flange. By assuming a linear relationship between the strains, this ratio corresponds to a neutral axis height of 74.8 in. from the bottom of the girder, as opposed to a theoretical value of 48.3 in. As indicated by the data, the concrete decking and the steel girder do create enough friction to noticeably adjust the neutral axis. This change in height would create an increase of 65 percent in the stiffness of the member. Although designed as a non-composite system, the concrete decking does provide some support. This result will be helpful in adjusting the finite element model for web-gap distortion to better model the actual behavior of the structure.

4.2 Bracing Gages

The purpose of testing the bracing was to provide a future graduate student with field information to improve the finite element model. The information gathered may not be critical in evaluating the future retrofits, since the forces in the diaphragms should not change drastically. The collected data, however, should assist in the theoretical study of the fatigue cracking found on the bridge. Since the

information collected will be most useful to the student creating the finite element models, little evaluation is provided in this report.

In addition to studying the fatigue cracking, the collected data from the bracing may prove useful for another circumstance. Wipf, et al., researched loosening or removing diaphragm bracing to prevent web-gap cracking. Whether this is a possibility for retrofit is debatable, particularly due to the deepness of the girders and the high winds in the region. Regardless, information gathered from field-testing certainly would aid in considering this retrofit measure.

4.2.1 Gage Locations

Diaphragm bracings found in the upper web-gap and gusset plate regions were gaged to measure the forces within these regions of interest. The gages measured the axial forces found in each of these two-force members. Since the diaphragm bracing creates web-gap stresses, as described in Chapter 2, the axial forces within the diaphragm bracing were measured. The lateral braces within the diaphragm were also instrumented. Figures 4-3 through 4-5 display the gage placement locations for the web-gap region.

The gusset plate region was investigated much like the web-gap region. Gages were placed on the lateral bracing, which are believed to be the cause of the gusset plate cracking. Figures 4-6 through 4-8 show the gages placed on the bracing.

4.2.2 Results

Maximum and minimum values from the gages were determined, but no further analysis was performed. The maximum and minimum values found from the web-gap gages can be found in Tables 4-5 through 4-8. Results from the gages investigating the gusset plate are located in Tables 4-9 through 4-12.

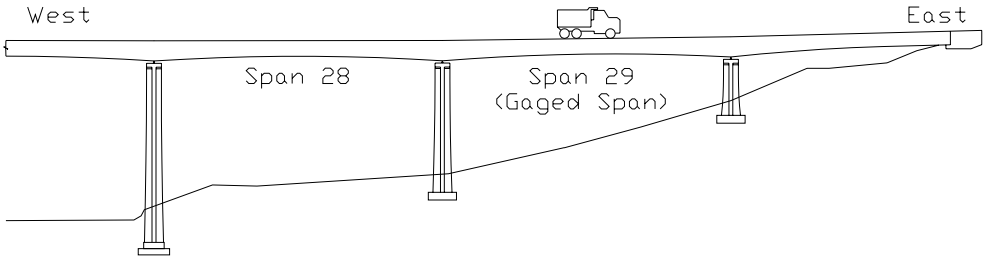

Positive Moment			Gage Number 9	10
Eastbound	65 mph	A	-0.8	2.6
		B	-0.6	3.0
	45 mph	A	-1.0	3.3
		B	-0.6	2.7
	25 mph	A	-1.0	2.3
		B	-0.7	2.6
	5 mph	A	-1.0	2.7
		B	-1.1	3.0
Average Stress (ksi)			**-0.8**	**2.8**

Gage 9 – Top Flange
Gage 10 – Bottom Flange

See Figures 4-2 through 4-5 for locations of Gages 9-10

Table 4-1 Flange Stresses (E29)

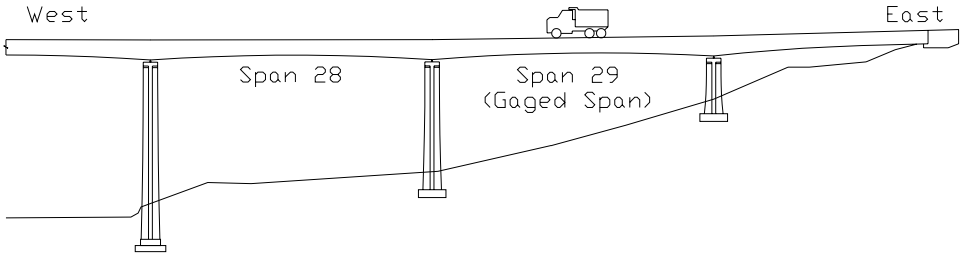

Positive Moment			Gage Number 9	10
Westbound	65 mph	A	-0.1	2.1
		B	-0.2	2.2
	45 mph	A	-0.9	1.4
		B	-0.6	1.4
	25 mph	A	-0.7	1.6
		B	-0.4	1.7
	5 mph	A	-0.7	1.7
		B	-0.8	1.5
Average Stress (ksi)			**-0.6**	**1.7**

Table 4-2 Flange Stresses (W29)

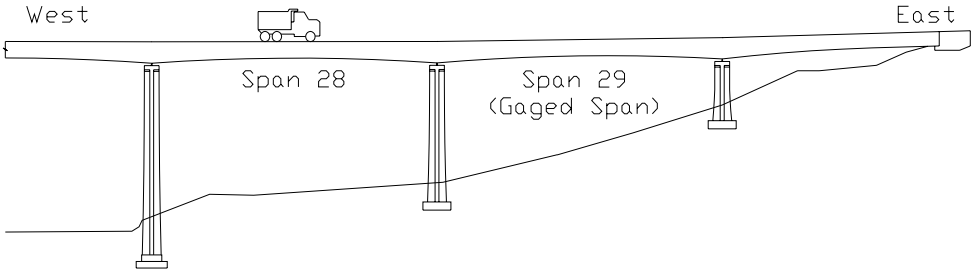

Negative Moment			Gage Number 9	10
Eastbound	65 mph	A	1.1	-0.8
		B	0.9	-1.6
	45 mph	A	0.7	-1.1
		B	0.6	-0.8
	25 mph	A	0.4	-1.7
		B	0.7	-1.0
	5 mph	A	0.7	-1.4
		B	0.9	-0.9
Average Stress (ksi)			**0.8**	**-1.2**

Table 4-3 Flange Stresses (E28)

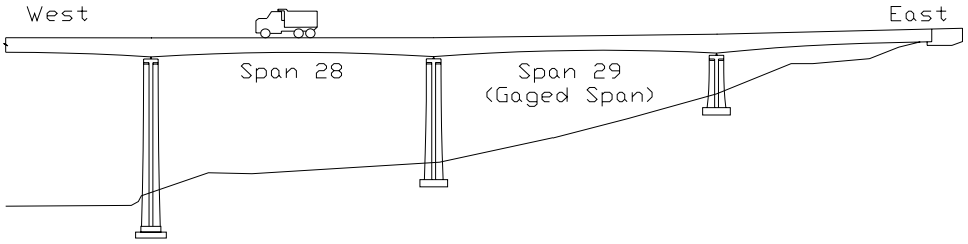

Negative Moment			Gage Number 9	10
Westbound	65 mph	A	1.2	-0.7
		B	1.0	-1.0
	45 mph	A	0.5	-1.8
		B	0.5	-1.1
	25 mph	A	0.5	-1.2
		B	0.7	-1.0
	5 mph	A	0.6	-1.5
		B	0.5	-1.4
Average Stress (ksi)			**0.7**	**-1.2**

Table 4-4 Flange Stresses (W28)

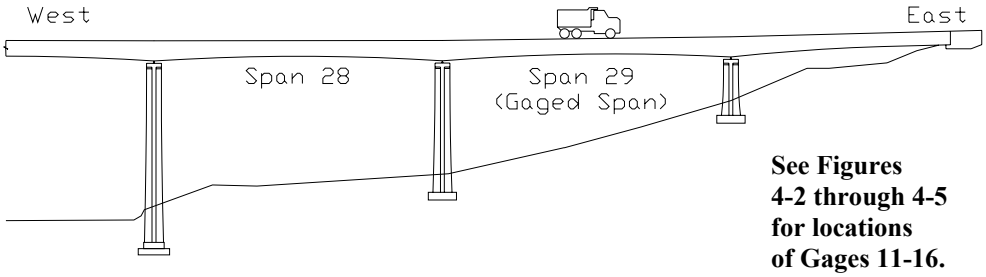

See Figures 4-2 through 4-5 for locations of Gages 11-16.

			Gage Number					
Positive Moment			11	12	13	14	15	16
Eastbound	65 mph	A	0.9	-0.3	0.8	-0.3	-0.4	1.0
		B	1.0	-0.4	0.8	-0.3	-0.7	1.1
	45 mph	A	1.2	-0.6	0.8	-0.5	-0.7	1.4
		B	0.7	-0.3	0.5	-0.3	-0.4	1.2
	25 mph	A	0.6	-0.7	0.4	-0.5	-1.0	1.0
		B	0.8	-0.4	0.5	-0.4	-0.6	1.2
	5 mph	A	0.8	-0.6	0.6	-0.5	-0.9	1.1
		B	0.9	-0.5	0.8	-0.4	-0.8	1.6
Average Stress (ksi)			**0.9**	**-0.5**	**0.6**	**-0.4**	**-0.7**	**1.2**

Table 4-5 Web-Gap Bracing Stresses (E29)

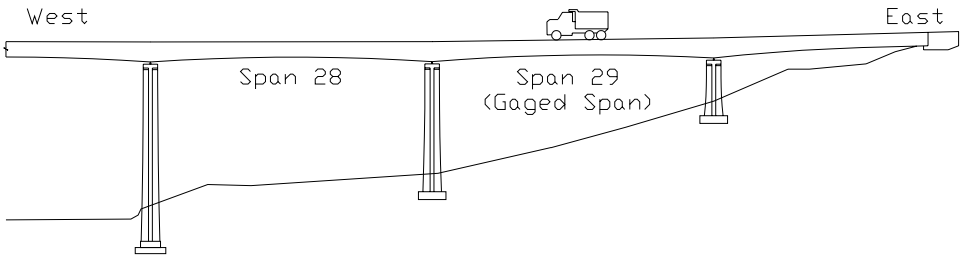

			Gage Number					
Positive Moment			11	12	13	14	15	16
Westbound	65 mph	A	1.4	1.0	-0.2	-0.3	1.6	1.0
		B	1.3	0.9	-0.2	-0.3	1.7	1.0
	45 mph	A	0.9	0.5	-0.7	-0.8	1.1	0.6
		B	0.8	0.6	-0.6	-0.7	1.1	0.7
	25 mph	A	1.0	0.6	-0.6	-0.7	1.2	0.8
		B	1.0	0.7	-0.4	-0.6	1.3	0.9
	5 mph	A	1.1	0.7	-0.5	-0.8	1.3	0.7
		B	1.0	0.7	-0.6	-0.8	1.2	0.7
Average Stress (ksi)			**1.1**	**0.7**	**-0.5**	**-0.6**	**1.3**	**0.8**

Table 4-6 Web-Gap Bracing Stresses (W29)

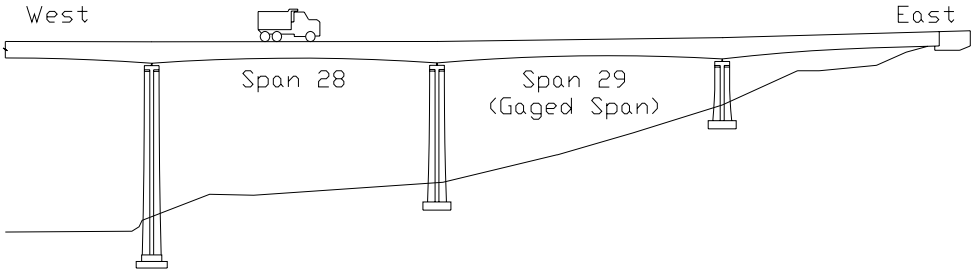

Negative Moment			Gage Number 11	12	13	14	15	16
Eastbound	65 mph	A	-0.3	0.8	-0.3	0.8	1.0	-0.4
		B	-0.4	0.7	-0.4	0.7	0.8	-0.8
	45 mph	A	-0.5	0.6	-0.4	0.5	0.8	-0.7
		B	-0.2	0.5	-0.2	0.4	0.6	-0.5
	25 mph	A	-0.5	0.3	-0.4	0.3	0.3	-0.7
		B	-0.2	0.5	-0.2	0.5	0.5	-0.4
	5 mph	A	-0.5	0.6	-0.4	0.5	0.6	-0.6
		B	-0.3	0.7	-0.3	0.7	0.8	-0.3
Average Stress (ksi)			**-0.4**	**0.6**	**-0.3**	**0.6**	**0.7**	**-0.6**

Table 4-7 Web-Gap Bracing Stresses (E28)

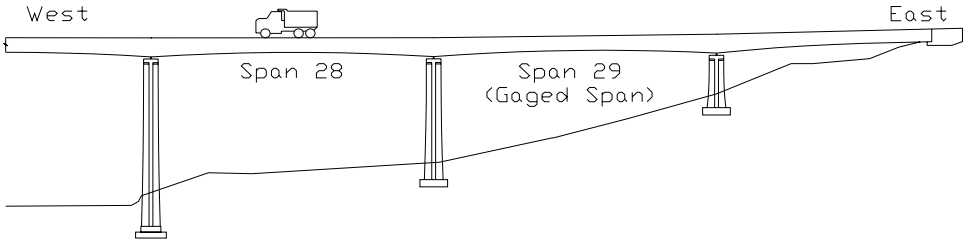

Negative Moment			Gage Number 11	12	13	14	15	16
Westbound	65 mph	A	-0.1	-0.1	0.7	0.7	-0.3	-0.3
		B	-0.2	-0.2	0.7	0.7	-0.4	-0.4
	45 mph	A	-0.8	-0.7	0.3	0.3	-1.0	-1.1
		B	-0.4	-0.4	0.4	0.3	-0.6	-0.5
	25 mph	A	-0.5	-0.4	0.3	0.4	-0.6	-0.7
		B	-0.4	-0.3	0.4	0.5	-0.5	-0.5
	5 mph	A	-0.5	-0.5	0.4	0.4	-0.8	-0.7
		B	-0.6	-0.5	0.3	0.3	-0.8	-0.7
Average Stress (ksi)			**-0.4**	**-0.4**	**0.4**	**0.5**	**-0.6**	**-0.6**

Table 4-8 Web-Gap Bracing Stresses (W28)

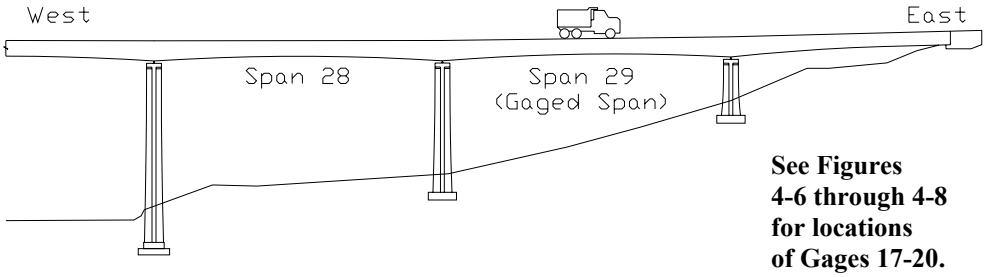

See Figures 4-6 through 4-8 for locations of Gages 17-20.

Positive Moment			Gage Number 17	18	19	20
Eastbound	65 mph	A	0.7	0.7	-0.9	1.3
		B	0.7	0.8	-0.9	1.5
	45 mph	A	0.8	0.7	-0.9	1.6
		B	0.6	0.6	-0.6	1.3
	25 mph	A	0.4	0.3	-1.1	1.2
		B	0.6	0.7	-0.7	1.3
	5 mph	A	0.7	0.7	-0.9	1.5
		B	0.8	0.8	-0.9	1.8
Average Stress (ksi)			**0.7**	**0.7**	**-0.9**	**1.4**

Table 4-9 Gusset Plate Bracing Stresses (E29)

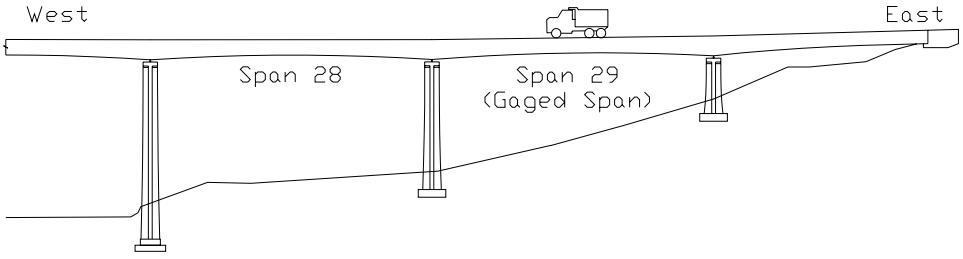

Positive Moment			Gage Number 17	18	19	20
Westbound	65 mph	A	-0.2	-0.2	1.2	-0.5
		B	-0.3	-0.3	1.2	-0.4
	45 mph	A	-0.8	-0.9	0.8	-1.1
		B	-0.5	-0.5	0.9	-1.0
	25 mph	A	-0.5	-0.5	1.0	-0.9
		B	-0.4	-0.4	1.2	-0.9
	5 mph	A	-0.5	-0.6	1.0	-1.0
		B	-0.6	-0.6	1.0	-1.0
Average Stress (ksi)			**-0.5**	**-0.5**	**1.1**	**-0.9**

Table 4-10 Gusset Plate Bracing Stresses (W29)

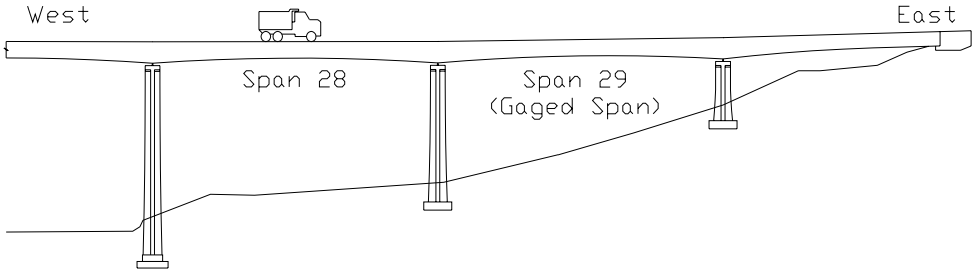

Negative Moment			Gage Number 17	18	19	20
Eastbound	65 mph	A	-0.4	-0.4	0.8	-0.5
		B	-0.7	-0.6	0.7	-1.0
	45 mph	A	-0.5	-0.6	0.6	-0.7
		B	-0.3	-0.3	0.6	-0.4
	25 mph	A	-0.6	-0.6	0.3	-0.9
		B	-0.3	-0.3	0.7	-0.5
	5 mph	A	-0.4	-0.3	0.7	-0.6
		B	-0.3	-0.4	0.7	-0.6
Average Stress (ksi)			**-0.4**	**-0.4**	**0.6**	**-0.6**

Table 4-11 Gusset Plate Bracing Stresses (E28)

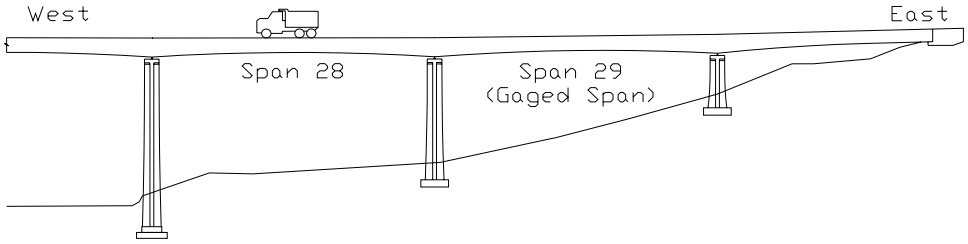

Negative Moment			Gage Number 17	18	19	20
Westbound	65 mph	A	0.9	1.0	-0.4	0.8
		B	0.9	1.0	-0.5	1.0
	45 mph	A	0.4	0.4	-0.9	0.5
		B	0.3	0.4	-0.6	0.4
	25 mph	A	0.4	0.5	-0.6	0.4
		B	0.6	0.7	-0.6	0.5
	5 mph	A	0.5	0.6	-0.9	0.5
		B	0.5	0.5	-0.8	0.5
Average Stress (ksi)			**0.6**	**0.6**	**-0.7**	**0.6**

Table 4-12 Gusset Plate Bracing Stresses (W28)

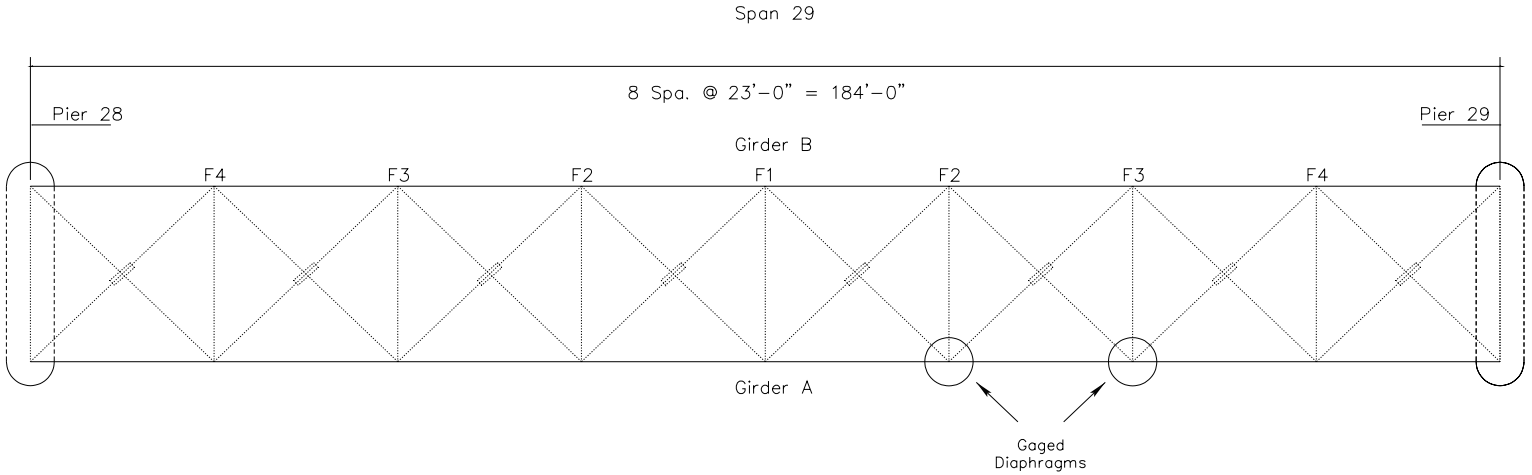

Figure 4-1 Gage Placement on Span 29

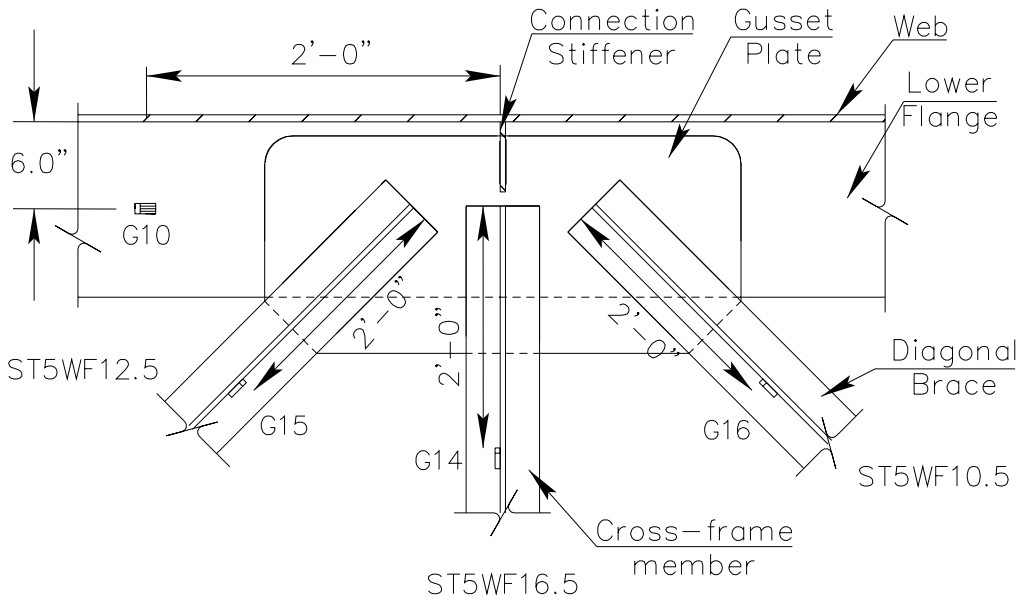

Figure 4-2 Lower Flange/ Bracing Gages (Diaphragm F2)

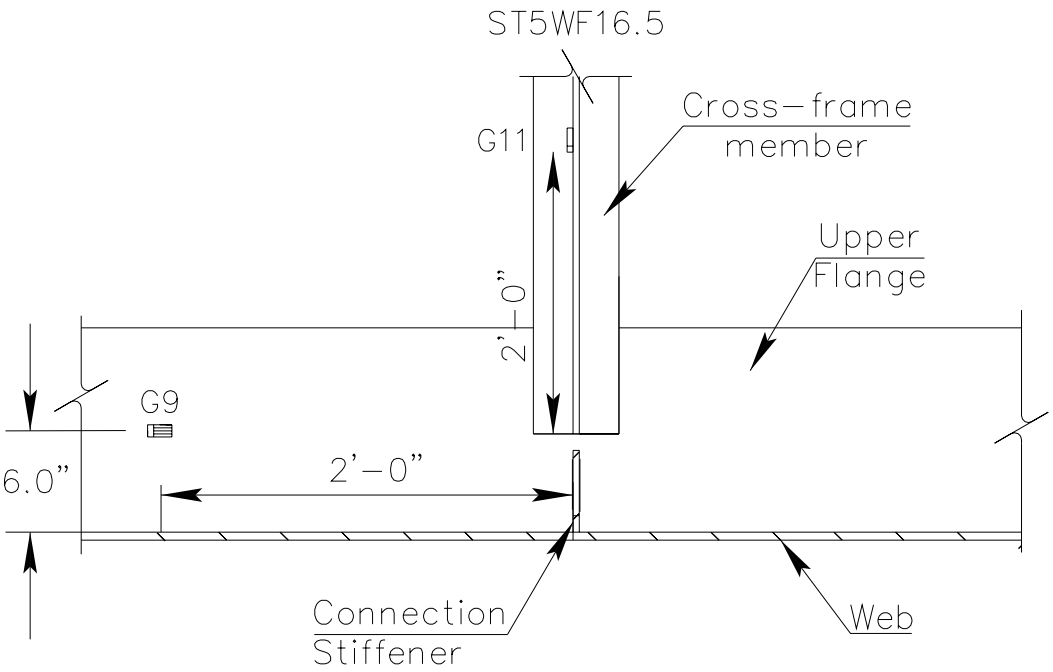

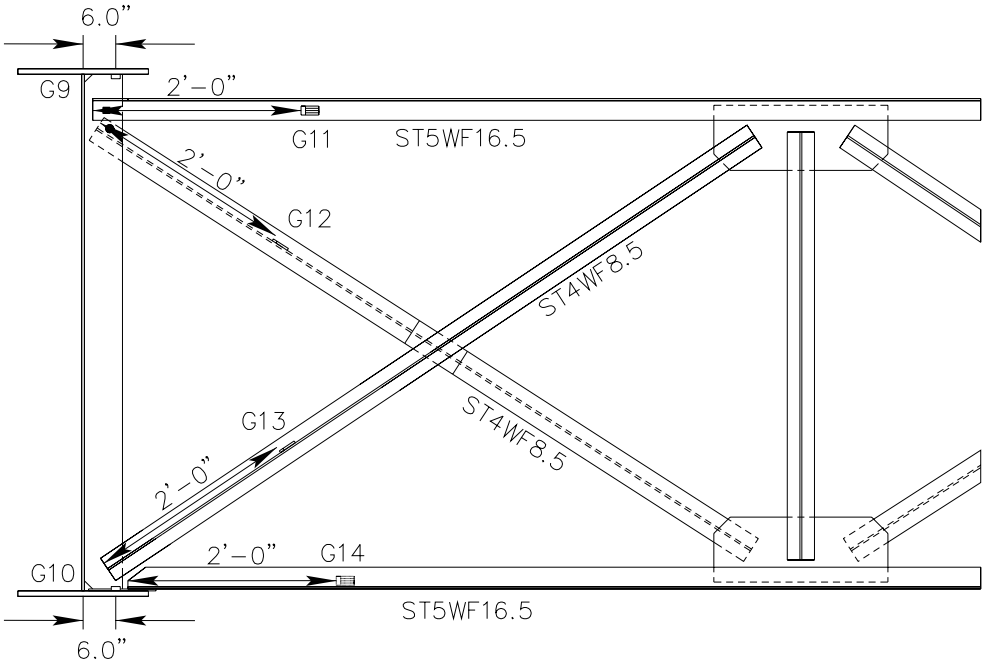

Figure 4-4 Flange/ Bracing Gages (Diaphragm F2)

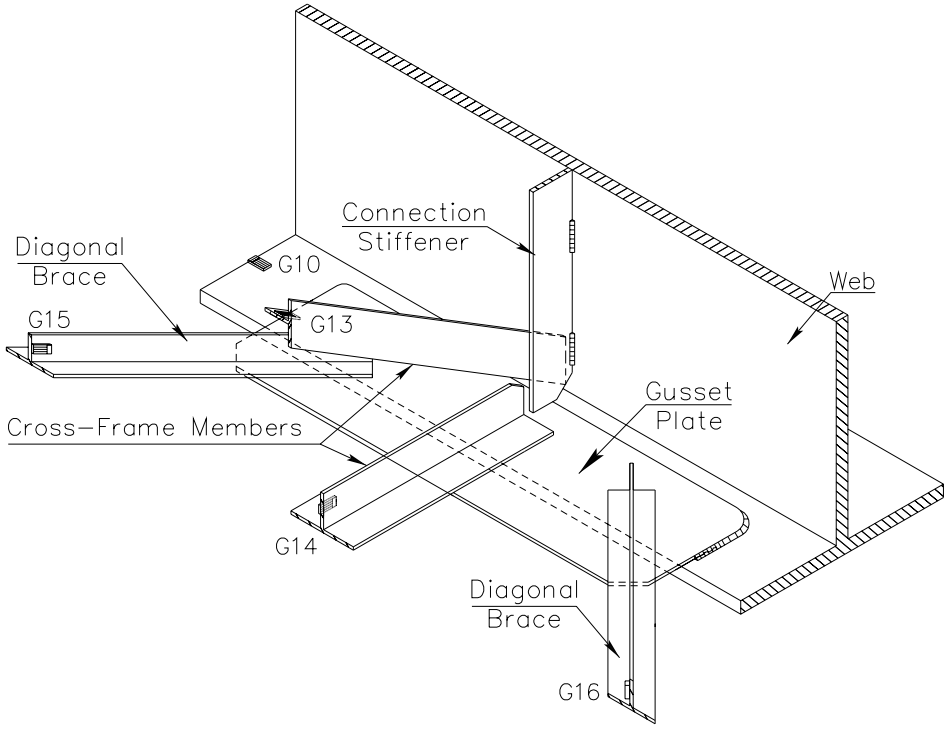

Figure 4-5 Lower Flange/ Bracing Gages (Diaphragm F2)

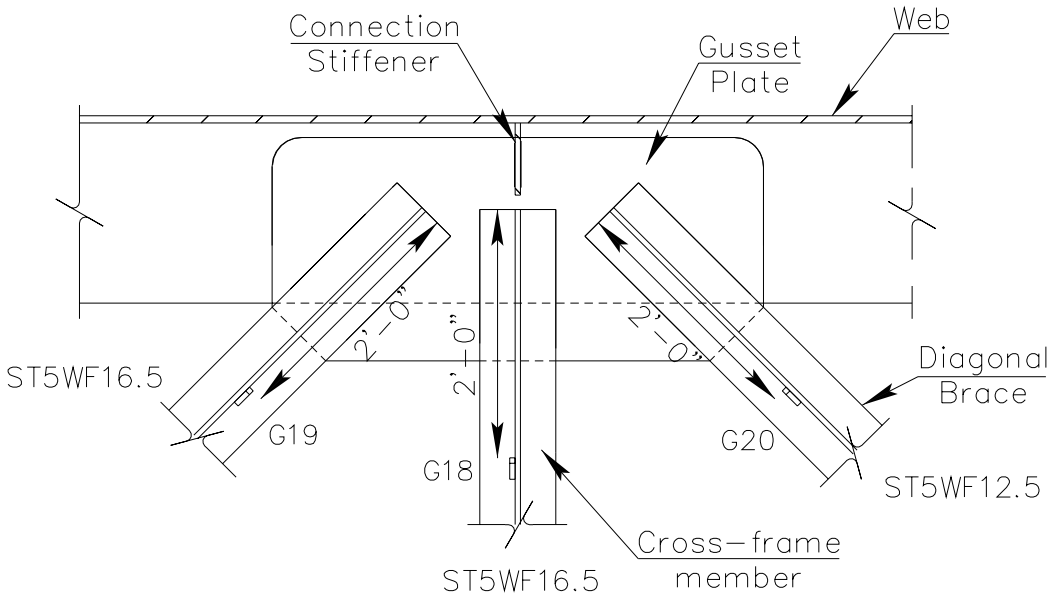

Figure 4-6 Lateral Bracing Gages (Diaphragm F3)

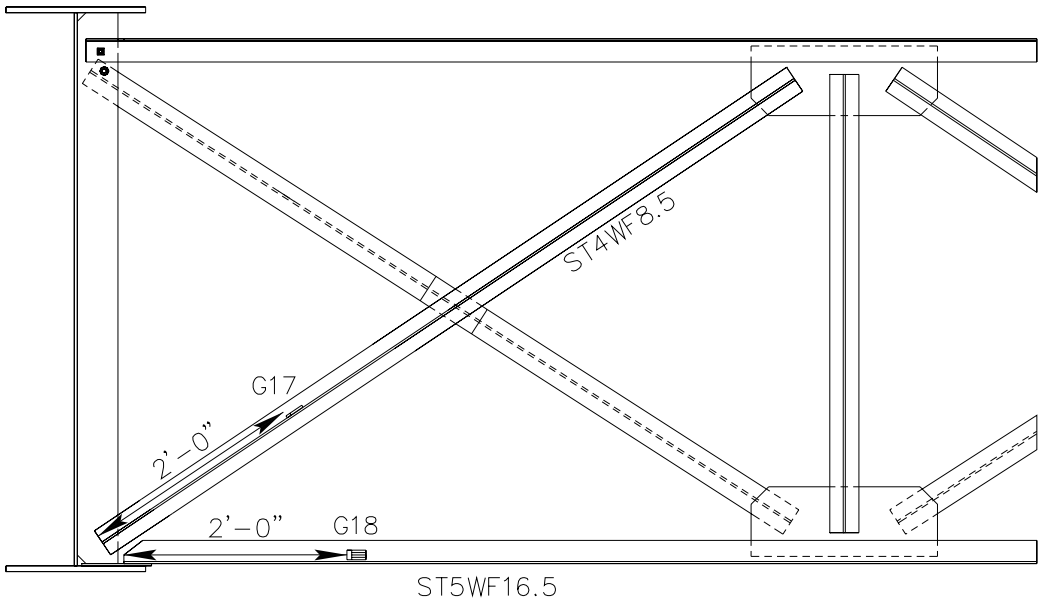

Figure 4-7 Diaphragm Bracing Gages (Diaphragm F3)

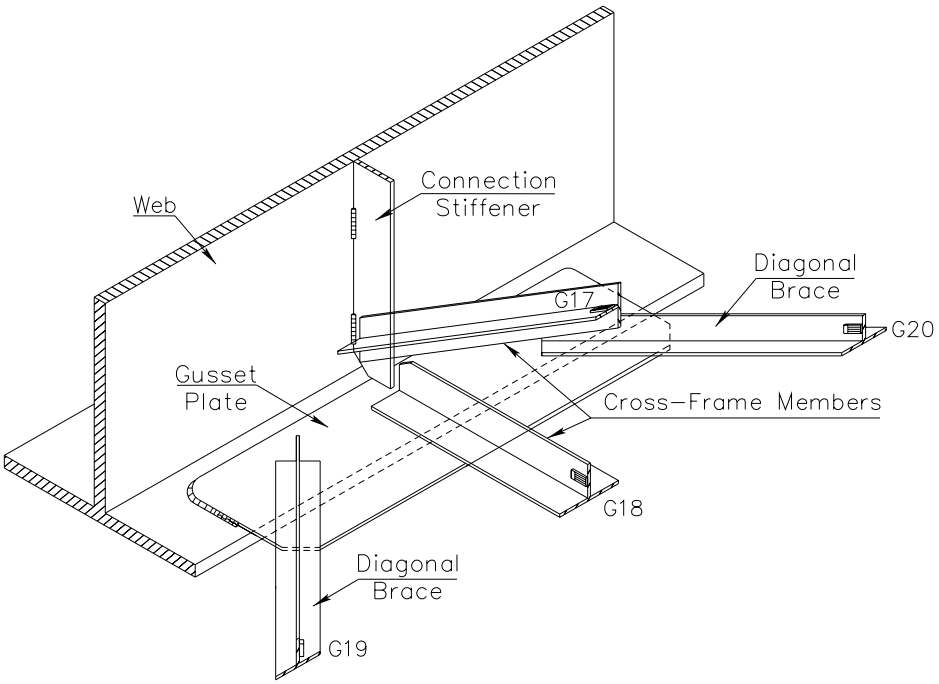

Figure 4-8 Bracing Gages (Diaphragm F3)

CHAPTER 5 WEB-GAP CRACKING

This chapter describes work performed on the web-gap region. The repairs, both past and future, are presented as a background to the testing. The purpose of each gage is explained and their position described. Finally, the results from the gages are presented as well as inferences from the data.

5.1 Repair Strategy

Many repair strategies have been adopted to alleviate web-gap cracking. The drilling of stop holes has been an economic solution in stopping crack propagation. However, for the Tuttle Creek Bridge, this repair has been ineffective. Softening measures, such as increasing the web-gap by slotting the connection stiffener, can also be a cost-effective solution. This retrofit strategy was also used for the Tuttle Creek Bridge, but like the stop holes, it too did not prevent further propagation. The repair strategy performed in 1986 is shown in Figure 5-1.

The most effective retrofit for web-gap cracking is positive attachment of the connection stiffener to the flange by either a bracket or fillet weld. Current standards require this design detail for both positive and negative moment regions. This retrofit method, however, is very costly and is a last resort for most designers.

For the Tuttle Creek Bridge, the repair design was the expensive retrofit of positively attaching the connection stiffener to the upper flange. Instead of difficult overhead welding, the stiffener will be attached to the upper flange by using two brackets, as shown in Figure 5-2. Two studs will be placed into the upper flange and will secure the bracket. The other end of the brackets will be bolted to the connection stiffener. Additional stop holes will also be drilled through the web to arrest further crack propagation.

Repairs were also made to the lower web-gap in 1986. An angle bracket was bolted to the connection stiffener and the lower flange, as shown in Figure 5-3. The repairs have been successful, although unretrofitted lower web-gaps have not had any

cracks found either. Since this retrofit was only performed on diaphragms labeled F4 in Figure 1-4, additional repairs were necessary for the other diaphragms in order to ensure no new cracks. The lower web-gap region will be repaired by fillet welding the stiffener to the existing gusset plate, as shown in Figure 5-4.

5.2 Gage Locations

Web-gap gages were used to determine the amount of stress created by the web distortion. Gages were placed in both the upper and lower web-gaps, since Zhao determined both gaps to be fatigue prone. The gages were placed on the girder web since the majority of the cracks and highest predicted stresses were found within it.

The single-element gages were placed vertically near the tip of the existing horizontal crack, as shown in Figures 5-5 through 5-6. The strain gages were placed as close to the tangent of the drilled hole without overlapping onto the fillet weld. Since the horizontal crack runs along a fillet weld, the gages could not be placed in this high stress region. Due to this restriction, two gages were placed in line with each other. Their values were used to extrapolate the maximum stress near the crack tip. Two sets of gages were used: one on the interior side of the girder and one on the exterior. The gages, in theory, should read equal but opposite strains due to pure bending in the web-gap. Having two sets also provided a backup in case one of the gages did not read strains properly. This gage setup was utilized in similar bridge load testing such as Stallings et al., Jajich and Schultz, and Wpif et al, as summarized in Appendix A.

The web-gap gages were placed on diaphragm F2, which is one diaphragm away from the center of the span. This diaphragm was chosen because the finite element model created by Zhao indicated this diaphragm created the highest web-gap stress. The inspection report indicated this diaphragm location had an existing weld tear and horizontal crack. The horizontal crack was previously drilled with no new growth.

5.3 Results

The gages placed in the web-gap regions worked exceptionally well. The upper gap gages placed on the inside of the girder observed compression during positive bending of the span, while the outside indicated tensile forces. The absolute values of the interior and exterior gages were nearly equal, indicating pure bending forces.

The alignment of the two gages also worked very well. As expected, the gage nearest to the flange had a higher stress value. For the upper flange regions, the extrapolated value was to the edge of the drilled hole, which was also the lower edge of the flange/web fillet weld. For the lower flanges, the extrapolated value was simply to the edge of the flange/web fillet weld.

The stress values for the upper web-gap regions were much higher in the westbound direction than eastbound, as seen in Tables 5-1 through 5-2. This observation reinforces Zhao's model. Zhao's model indicated maximum tension values, σ_y, of 46 ksi and 12 ksi for westbound and eastbound traffic, respectively. After extrapolating the two gages, the values obtained from this test reported average maximum stresses of 35.4 ksi for westbound and 12.6 ksi for eastbound. Figure 5-9 displays the predicted web-gap stresses with those measured during the load test. In general, there is a good agreement between the maximum stresses theoretically calculated for the upper web-gap and those measured on the bridge.

Minimum stresses were also in agreement with predicted values. Zhao predicted the minimum stresses to be close to zero. During the load test, the minimum value of σ_y was found to be approximately 3.6 ksi for eastbound and 2.4 ksi for westbound.

Lower web-gap stresses, however, were below those predicted by Zhao's model. A maximum stress of 14 ksi for eastbound and 8.6 ksi for westbound was theoretically calculated. After load testing, maximum values of 2.4 ksi and 3.0 ksi were extrapolated for eastbound and westbound traffic, respectively. Zhao's model

appears to be overly conservative when predicting the amount of lower web-gap stresses. Figure 5-10 compares the measured lower web-gap stresses with those predicted by Zhao.

The difference in lower web-gap stresses is probably due to the difficulty of predicting the amount of horizontal translation of the girder under load. While the deck rigidly holds the upper flange, the lower flange is free to move sideways and rotate. Since stresses in the lower web-gap are a function of the rigidity of the girder, any difference in rigidity would alter the calculated lower web-gap stresses. Given that the extent of this movement is difficult to predict, any differences in the theoretical model and the load test would be understandable. The important point is that the model is conservative. The measured stresses support Zhao's prediction that the lower web-gap should not develop any cracking.

After determining the average stresses in the detail, the fatigue life can be calculated. Fatigue life calculations were determined for the web-gap region. The web-gap region is a category C detail, which corresponds to a fatigue category constant of 44×10^8 ksi^3. After performing the fatigue life calculations, which are summarized in Chapter F, the fatigue life of the web-gap detail without retrofit is approximately 50 years. Since the bridge was built 1962, the current detail is approaching the end of its lifespan.

5.4 Cracking Theories

The stresses obtained by the strain gages were in good agreement with the values from Yuan Zhao's finite element model. However, the web-gap stress concentrations do not support all of the cracking patterns found on the bridge. Weld tearing is fully supported by the finite element model; however, horizontal cracking found on the interior side of the girder does not appear logical. Both the finite element model and the field-testing show that the region is predominately in compression due to live loads. If the live load is the only loading in this region, a fatigue crack should not be initiating.

Several theories exist of why there is cracking occurring in the web-gap. The first possibility is the existence of residual stresses due to the fillet weld. Welding can create tensile residual stresses in the vicinity of a weld. These residual stresses would make the apparent compressive cycle actually a tension cycle. One drawback to this theory is that if residual stresses are occurring on the interior side of the girder, logically, the exterior side should also have residual stresses. The residual stresses would magnify the tensile cycles found in the exterior side, thus increasing crack initiation. Residual stresses would increase the possibility of crack initiation for both sides, but they do not explain why more horizontal cracks are found on the interior side than the exterior.

Perhaps unforeseen loads from the dead weight of the structure caused the crack patterns. An imbalance of the deck load on the upper flange could cause tensile forces within the interior, web-gap region. If the weight of the deck cantilevered over the girder flange were high compared to the deck weight, the flange would rotate outwardly, as shown in Figure 5-11. This rotation would create tensile forces within the web-gap region. This would explain the abundance of cracks on the interior side of the girder.

Another theory would be binding of the connection stiffener. The connection stiffeners, found only on the interior side, were designed to be the same height as the web at the diaphragm locations. Although designed as a secondary-loaded member, the connection stiffeners may have inadvertently created stress in the web-gap. When constructed in 1962, the girders were first loaded with the dead weight of the decking. The weight of the decking was transferred directly to the upper flange of the girders. The load may have then transferred to portions of the connection stiffener, which were at the same height as the girder web. Additional deformation of the web-gap, due to double curvature bending from differential deflection of the girders, would cause further load to be applied to the stiffener. Since the stiffener is found only on the interior side, the distributed load from the decking onto the upper flange would be unbalanced. A moment is thus created in the web-gap region, placing the interior side

into tension, as shown in Figure 5-12. If the interior side of the web-gap were in tension prior to large live loads, fatigue cracks would be likely to initiate. The live loads producing compressive stress cycles would actually be creating tensile residual stress cycles, thus causing crack initiation.

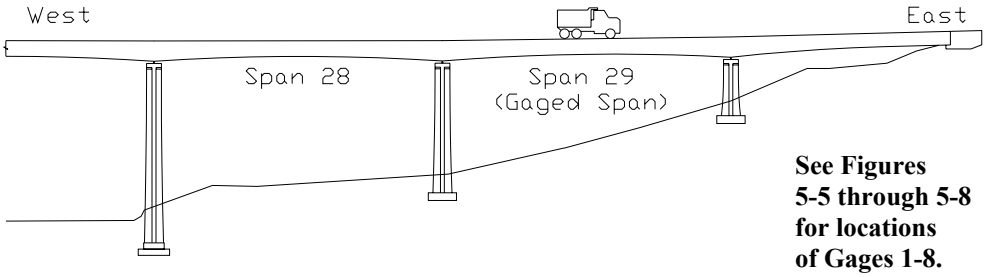

See Figures 5-5 through 5-8 for locations of Gages 1-8.

Positive Moment			Gage Number 1	2	3	4	5	6	7	8
Eastbound	65 mph	A	-7.4	-3.8	8.1	4.4	1.1	-1.0	-2.3	-0.4
		B	-7.4	-3.7	8.7	4.9	1.4	-1.0	-2.3	-0.6
	45 mph	A	-9.3	-4.3	10.7	5.7	1.4	-1.3	-2.3	-0.8
		B	-9.8	-4.7	10.3	5.2	1.1	-1.0	-2.2	-0.4
	25 mph	A	-8.4	-4.4	8.8	4.6	1.0	-1.5	-2.6	-0.7
		B	-11.4	-5.3	11.8	5.8	1.1	-1.1	-2.5	-0.5
	5 mph	A	-10.9	-5.4	10.6	5.3	1.2	-1.5	-2.8	-0.6
		B	-7.8	-4.3	8.5	4.7	1.4	-1.4	-2.7	-0.4
Average Stress (ksi)			**-9.1**	**-4.5**	**9.7**	**5.1**	**1.2**	**-1.2**	**-2.5**	**-0.5**

Table 5-1 Web-Gap Stresses (E29)

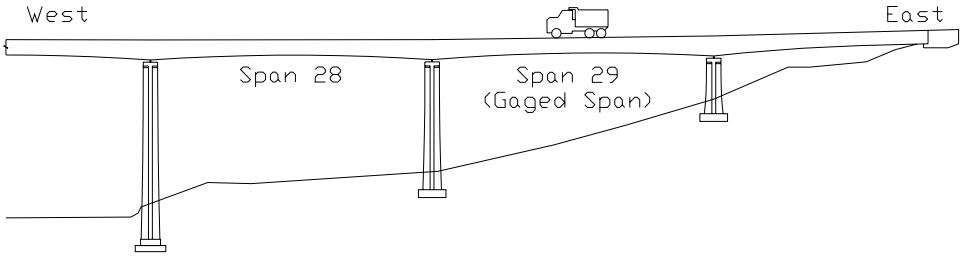

Positive Moment			Gage Number 1	2	3	4	5	6	7	8
Westbound	65 mph	A	-24.1	-8.9	25.7	9.7	-0.3	1.9	1.4	-1.4
		B	-24.8	-9.3	26.4	9.8	-0.4	2.0	1.4	-1.5
	45 mph	A	-23.9	-9.0	24.4	8.8	-0.9	1.6	0.6	-2.3
		B	-24.2	-9.3	24.4	8.7	-0.9	1.5	0.6	-2.2
	25 mph	A	-24.8	-9.2	25.3	9.2	-0.8	1.6	0.8	-2.2
		B	-24.6	-9.2	25.1	9.0	-0.7	1.8	0.9	-2.0
	5 mph	A	-26.0	-9.5	26.0	9.5	-0.8	1.8	0.9	-2.3
		B	-25.2	-9.6	25.4	9.4	-0.9	1.8	0.8	-2.3
Average Stress (ksi)			**-24.7**	**-9.3**	**25.3**	**9.2**	**-0.7**	**1.7**	**0.9**	**-2.0**

Table 5-2 Web-Gap Stresses (W29)

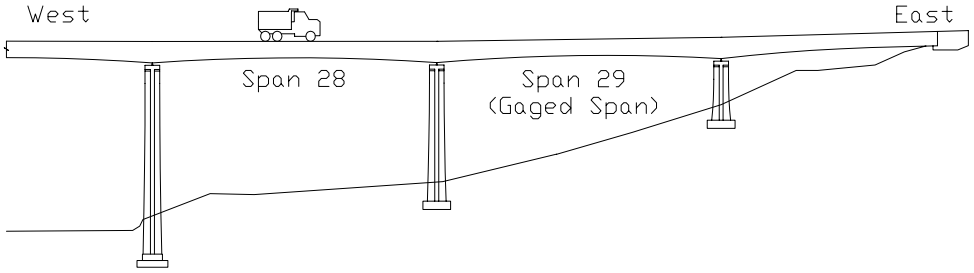

Negative Moment			Gage Number 1	2	3	4	5	6	7	8
Eastbound	65 mph	A	2.8	1.0	-2.1	-0.5	-0.3	0.9	1.1	1.3
		B	2.5	0.8	-2.3	-0.7	-0.4	0.8	1.1	1.2
	45 mph	A	2.5	1.0	-1.9	-0.7	-0.6	0.6	0.9	0.9
		B	1.8	0.8	-1.7	-0.4	-0.3	0.5	0.8	0.8
	25 mph	A	2.6	0.7	-2.7	-1.1	-0.5	0.3	0.4	0.5
		B	2.2	0.9	-2.0	-0.6	-0.2	0.6	0.9	0.9
	5 mph	A	2.6	0.9	-2.5	-0.9	-0.4	0.6	0.9	0.9
		B	3.8	1.3	-3.0	-1.0	-0.3	0.8	1.1	1.1
Average Stress (ksi)			**2.6**	**0.9**	**-2.3**	**-0.7**	**-0.4**	**0.6**	**0.9**	**0.9**

Table 5-3 Web-Gap Stresses (E28)

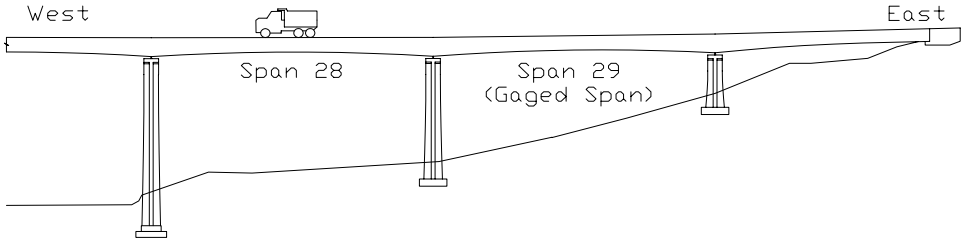

Negative Moment			Gage Number 1	2	3	4	5	6	7	8
Westbound	65 mph	A	1.8	0.9	-1.3	-0.5	1.0	-0.3	-0.2	1.5
		B	1.8	0.8	-1.6	-0.7	0.9	-0.5	-0.3	1.2
	45 mph	A	1.5	0.4	-1.7	-1.0	0.4	-0.9	-1.0	0.5
		B	1.4	0.4	-1.5	-0.7	0.5	-0.6	-0.5	0.7
	25 mph	A	1.6	0.6	-1.7	-0.8	0.6	-0.7	-0.7	0.8
		B	1.6	0.7	-1.6	-0.7	0.8	-0.6	-0.5	1.1
	5 mph	A	1.0	0.6	-1.4	-0.9	0.6	-0.8	-0.8	0.9
		B	3.1	0.6	-1.9	-1.0	0.6	-0.8	-0.8	0.9
Average Stress (ksi)			**1.7**	**0.6**	**-1.6**	**-0.8**	**0.7**	**-0.6**	**-0.6**	**1.0**

Table 5-4 Web-Gap Stresses (W28)

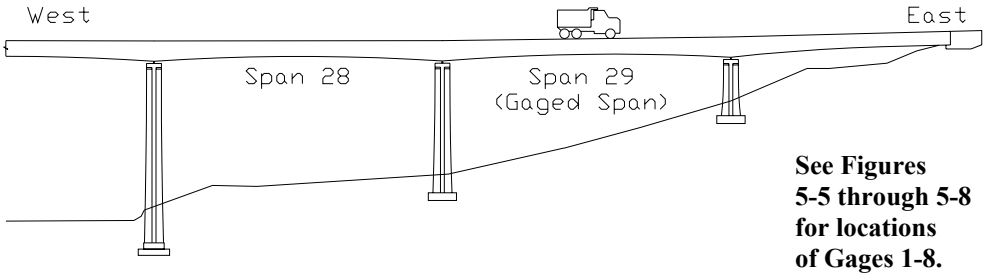

See Figures 5-5 through 5-8 for locations of Gages 1-8.

Positive Moment			Extrapolated Gages 1 & 2	3 & 4	5 & 6	7 & 8
Eastbound	65 mph	A	-9.7	10.4	-2.1	2.1
		B	-9.7	11.1	-2.2	1.6
	45 mph	A	-12.4	13.8	-2.6	1.2
		B	-12.9	13.5	-2.0	1.7
	25 mph	A	-10.8	11.5	-2.8	1.7
		B	-15.2	15.5	-2.2	2.0
	5 mph	A	-14.3	13.9	-2.8	2.1
		B	-10.1	10.8	-2.8	2.4
Average Stress (ksi)			**-11.9**	**12.6**	**-2.4**	**1.8**

Table 5-5 Extrapolated Web-Gap Stresses (E29)

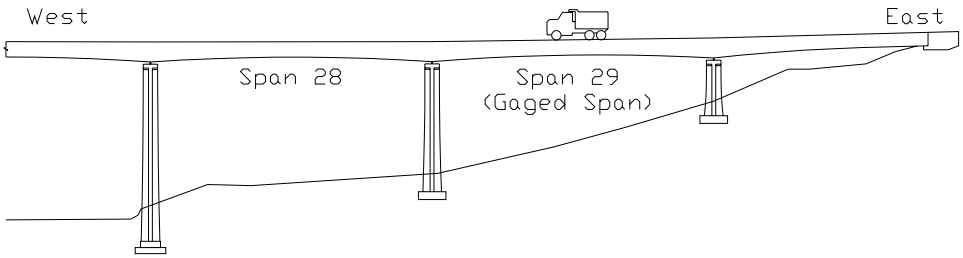

Positive Moment			Extrapolated Gages 1 & 2	3 & 4	5 & 6	7 & 8
Westbound	65 mph	A	-33.7	35.6	3.0	-4.9
		B	-34.5	36.8	3.2	-5.0
	45 mph	A	-33.2	34.1	2.9	-5.9
		B	-33.6	34.1	2.7	-5.8
	25 mph	A	-34.5	35.4	2.8	-6.0
		B	-34.1	35.2	3.0	-5.6
	5 mph	A	-36.2	36.3	3.1	-6.3
		B	-35.0	35.4	3.1	-6.2
Average Stress (ksi)			**-34.4**	**35.4**	**3.0**	**-5.7**

Table 5-6 Extrapolated Web-Gap Stresses (W29)

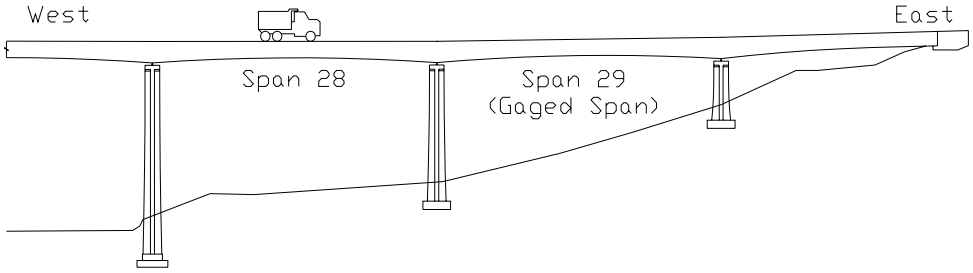

Negative Moment			Extrapolated Gages 1 & 2	3 & 4	5 & 6	7 & 8
Eastbound	65 mph	A	3.9	-3.1	1.5	1.4
		B	3.6	-3.4	1.4	1.2
	45 mph	A	3.5	-2.6	1.3	0.9
		B	2.4	-2.5	1.0	0.8
	25 mph	A	3.8	-3.7	0.7	0.5
		B	3.1	-2.9	1.0	1.0
	5 mph	A	3.6	-3.4	1.1	1.0
		B	5.4	-4.2	1.4	1.3
Average Stress (ksi)			**3.6**	**-3.2**	**1.2**	**1.0**

Table 5-7 Extrapolated Web-Gap Stresses (E28)

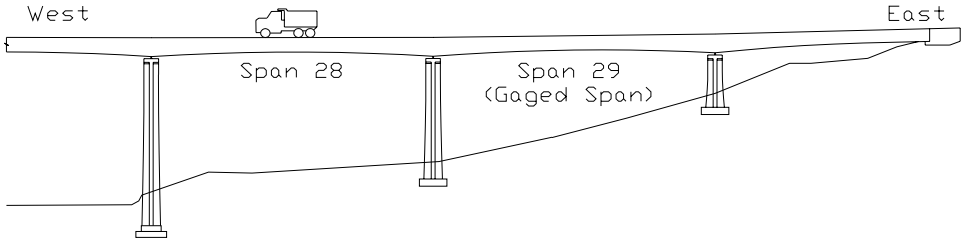

Negative Moment			Extrapolated Gages 1 & 2	3 & 4	5 & 6	7 & 8
Westbound	65 mph	A	2.4	-1.8	-1.0	3.6
		B	2.5	-2.3	-1.2	3.1
	45 mph	A	2.2	-2.2	-1.5	2.4
		B	2.0	-2.0	-1.1	2.3
	25 mph	A	2.3	-2.2	-1.3	2.7
		B	2.1	-2.1	-1.2	3.1
	5 mph	A	1.2	-1.7	-1.5	3.1
		B	4.7	-2.4	-1.5	3.0
Average Stress (ksi)			**2.4**	**-2.1**	**-1.3**	**2.9**

Table 5-8 Extrapolated Web-Gap Stresses (W28)

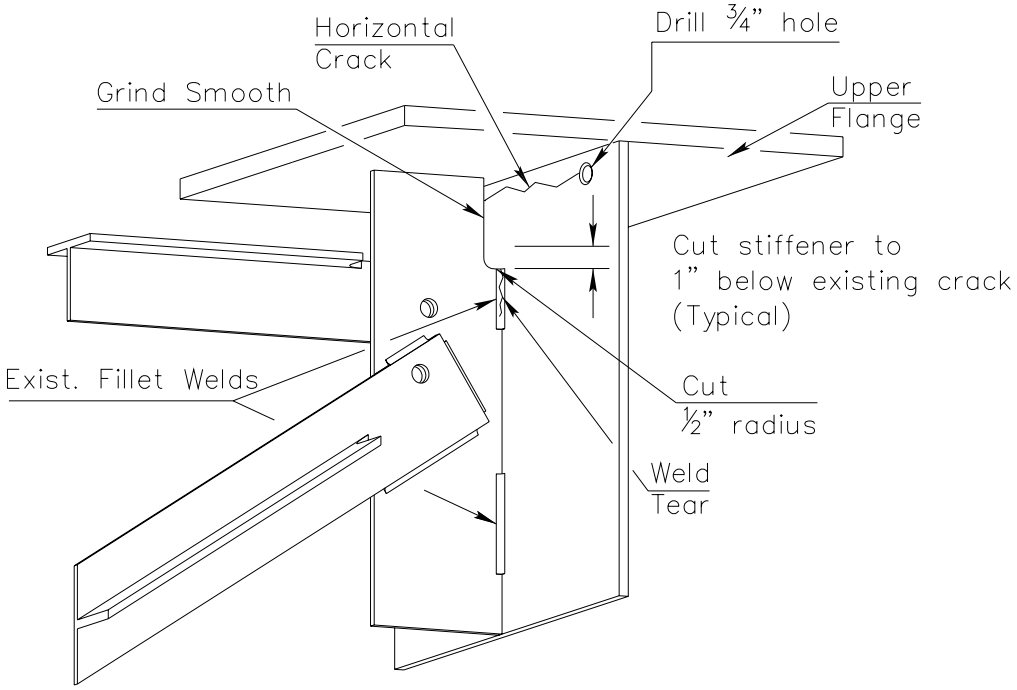

Figure 5-1 1986 Repair of Upper Web-Gap

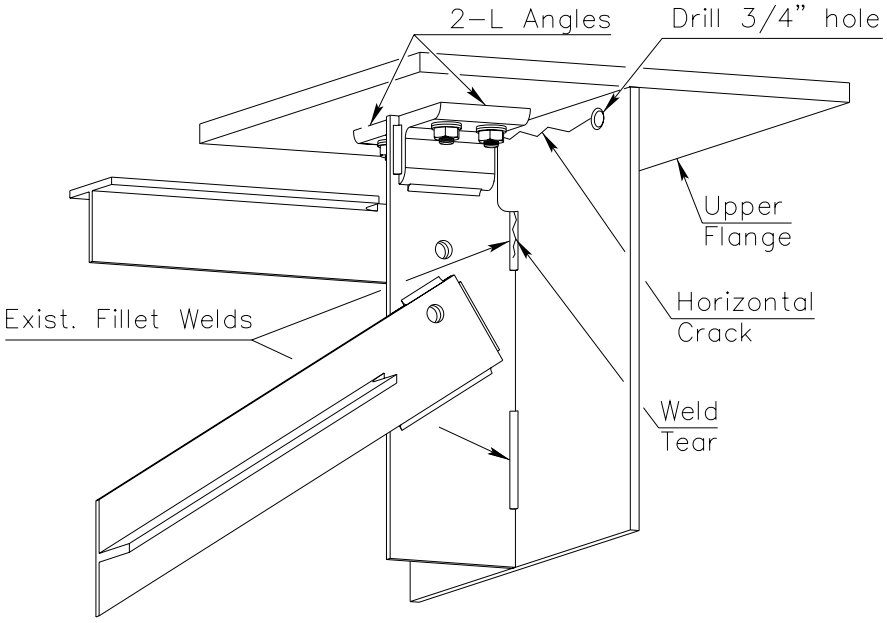

Figure 5-2 2005 Repair of Upper Web-Gap

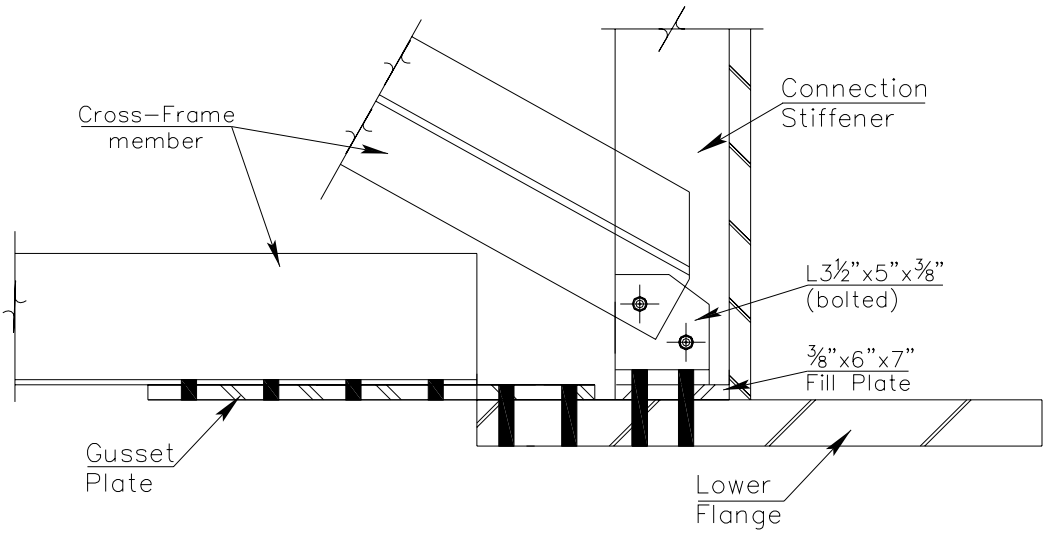

Figure 5-3 1986 Repair of Lower Web-Gap

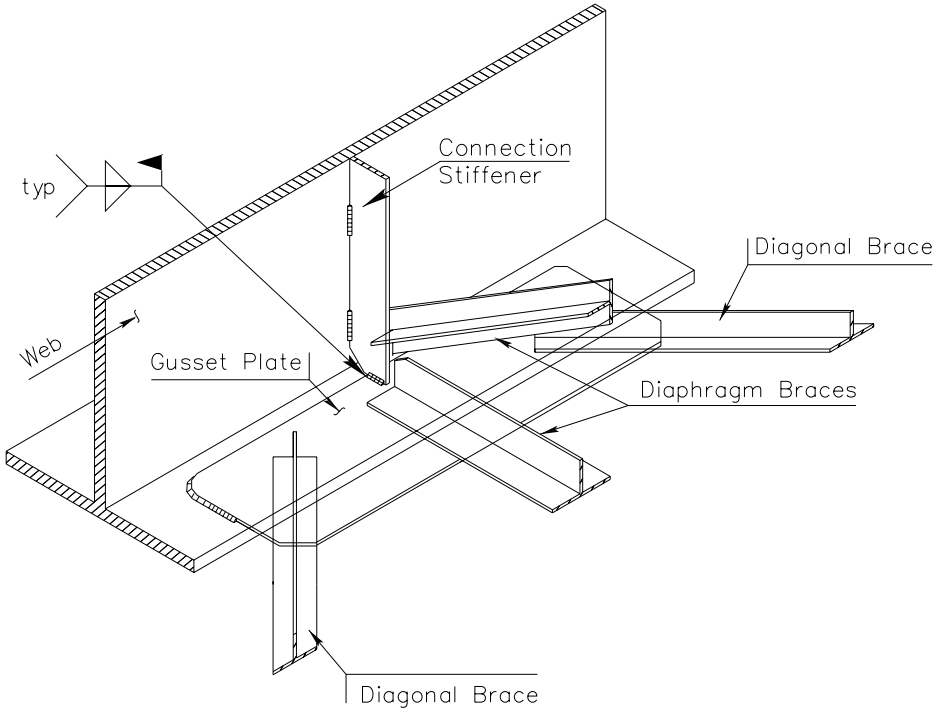

Figure 5-4 2005 Repair of Lower Web-Gap

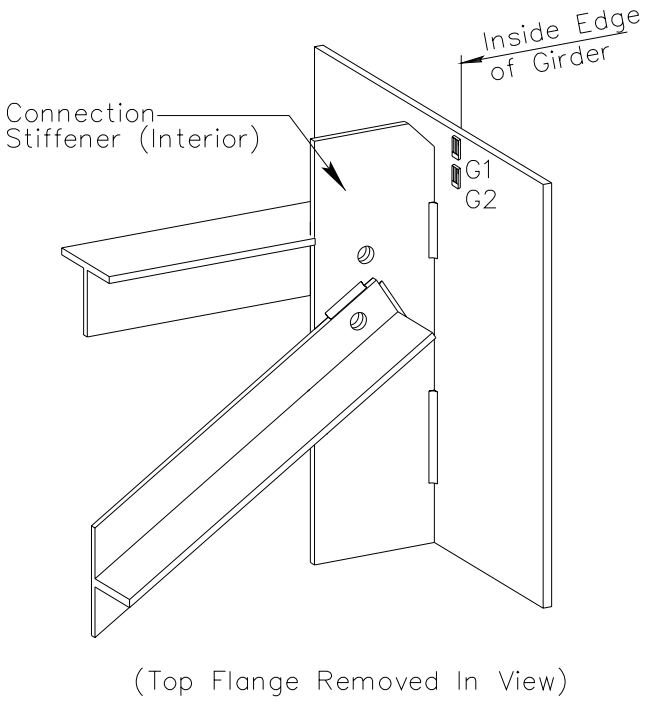

Figure 5-5 Upper Web-Gap (Diaphragm F2)

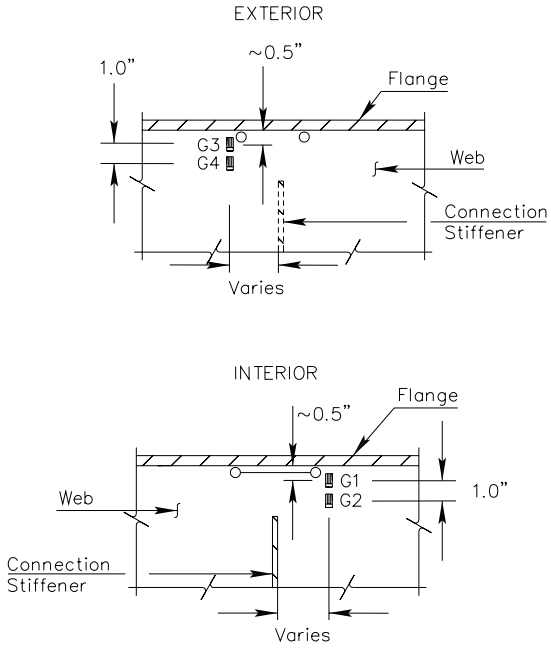

Figure 5-6 Upper Web-Gap (Interior and Exterior) (Diaphragm F2)

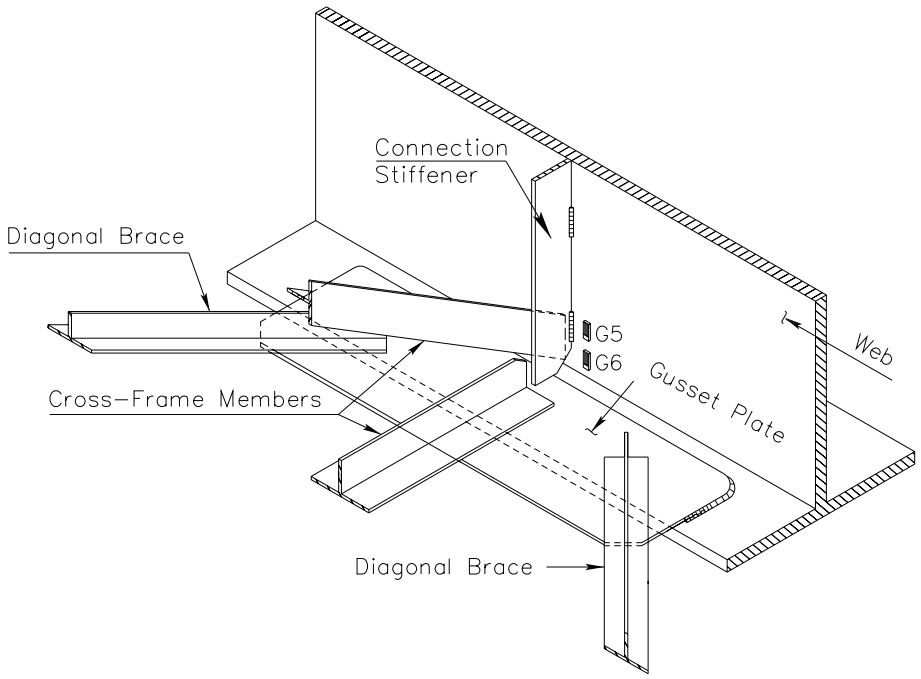

Figure 5-7 Lower Web-Gap (Diaphragm F2)

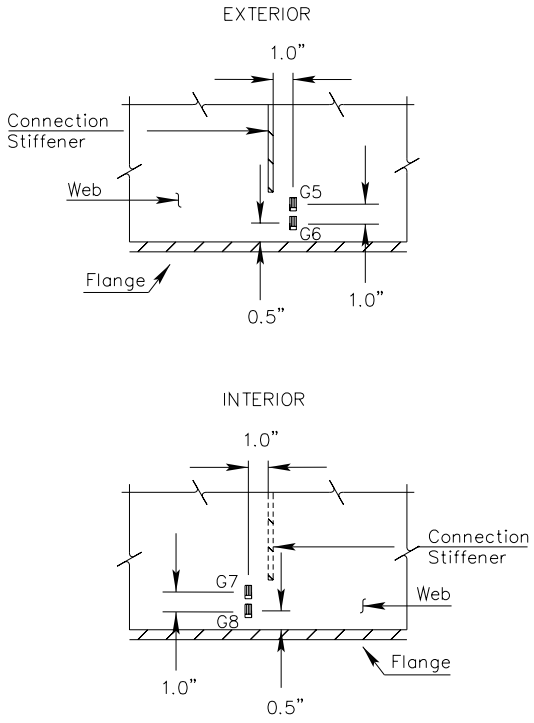

Figure 5-8 Lower Web-Gap (Interior and Exterior) (Diaphragm F2)

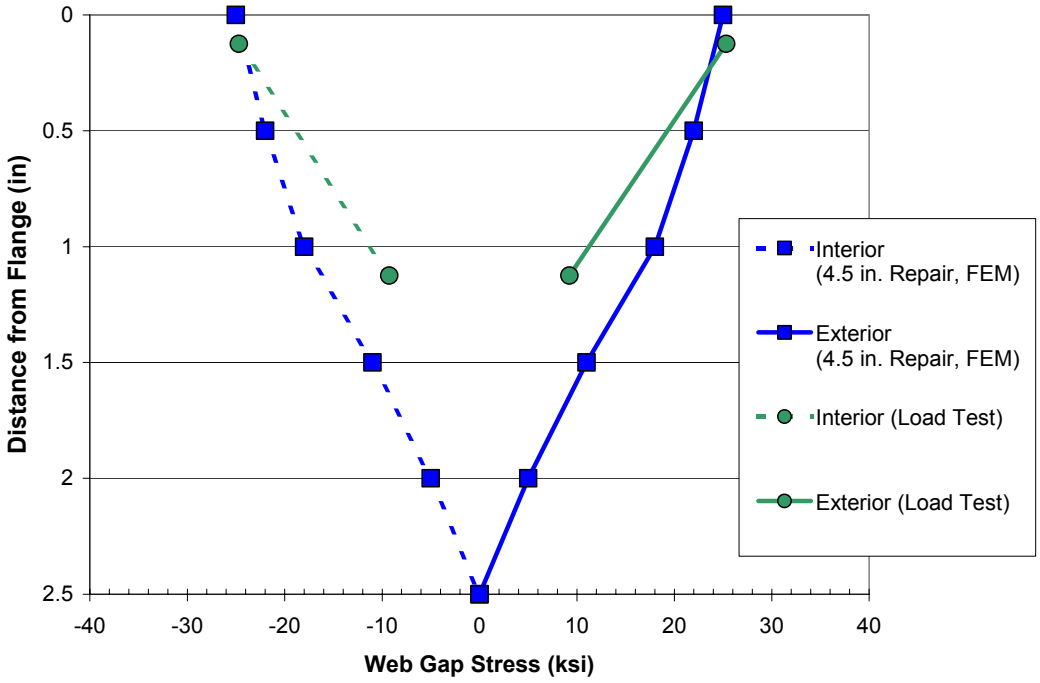

Figure 5-9 Measured vs. Theoretical Upper Web-Gap Stress

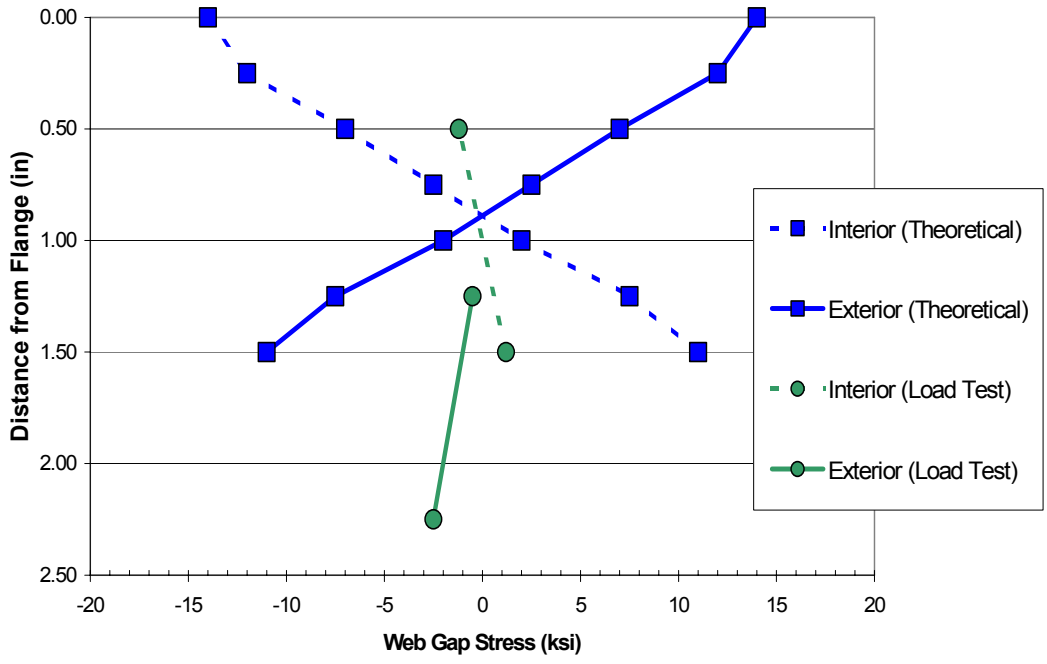

Figure 5-10 Measured vs. Theoretical Lower Web-Gap Stress

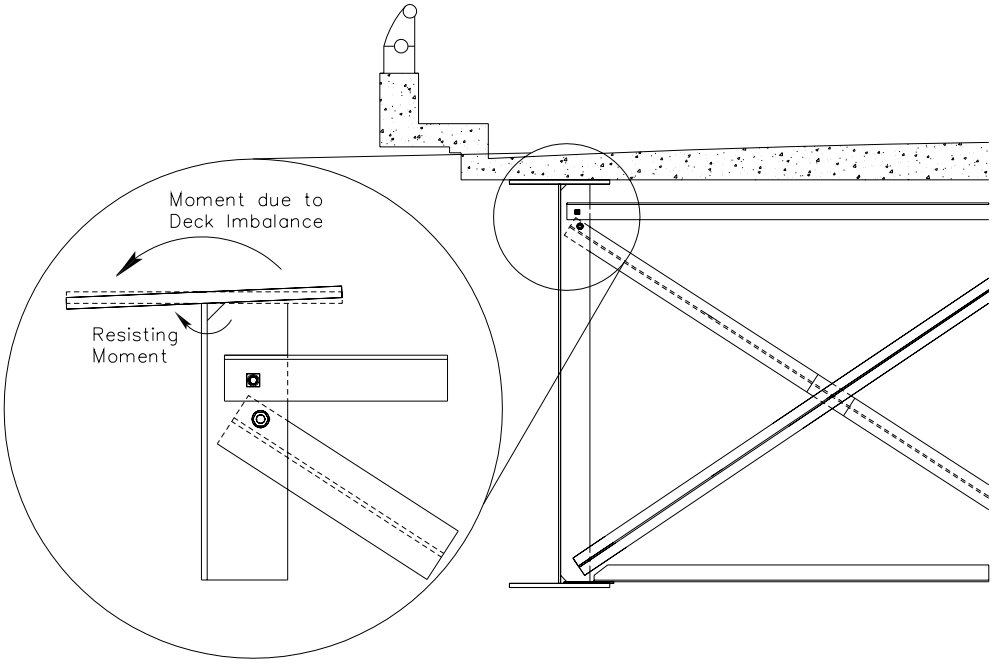

Figure 5-11 Cracking Theory (Cantilevering of the Deck)

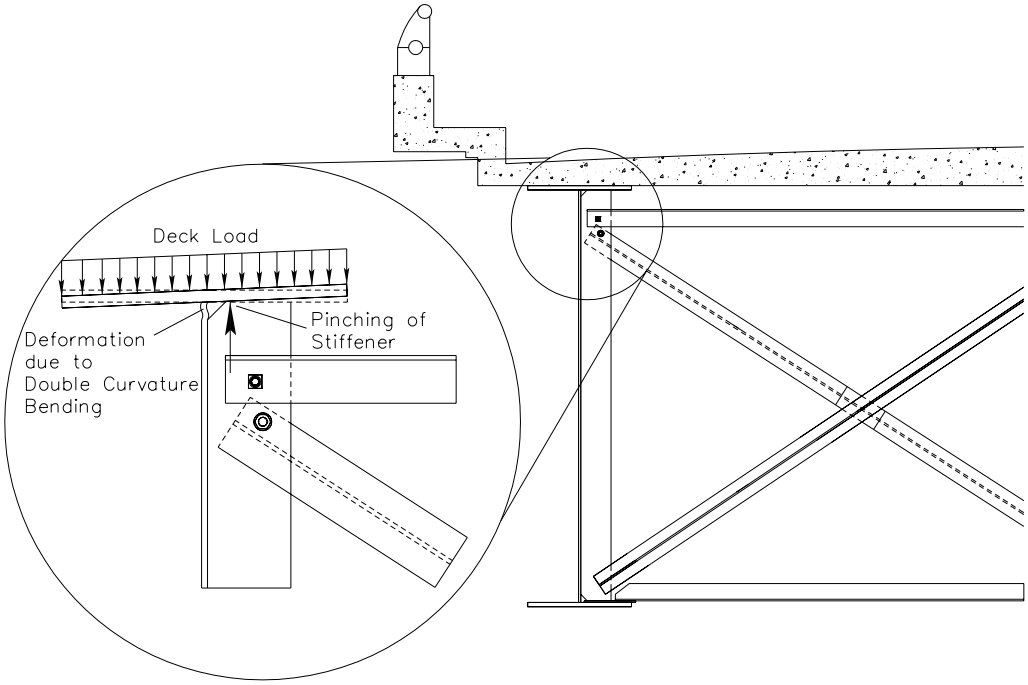

Figure 5-12 Cracking Theory (Binding of the Stiffener)

CHAPTER 6 GUSSET PLATE CRACKING

This chapter describes work performed on the gusset plate region. Both the 1986 and 2005 repairs are presented as backgrounds to the testing. The purpose of the strain rosette is explained, and its position is displayed. The gages results are presented as well as the inferences drawn them.

6.1 Repair Strategy

In 1986, repairs were made to gusset plates on the diaphragms located nearest to the piers. These diaphragms are labeled F4 in Figure 1-4. Repairs included bolting a larger gusset plate to the lower flange and eliminating all welds in the connection. The gusset repair can be found in Figure 6-1. To date, the repair has been effective with no new cracks reported.

Although the 1986 retrofit was successful, it only repaired two diaphragm locations per span. New cracks have developed at diaphragms adjacent to the repaired gusset plates. KDOT has decided to repair these diaphragms. However, economic factors have changed the repair plan from the 1986 retrofit design. Figure 6-2 displays the new proposed retrofit. In order to save money, the existing gusset plates will remain on the bridge. The gusset plates will be repaired by first grinding out existing cracked welds and then will be re-welded to the previous dimensions. In addition to welding the gusset plate, four bolts will be placed through the gusset plate and the lower flange. The bolts should prevent any uplift force on the gusset plate. The existing tack welds will also be ground off.

6.2 Gage Locations

The exact source of the gusset plate cracks was not certain during retrofit design. The cracking of the gusset plate welds could have been due to distortion-based stress from the bracing or by the stress induced by the bending strains of the

primary girder. In order to determine the nature of the cracking, the region with gusset plate cracking was gaged.

A rosette placed on the gusset plate, as shown in Figure 6-3, was used to measure the magnitude and direction of the forces within the plate. If the measured stresses were primarily parallel with the girder, bending of the girder would be the logical culprit for the cracking. However, if the forces were parallel with the diagonal brace attached to the plate, distortion caused by this brace would be the source of the problem.

6.3 Results

Gages placed on the gusset plate assisted in explaining the source of the weld cracking. For a vehicle traveling westbound on span 29, the gage readings indicate that the plate is being stretched to 0.5 ksi parallel and perpendicular with the girder. When the truck was eastbound on span 29, the average perpendicular stress was equal magnitude, but opposite direction, than the westbound vehicle. Maximum and minimum values for the different load cases, located in Tables 6-1 through 6-4, summarize these findings.

These measurements indicate that the stresses within the gusset plate are not solely from bending forces of the girder. As the truck passes over the bridge, the lateral bracing is shown to apply stress to the gusset. This data supports the theory that the gusset plate cracking is caused partly by distortion of the lateral brace. If the lateral brace were pushing against the plate, then it would be deforming. This distortion would create a prying action on the gusset plate. This prying would be a logical cause of the cracking. The data refutes the theory that only bending forces of the girder are solely causing the cracking, but it does not disprove that the girder stresses are not contributing.

Since bending stresses on girder A is more in the eastbound direction, the westbound traffic is of particular interest when investigating the effects of the lateral bracing. Westbound loadings would isolate the effects of the lateral bracing better

than the eastbound loadings. After comparing the values of the two gages, the average ratio of gage 21 versus gage 22 for westbound traffic is approximately 1.0 with a vector of magnitude 0.7 ksi. This ratio corresponds to an angle of approximately 42º parallel with the girder. This angle is close to the angle of 45º of the lateral brace entering into the gusset plate. The average stress from this lateral bracing, which is detailed in Chapter 4, is approximately 0.9 ksi, which is comparable to the stress vector found in the gusset plate.

Information gathered from the inspection reports also supports the theory that the lateral bracing is inducing crack initiation. The observed cracking patterns indicate that the cracks are not load-induced from the girders. The diaphragm locations with cracks are not in regions with high bending stress. Since gusset plates in regions of higher stress have not been found cracking, the theory of bending forces inducing cracking seems unlikely.

The other cracking theory mentioned previously is prying forces from the diagonal bracing. This theory appears logical since the gusset plates with cracks are found in regions of large height transition of the web. The bracing is approaching the gusset plate from an upward angle due to its other end being attached to a gusset plate at a lower elevation. When placed in compression, the bracing will push slightly upward on the gusset plate. The slight upward angle of the bracing could be causing the cracking in the gusset plate.

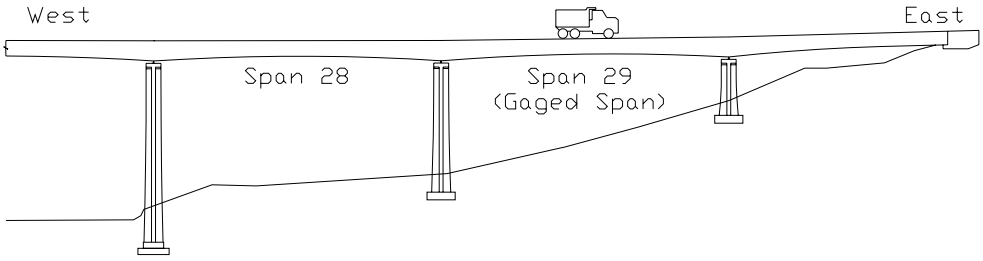

Positive Moment			Gage Number 21	22
Eastbound	65 mph	A	-0.5	0.9
		B	-0.5	1.0
	45 mph	A	-0.5	1.1
		B	-0.3	1.0
	25 mph	A	-0.6	0.9
		B	-0.4	1.1
	5 mph	A	-0.6	1.2
		B	-0.6	1.3
Average Stress (ksi)			**-0.5**	**1.1**

Gage 21
Perpendicular with Girder
Gage 22
Parallel with Girder

See Figure 6-3 for location of Gages 21-22.

Table 6-1 Gusset Plate Stresses (E29)

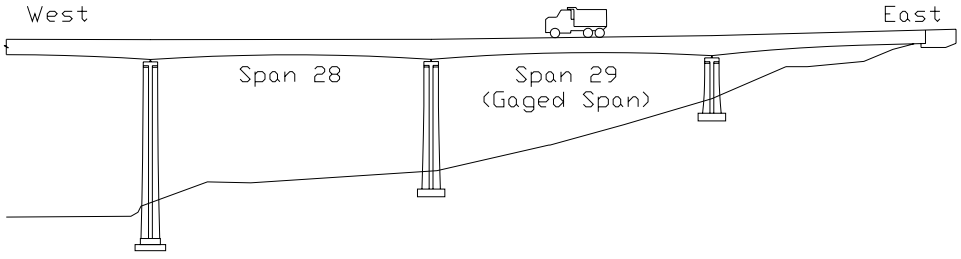

Positive Moment			Gage Number 21	22
Westbound	65 mph	A	0.8	0.7
		B	0.8	0.9
	45 mph	A	0.3	0.4
		B	0.3	0.4
	25 mph	A	0.4	0.4
		B	0.6	0.6
	5 mph	A	0.5	0.4
		B	0.5	0.4
Average Stress (ksi)			**0.5**	**0.5**

Table 6-2 Gusset Plate Stresses (W29)

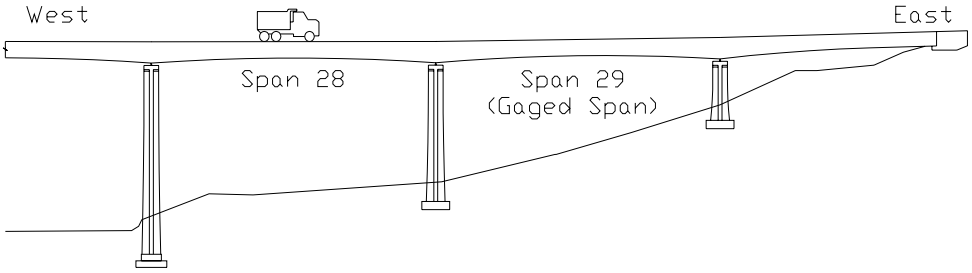

			Gage Number 21	22
Negative Moment				
Eastbound	65 mph	A	0.7	-0.6
		B	0.7	-1.0
	45 mph	A	0.7	-0.6
		B	0.6	-0.5
	25 mph	A	0.3	-0.9
		B	0.6	-0.5
	5 mph	A	0.7	-0.7
		B	0.7	-0.7
Average Stress (ksi)			**0.6**	**-0.7**

Table 6-3 Gusset Plate Stresses (E28)

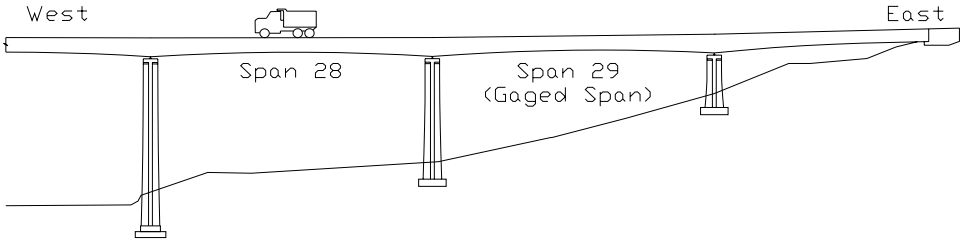

			Gage Number 21	22
Negative Moment				
Westbound	65 mph	A	-0.1	-0.3
		B	-0.3	-0.3
	45 mph	A	-0.7	-0.8
		B	-0.4	-0.5
	25 mph	A	-0.4	-0.5
		B	-0.3	-0.4
	5 mph	A	-0.5	-0.7
		B	-0.5	-0.7
Average Stress (ksi)			**-0.4**	**-0.5**

Table 6-4 Gusset Plate Stresses (W28)

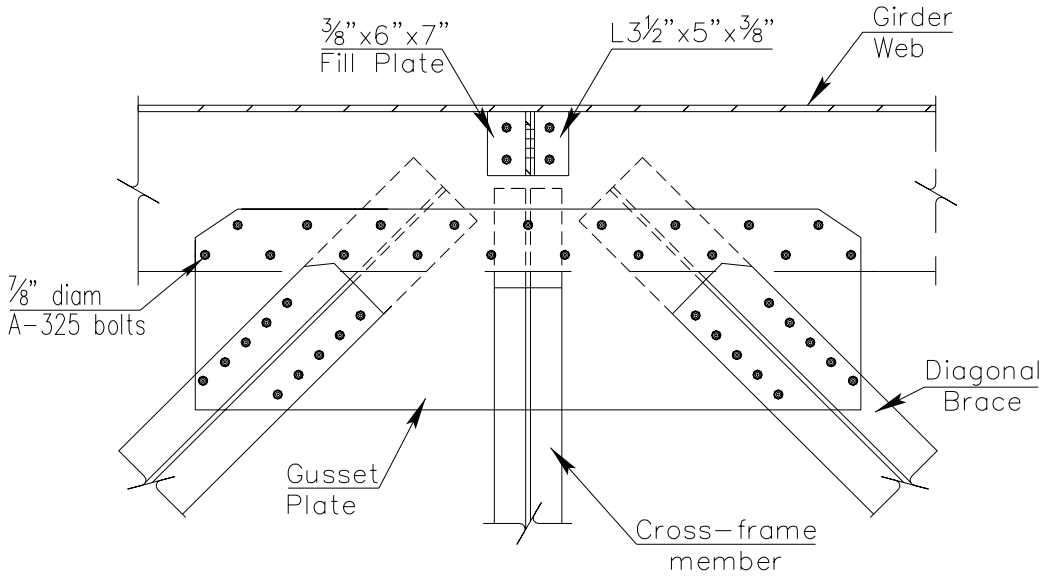

Figure 6-1 1986 Repair of Gusset Plate

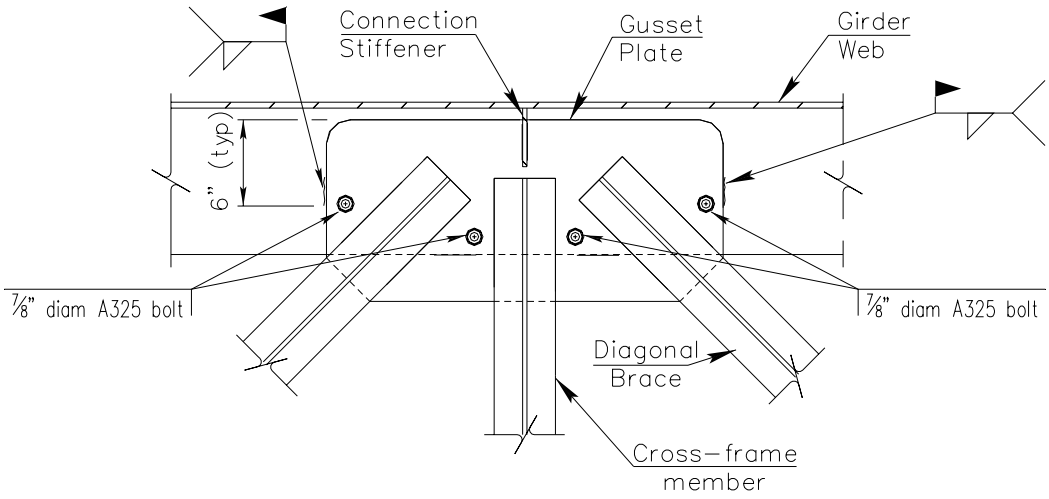

Figure 6-2 2005 Repair of Gusset Plate

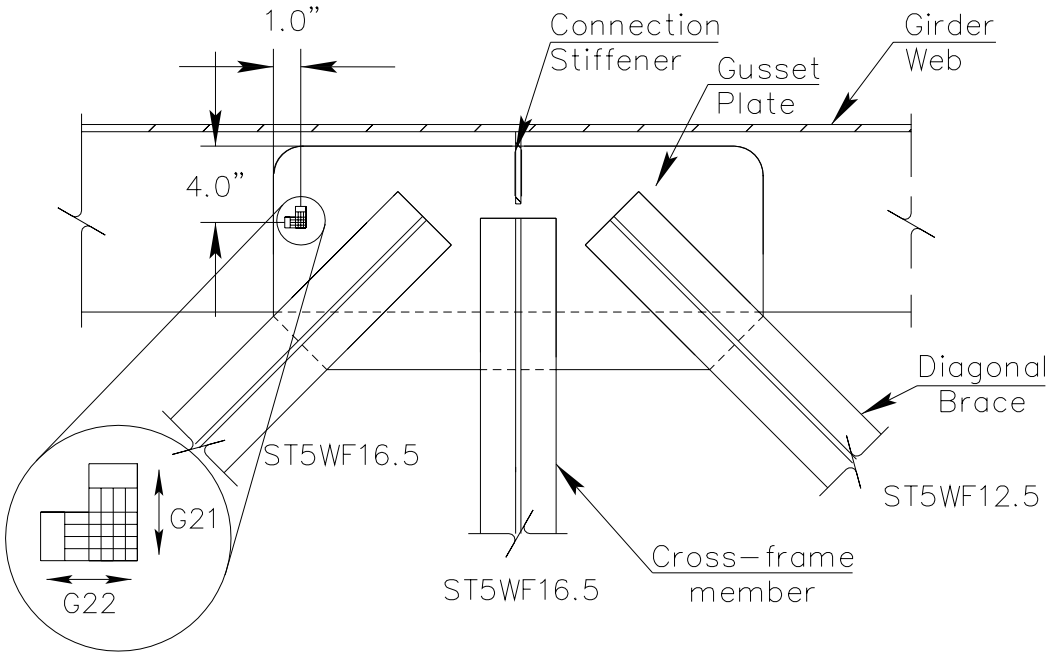

Figure 6-3 Gusset Plate Rosette (Diaphragm F3)

CHAPTER 7 LONGITUDINAL STIFFENER CRACKING

This chapter describes work performed on the longitudinal stiffeners. Repairs will be performed to reduce the potential for fatigue damage of the connection. Details of the 2005 repairs are presented. A gage was used to test the stresses at the end of a longitudinal stiffener. The purpose of the strain gage is explained, and its position is displayed. The gage results are presented and will be compared with the data collected after the retrofit is performed.

7.1 Repair Strategy

Two repairs are scheduled for the longitudinal stiffeners. The first repair, re-welding the cracks in the butt welds of the stiffener, is required to fix an existing problem. The other repair, tapering the end of the stiffener, is a preventive measure. For the cracks in the butt welds, the welds will be ground off and re-welded. Although not displaying any fatigue cracking, the termination of the longitudinal stiffener will also be retrofitted since it is a fatigue-prone detail. The repair is a preventive measure to reduce the fatigue category of the design from an E. The ends will be tapered to reduce the stress concentration at the ends, as shown in Figure 7-1. This repair strategy is similar to the tapering of the end of a cover plate welded to a flange. Stress induced by girder bending should gradually enter into the longitudinal stiffener, rather than abruptly at the end.

7.2 Gage Location

One, single-element gage was used to provide a prior-to-retrofit measurement. Only the tapering repair was investigated, since the butt weld repair was not a new structural configuration. The gage was placed close to the end of the lower longitudinal stiffener, as shown in Figure 7-2. The very tip of the stiffener, in theory, should have the highest stress. The gage, however, could not be placed directly on the tip, therefore the stresses may be higher than those measured. Nevertheless, its

values can be used to compare with post-retrofit values and help determine the effectiveness of the repair.

7.3 Results

Results from the various loadings can be found in Tables 7-1 through 7-4. For the eastbound truck, the average stress cycle was 4.6 ksi, while the westbound truck created a 3.4 ksi cycle. Since the cycle entered into the tensile region, this detail is particularly vulnerable to fatigue. Residual stresses could make this tensile cycle even more damaging. This stress value will be good to compare with the post-retrofit stresses to see the effectiveness of the repair.

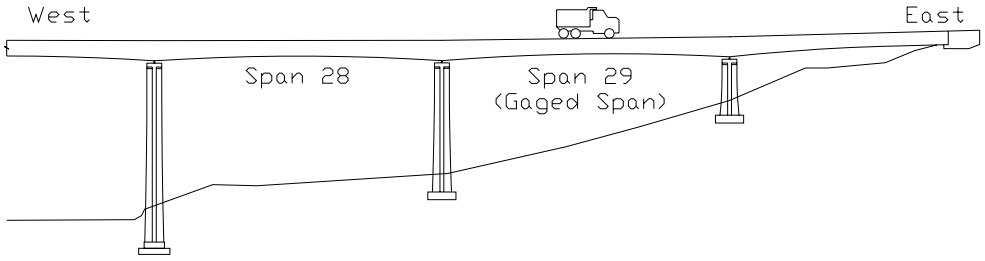

			Gage Number
	Positive Moment		23
Eastbound	65 mph	A	4.5
		B	4.7
	45 mph	A	4.9
		B	4.6
	25 mph	A	4.0
		B	4.3
	5 mph	A	4.7
		B	5.3
Average Stress (ksi)			**4.6**

See Figure 7-2 for location of Gage 23.

Table 7-1 Longitudinal Stiffener Stresses (E29)

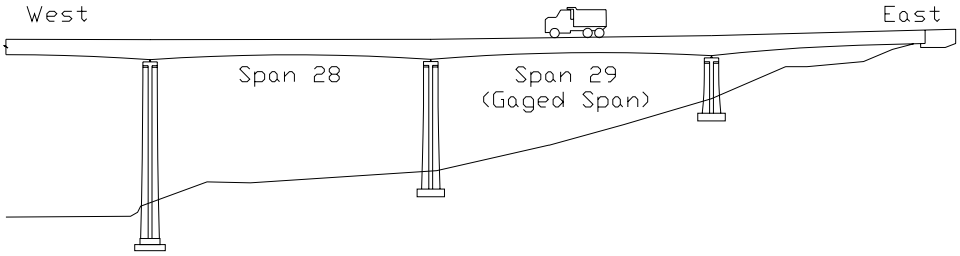

			Gage Number
	Positive Moment		Gage 23
Westbound	65 mph	A	4.1
		B	4.1
	45 mph	A	3.0
		B	2.9
	25 mph	A	3.4
		B	3.3
	5 mph	A	3.4
		B	3.4
Average Stress (ksi)			**3.4**

Table 7-2 Longitudinal Stiffener Stresses (W29)

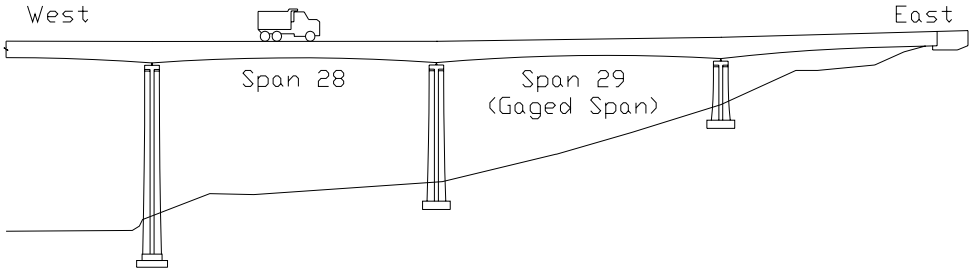

			Gage Number
Negative Moment			23
Eastbound	65 mph	A	-1.5
		B	-2.5
	45 mph	A	-1.9
		B	-1.3
	25 mph	A	-2.4
		B	-1.5
	5 mph	A	-1.9
		B	-1.5
Average Stress (ksi)			**-1.8**

Table 7-3 Longitudinal Stiffener Stresses (E28)

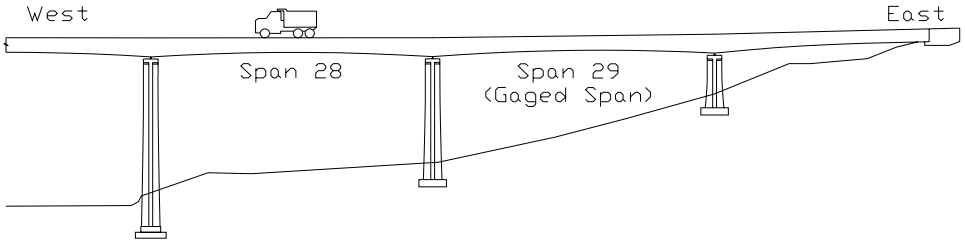

			Gage Number
Negative Moment			Gage 23
Westbound	65 mph	A	-1.2
		B	-1.5
	45 mph	A	-2.6
		B	-1.6
	25 mph	A	-1.8
		B	-1.5
	5 mph	A	-2.1
		B	-1.9
Average Stress (ksi)			**-1.8**

Table 7-4 Longitudinal Stiffener Stresses (W28)

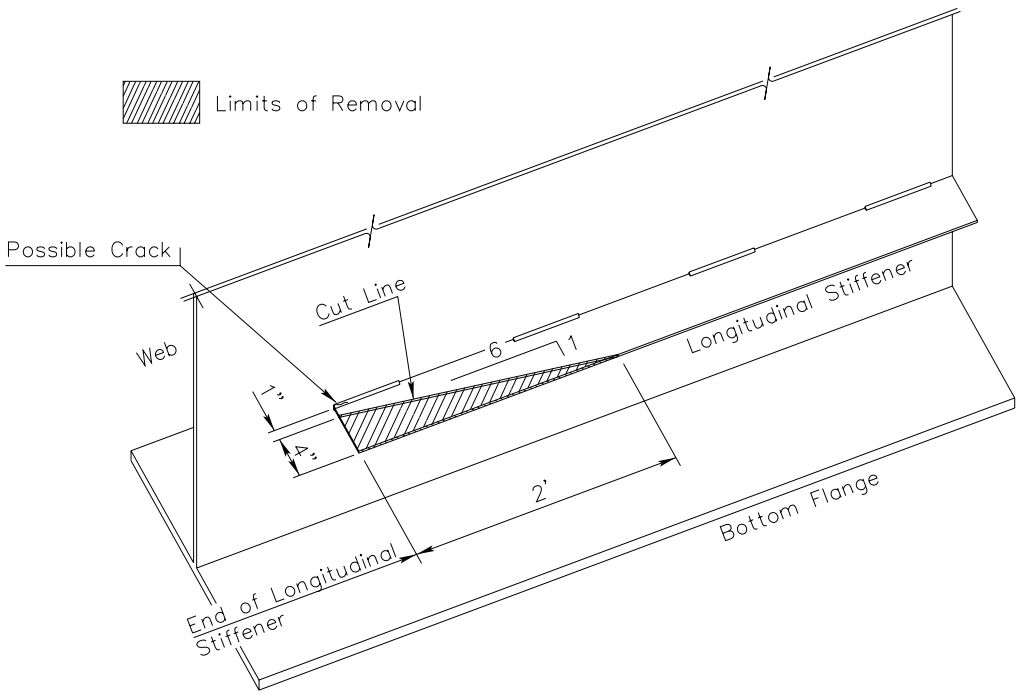

Figure 7-1 2005 Longitudinal Stiffener Repair

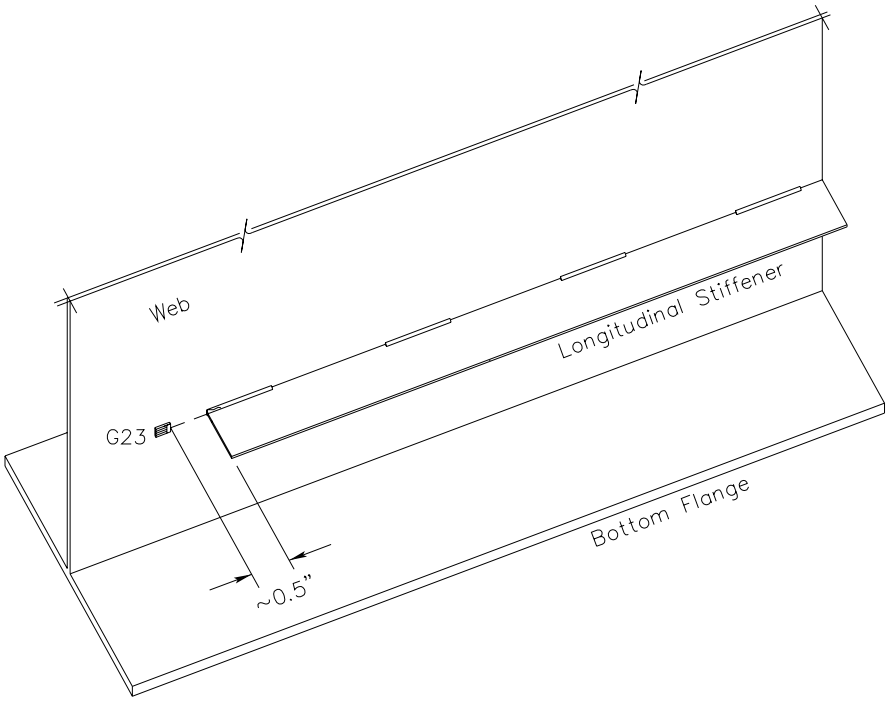

Figure 7-2 Longitudinal Stiffener Gage (Span 29)

CHAPTER 8 CONCLUSIONS

Testing of the Tuttle Creek Bridge has been performed successfully. Twenty-three strain gages were used to obtain data from 16 truck loadings. The web-gap, gusset plate, and longitudinal stiffener regions were all investigated to understand better the stresses within the bridge. Data acquired from the test should aid in the evaluation of the retrofits to be completed. Although the data acquired will be best utilized after the second load test is conducted, the following conclusions can be inferred from the measurements taken.

1. Comparison of the upper web-gap data with the finite element models of Zhao shows that the acquired data is in good agreement with the model. The upper web-gap stresses were slightly less than those theoretically calculated. This agreement adds validity to both methods of stress evaluation.

2. Stresses in the lower web-gap were much less than those predicted in the model. The measurements indicated that this portion of the model is conservative. Initiation of cracks appears unlikely in this region, particularly after the retrofit. Although the repair's purpose is to stiffen the entire structural system, the retrofit also should reduce stresses within the lower web-gap.

3. The field measurements taken in the gusset plate region suggest a source of the fatigue cracking. Although the cyclic loadings of the girders may create additional fatigue loading on the weld, the primary source of the gusset plate cracks is believed to be from cyclic loading of the lateral braces. Stresses measured on the gusset plate indicate perpendicular load cycling. The inspection reports indicate that the majority of the cracks are located in lower stress regions within the girder, which would indicate that the bending stresses are not creating the cracks. Cyclic loading of the lateral braces is believed to be the source of the gusset plate cracks.

4. The degree of composite action was also measured for the Tuttle Creek Bridge. Strain gage results of the upper and lower flanges of the symmetric girder indicated higher strains in the lower flange than the upper flange. Thus as expected, the girders exhibited partial composite action. The increased moment of inertia due to this partial composite action was found to be approximately 65 percent. This increase in flexural strength would not be expected near failure, since the interlocking of the deck and the girder would eventually breakdown. Fatigue calculations, however, should include this strength increase. Web-gap distortion is a function of differential deflection of the girders. If the girders do not deflect as much as expected due to unintended composite action, fatigue calculations may be unnecessarily high.

REFERENCES

AASHTO LRFD, 2004

LRFD Bridge Design Specifications, 3rd Edition. LRFDUS-3 or LRFDSI- 3, American Association of State Highway and Transportation Officials, Washington, D.C.

AASHTO, 2002.

Standard Specifications for Highway Bridges, 17th Edition, HB-17, American Association of State Highway and Transportation Officials, Washington, DC.

AASHTO, 1990.

Guide Specifications for Fatigue Evaluation of Existing Steel Bridges, 1st Edition, GSFEB-1, American Association of State Highway and Transportation Officials, Washington, DC.

AASHTO, 1989.

Fatigue Design of Steel Bridges, 1st Edition, GPEB-1, American Association of State Highway and Transportation Officials, Washington, DC.

AASHTO, 1989.

Guide Specifications for Strength Evaluation of Existing Steel and Concrete Bridges, 1st Edition, GSEC-1, American Association of State Highway and Transportation Officials, Washington, DC.

Barsom and Rolfe, 1999

John M. Barsom and Stanley T. Rolfe. Fracture and Fatigue Control in Structures: Applications of Fracture Mechanics, 3rd Edition. ASTM, West Conshohocken, Pennsylvania.

Fisher et al., 1980

J.W. Fisher, B.M. Barthelemy, D.R. Mertz, and J.A. Edinger. "Fatigue Behavior of Full-Scale Welded Bridge Attachments". Transportation Research Board 227, Transportation Research Board, National Research Council, Washington, D.C.

Foster and Oehler, 1954

George M. Foster and LeRoy T. Oehler. "Vibration and Deflection of Rolled Beam and Plate Girder Type Bridges" Highway Research Board. Research Laboratory Testing and Research Division. No. 219

IOtech, Inc., 1997

IOtech, Inc. Wave Book User's Manual, Cleveland, Ohio.

Jajich, D. and A.E. Schultz, 2003

D. Jajich and A.E. Schultz. **"**Measurement and Analysis of Distortion-Induced Fatigue in Multigirder Steel Bridges", Journal of Bridge Engineering, Vol 8, No. 2, pp. 84-91. ASCE, Reston, Virginia

Jáuregui, et al., 2002

D. V. Jáuregui, J. A. Yura, K. H. Frank, and S. L. Wood. "Field Evaluation of Decommissioned Noncomposite Steel Girder Bridge", Journal of Bridge Engineering, Vol 7, No. 1, pp. 39-48. ASCE, Reston, Virginia.

Kansas Department of Transportation, 2000

Fracture Critical Inspection: Special Bridge Inspection Report, Bridge No. 16-81-2.24 (017). Aug 28, 2000.

Kansas Department of Transportation, 2002

Fracture Critical Inspection: Special Bridge Inspection Report, Bridge No. 16-81-2.24 (017). September 9, 2002.

Stallings, et al., 1993

J. Michael Stallings, Thomas E. Cousins, and Scott K. Rutland. "Evaluation of Fatigue Cracking in I-65 Mobile Delta Crossing Bridges, Volume III: Floortruss-Girder Connections." Highway Research Center, Harbert Engineering Center, Auburn University, Alabama.

Vishay Micro Measurements, Inc., 2000

Vishay Micro Measurements Group, Inc. (2000). Products and Technical Binder, Raleigh, North Carolina.

Wipf, et al. ,1998

T.J. Wipf, L.F. Greimann, A.H. Khalil, and D. Wood. Preventing Cracking at the Diaphragm/ Plate Girder Connections in Steel Bridges. Iowa State University, Ames, Iowa.

Zhao and DeWolf, 2002

Jun Zhao and John T. Dewolf. "Dynamic Monitoring of Steel Girder Highway Bridge", Journal of Bridge Engineering, Vol 7, No. 6, pp. 350-356. ASCE, Reston, Virginia

Zhao and Roddis, 2003

Yuan Zhao and W. M. Kim Roddis. "Fatigue Prone Steel Bridge Details: Investigation and Recommended Repairs", Report No. KTRAN: KU-99-2, Kansas Department of Transportation, Topeka, Kansas.

APPENDIX A PREVIOUS RESEARCH

A.1 Web-Gap Cracking

Web-gap cracking research has been abundant due to the large number of steel bridges affected by this type of fatigue. Research has focused on causes of cracking and retrofit measures used to prevent further fatigue crack initiation and growth. Many of the retrofit designs have been tested in full-scale field tests. Field-testing provides engineers with data to better understand the in-service behavior of a structure before and after a retrofit. For this report, the analysis of web-gap research will focus on the use of full-scale load tests to study this distortion-based fatigue cracking.

A.1.1 Stallings, et al (1993)

Stallings, et al performed a field evaluation of retrofits designed to prevent web-gap cracking. The purpose of the study was to test the effectiveness of two different repairs by comparing stress values to the original condition.

The I-65 Mobile Delta Crossing Bridges had developed similar cracking patterns as the ones found in the Tuttle Creek Bridge. These bridges are floor-truss systems with non-composite decks. Horseshoe cracks were found in the connection of the web stiffener to the truss gusset plate. The cracks were found only in the weld material. A "softening" repair strategy was undertaken to lower crack-propagating stresses. The retrofit investigated was to lengthen the web-gap by cutting a slot in the web stiffener. Two different slot lengths, 6 and 10 inches, were tested.

In-service load tests were conducted to measure the stress differences due to the retrofit. A total of 110 instruments, including strain gages and displacement transducers, were used to investigate the bridge. Strain gages were used to investigate the vertical stress in the web-gap. Extrapolation of inline gages located in the web-gap estimated the peak vertical stress. Gages were also placed horizontally along the length of the web stiffener to measure the stress distribution into the web.

Diaphragm braces were gaged to relate bracing stress with web-gap stresses. Displacement transducers measured the translation of the girder due to diaphragm distortion.

Testing consisted of loading a span with both pre-weighed trucks and ambient truck traffic. The pre-weighed vehicles consisted of a 3-axle dump truck and a 5-axle lowboy. The tests consisted of static loadings, crawling speed runs, and normal highway-speed passes. For the ambient traffic, the data acquisition system was setup to record only truck passes that created a stress exceeding a predetermined value in the bridge.

The load tests indicated an improvement in the bridges performance due to the retrofit. The web-gap stresses were lowered by 50 to 75 percent. The retrofit was found to extend the service life of the structure, however, it would not prevent eventual crack initiation.

A.1.2 Jajich and Schultz (2003)

Jajich and Schultz investigated the web-gap region of a multi-girder steel bridge set on a skew. The purpose of the research was to validate the assumptions used by designers to select fatigue-resistant bridge details. An engineer will often use the theoretical deflection of a girder to estimate the web-gap stresses. This study examined the relationship between the differential deflection of girders to the distortion stress in the web-gap.

Sixteen strain gages were placed on the bridge at four diaphragm locations. Seven gages were used to measure the flexural bending of the web-gap in the vertical direction. Longitudinal strains of the girders were measured at the four diaphragm locations. Gages also were used to monitor stresses at the weld toe of the diaphragm stiffener. Four string potentiometers were used to measure the differential deflection of the girders at two diaphragms.

Trucks of known weight and ambient traffic were used to load the structure. For the ambient loadings, data was recorded for only pulses of high stresses, which

could only be initiated by large vehicles. Each recording was placed into a histogram, which indicated a typical loading cycle. For the load test, two trucks weighing 50 kips each were used to load the structure. The trucks were sent over the multi-lane bridge in various configurations and speeds.

After analysis of the collected data, several conclusions were determined. Results of the potentiometers indicated that rotation of the web-gap, rather than translation, was the cause of the web-gap stress concentrations. For all four diaphragms, bottom web-gap stresses were found to be too small to initiate cracks. Upper web-gap stresses, however, were found to be very high, with some web-gap stresses being up to twenty times larger than the flange stresses. The connection of the stiffener to the girder web has been tested to be a category C detail. By using the AASHTO fatigue life (S-N) curve and the average stress cycle magnitude, the number of cycles until failure was calculated. By using data from the stress cycle histogram, the fatigue life of the bridge was determined to be approximately 45-76 years.

A.1.3 Wipf et al. (1998)

Wipf et al. investigated diaphragm/ plate girder connections of five bridges in Iowa. The bridges were experiencing web-gap fatigue problems due to lack of attachment of the connection plate to the upper flange. Stop holes had been drilled, but were not effectively ceasing propagation. In an attempt to shortcut the high costs of attaching the connection plate to the upper flange, Iowa DOT proposed simply loosening the connections of the diaphragm to the girder. The retrofit would hopefully reduce the stresses within the web-gap at a reasonable price. Wipf et al performed load tests to investigate the viability of this retrofit.

Load testing was performed on several bridges, including X and K-type diaphragms. The bridges were instrumented with strain gages and displacement transducers before and after the retrofits. Rear tandem axle trucks weighing 50 kips were used to load the structures. Strain gages were placed vertically within the web

gap region to extrapolate the strain at the web/flange fillet weld. Gages were also placed on bracing to quantify the load placed on the connection plate. The displacement transducers measured the out-of-plane rotation of the girder.

Results showed that stresses in gaps with stop holes exceeded stresses found in non-cracked web-gaps. These results indicated that the drilled holes were not effective in preventing additional cracking. Loosening the connections greatly reduced stresses in the diagonal bracing, which were the causes of web-gap stresses. The web-gap stresses, consequently, were reduced by at least 25%. The effects of loosening the connections on the lateral distribution of forces were estimated to be within 10-15% of pre-retrofit conditions. For this experiment, load testing was successful in investigating the effectiveness of retrofits for steel bridges with fatigue damage.

A.2 Gusset Plate Cracking

No research was found for the monitoring of gusset plate cracks in-service. This lack of research may be due to gusset plate cracking not being as common in steel bridges as compared to web-gap cracking. Although less common, gusset plate cracking is just as critical as web-gap cracking, particularly if the weld cracks propagate into the tension flange. Although no in-service tests have been reported, gusset plate cracking has been performed in the lab. An example of gusset plate research is presented below.

A.2.1 Fisher et al. (1980)

Fisher et al. investigated the fatigue behavior of several gusset plate configurations. Gusset plates, which attach lateral bracing to the girders, were fatigued in a lab simulation. One of the plate configuration tested by Fisher is similar to those found on the Tuttle Creek Bridge. Since the configuration is similar, gusset plates tested that were transversely welded to the girder flange are highlighted in this summary.

Testing consisted of loading a rolled beam using hydraulic pulsators. The lateral attachments extended from the loaded girder to a stationary beam. A sinusoidal load was placed on the beam until gusset cracking was evident. The beam's lower flange was loaded under various tensile, stress cycles. After cracking of the gusset plate, different types of retrofits were used to repair the crack. Repair types included remelting the weld toe using a gas tungsten arc process, peening, drilling only holes at the crack tips, and placing high strength bolts within the drilled holes.

All gusset plate configurations were found to equal or exceed the fatigue resistance of a Category E detail. Although retrofitting of shallow cracks significantly improved fatigue life, retrofitting deeper cracks was shown to be ineffective. Tests indicated that the attachment of the gusset plate to the flange only with transverse welds was particularly fatigue prone. For the transversely welded gusset plate, fatigue cracks initiated at the ends of the fillet weld. Fatigue cracks severed the gusset plate attachment at a fatigue life less than Category E. In one case, cracking propagated into the tension flange. Fisher et al. recommended that gusset plates with only transverse welds not be used.

A.3 Composite Action

Field-testing of composite action has been common for fitness-for-service evaluations. Bridges may have much more capacity than previous known due to unexpected composite action. Load tests can be used to measure the degree of composite action and assist engineers in making critical decisions on a structure. An example of composite action testing is summarized below.

A.3.1 Jauregui et al. (2002)

Jauregui et al. investigated a non-composite, multi-girder steel bridge that had been taken out of commission. Their research focused on the interaction of the bridge deck with the steel girders. Although the assumption of no interaction between the

deck and the steel girders is conservative, additional capacity can be added to a structure if the degree of partial composite action can be determined. A load test was performed to measure this composite action.

Since the structure was being removed, the bridge was loaded until yielding of the girders occurred. In order to yield the structure with minimal amounts of weight, a pier bent was removed from the structure. Two forms of loading were used: placement of concrete traffic barriers on the bridge shoulder and a flatbed tractor-trailer with barriers as payload. At midspan, strain gages were placed longitudinally on the web at mid-height, on the underside of the upper flange, and on the top of the lower flange. The strains indicated the neutral axis height, and thus the degree of composite action.

Partial composite action was measured for all girders. When compared to interior girders, exterior girders demonstrated higher degrees of interaction due compressive area from the concrete curbing. Results also showed that the girders were slightly inelastic prior to yielding due to deterioration of the partial composite action. The partial composite action, which increased the moment of inertia, caused the actual yielding of the structure to occur at 7% higher load than anticipated. In conclusion, the girders were shown to act partially composite due to the friction and mechanical interlock between the bridge deck and the upper flange.

A.4 Vibrations

Testing of dynamic properties has been used to diagnose bridge structural problems. A dramatic change in the structural system will alter the dynamic properties, which can be measured by monitoring systems. Dynamic testing can be used to continuously monitor a structure.

A.4.1 Zhao and DeWolf (2002)

Zhao and DeWolf studied the changes in natural frequencies and mode shapes of a steel bridge due to partially restrained bearings occurring in the winter. The

purpose of the experiment was to demonstrate the effectiveness of a dynamic monitoring system. Without physically altering the bridge, a change in structural behavior due to changes in temperature could be monitored.

The bridge was equipped with 16 accelerometers to measure the vibration responses at different temperatures. Eleven sets of data were collected throughout the winter period to measure the different structural responses. Rather than use vibration-inducing equipment, ambient traffic was used to load the structure. The lowest three modes, two bending and one torsional, were measured by the accelerometers.

During testing, a noticeable increase in the bridge's natural frequencies was found at lower temperatures due to the partially restrained bearings. The maximum percent difference between the natural frequencies was found to be 15.4%, which was a clear indication that the structure was behaving differently. This experiment demonstrated the effectiveness of dynamic testing in monitoring the condition of a structure.

APPENDIX B PREVIOUS KU RESEARCH

Yuan Zhao, a former University of Kansas Ph.D. student, performed extensive research on distortion-induced cracking and proposed retrofit measures. Details of her research can be found in her report, *Fatigue Prone Steel Bridge Details: Investigation and Recommended Repairs*. Her dissertation focused on the investigation of five Kansas bridges, including the Tuttle Creek Bridge. The purpose of her studies was to theoretically compare different retrofit details by determining the amount of additional fatigue life each would provide. By knowing the AASHTO category of the design detail and the estimated stress values, the fatigue life could be determined. By using finite element modeling, she was able to estimate the stresses experienced by each detail. For one of the investigated bridges, a load-test was conducted to determine the accuracy of her models. This investigation is also discussed.

B.1 Tuttle Creek Bridge

For the Tuttle Creek Bridge, web-gap cracking was the focus of her modeling. Her theoretical models, which were created in ANSYS, estimated the stresses produced in the web-gap region. In addition to modeling the pre-retrofit situation, models were created for the following four retrofit strategies, which are shown in Figure B-1

- Simply allowing the stiffener welds to break
- Positively connecting the stiffener to the flanges
- Cutting a 4.5 in slot into the stiffener
- Cutting a 12.5 in slot into the stiffener

B.1.1 Coarse Model

The first model produced by Zhao was used to determine the transfer path of the forces due to a HS15 truck. One, full-length span was modeled in the program, as

shown in Figure B-2. The deck was assumed to act non-compositely. The truck was moved incrementally along the length of the bridge for a total of 40 load cases. The model only included loading of the westbound lane, since the bridge was assumed to act symmetrically. For the Tuttle Creek Bridge, the effects of a westbound truck on girder A should be the same as an eastbound truck on girder B. The coarse model generated the forces imposed on the web-gap region, but did not accurately predict the stresses within the gap. A more precise model was created to determine these stresses.

B.1.2 Sub-models

After creating the coarse model, Zhao focused her analysis on both the upper and lower web-gap regions. Separate submodels for each retrofit were created. The submodels used the forces found in the coarse model to determine the stress distribution in the web-gap region. An example of one of the submodels is shown in Figure B-3. Stress values were found in the x, y and z direction for the girder web. Stresses in the x direction were found for the web stiffener. The stress values for each retrofit were compared to determine the most effective repair option.

B.1.3 Conclusions

Zhao's models concluded that the positive attachment of the stiffener to the girder flange would be the most effective retrofit option considered. The stress ranges were lowered approximately 90%. These values are well below half the CAFT of 12 ksi for a C detail. The constant amplitude fatigue threshold, CAFT, refers to the stress range in which the detail can endure 2 x 10^6 cycles. A stress range of half of the CAFT can endure infinite fatigue cycles. The other retrofit measures did have reductions in stress ranges, however their ranges were still above the CAFT threshold. Crack initiation could still occur for these retrofits.

Prior to load testing, the 4.5 in. slotted retrofit had already been cut from the tested stiffener. This retrofit had been performed in 1986. Therefore, the initial

condition for load testing was actually comparable to the 4.5 in. retrofit, rather than the original condition modeled by Zhao. Since the condition of the web-gap tested matched the 4.5 in. retrofit, only results from this repair are displayed.

Results from Zhao's models were compared with those from the load test as discussed in Chapter 5. Figure B-4 shows the vertical stress distribution for the web gap region of diaphragm F2. This diaphragm was instrumented in the initial testing to measure differences between Zhao's model and the measured stress.

B.2 Other Bridges Investigated

Zhao investigated four other Kansas bridges with fatigue cracking in addition to the Tuttle Creek Bridge. She produced finite element models for each bridge to examine the specific fatigue problems. She also theoretically tested proposed retrofit measures for each fatigue problem. Although still distortion-induced, many of the other fatigue problems did not specifically relate to the fatigue problems experienced with the Tuttle Creek Bridge. One exception is the Westgate Bridge, which is highlighted in this report due to its similarities with the Tuttle Creek Bridge. The Arkansas River Bridge, another bridge investigated by Zhao, is discussed since a similar testing strategy was performed for it.

B.2.1 Westgate Bridge

The Westgate Bridge, a two-girder, floor/truss system, had developed fatigue cracks similar to the Tuttle Creek Bridge. Distortion-induced stresses had created cracking in the upper web-gap region at diaphragm locations. Horizontal cracks in the upper flange/web fillet welds were found on both side of the primary girder. Horseshoe cracks were found emanating from the top of the web stiffeners and entering into the girder web. A cross-section of the bridge and a diagram of the cracking patterns can be found in Figure B-5 and B-6, respectively. Repair methods used by KDOT included:

- Drilling stop holes at the ends of cracks
- In positive moment regions, fillet welding the stiffener to the upper flange
- In negative moment regions, adding stiffener plates to the exterior girder side

Zhao concluded that the positive moment repair would be satisfactory, however, the negative moment repair could allow cracks to continue to propagate. In addition to adding stiffener plates, Zhao recommended that removal of truss members would be necessary to improve the fatigue resistance in the negative moment region to an acceptable range. She recommended further studies be performed to determine if truss removal would maintain lateral stability.

B.2.2 Arkansas River Bridge

The Arkansas River Bridge is a non-composite steel bridge with a girder/floor-beam/stringer load-transfer system. Distortion-induced cracking had developed at many locations on the bridge. Cracking was being induced by the rotation of the floor-beam under live load. This rotation created horizontal cracks in the web stiffener and vertical cracks in the floor-beam. KDOT requested a study of the fatigue problem in order to select a proper retrofit.

Zhao modeled the bridge and offered a retrofit solution to KDOT. Zhao also recommended a load-test be performed to compare theoretical stresses with in-service values. The University of Kansas was selected to load-test the Arkansas River Bridge.

The bridge was field tested by Kaise Haris of the University of Kansas. Haris, a graduate research assistant, investigated the structure before and after retrofit. His report, *Field Instrumentation and Analysis of the Arkansas River Bridge,* details his testing procedure and results. Haris was responsible for measuring the stress differences due to the repair by using strain gages. The measured stress values were used to predict the additional service life of the bridge. By using the stress reductions, Haris estimated an additional service life between 25-65 years.

Although the bridges' geometry was different, the investigation of the Tuttle Creek Bridge was patterned after the testing of the Arkansas River Bridge. For both investigations, initial tests were used to determine the stress ranges prior to the retrofit. Like the Arkansas River Bridge, the Tuttle Creek Bridge will also be tested after the retrofit. After the repair of the fatigue-prone details, load testing will quantify the effectiveness of the repair.

Despite having many similarities, the goals for testing the Tuttle Creek Bridge were not completely identical with the Arkansas River Bridge. Unlike the Arkansas River Bridge test, the initial test of the Tuttle Creek Bridge was also used to assist in modeling of a second finite element model. In addition to providing data for the initial condition of the bridge, data was acquired to improve upon the models created by Zhao. A blending of these goals was used to properly locate the gages in areas of interest.

The same field-testing equipment used for testing the Arkansas River Bridge was utilized in the first Tuttle Creek Bridge load test. The testing setup and procedure, as detailed in Appendix C, was similar to the one used by Haris. The field-testing experience of Haris was helpful when designing a testing strategy and during instrument installation.

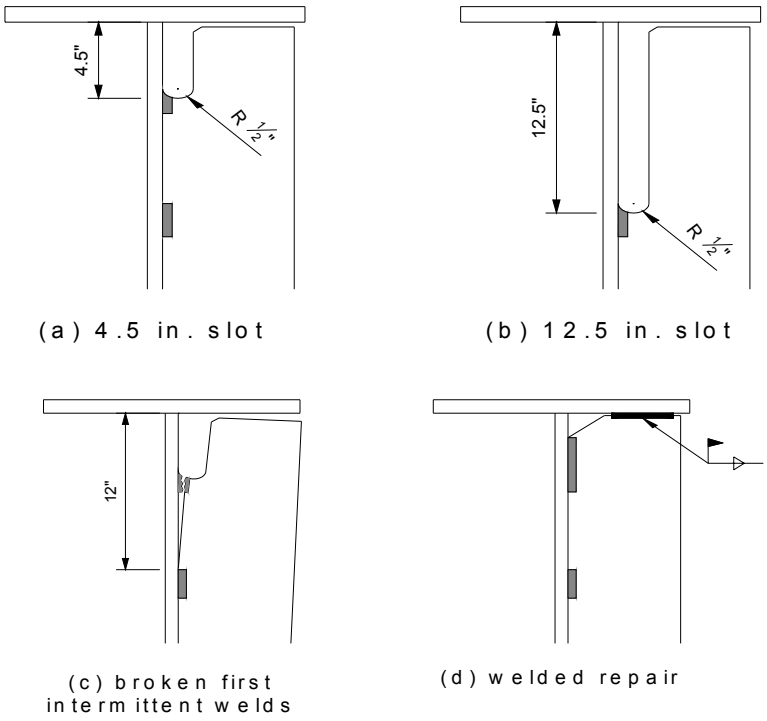

Figure B-1 Retrofits for the Tuttle Creek Bridge Modeled by Zhao

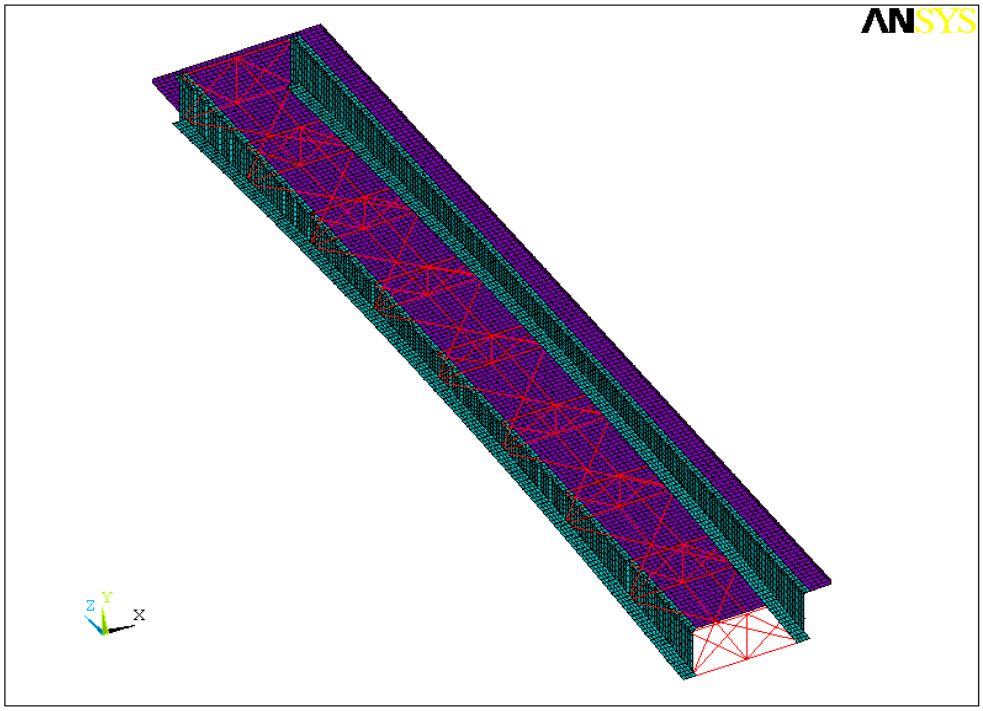

Figure B-2 Coarse Model of Typical Span

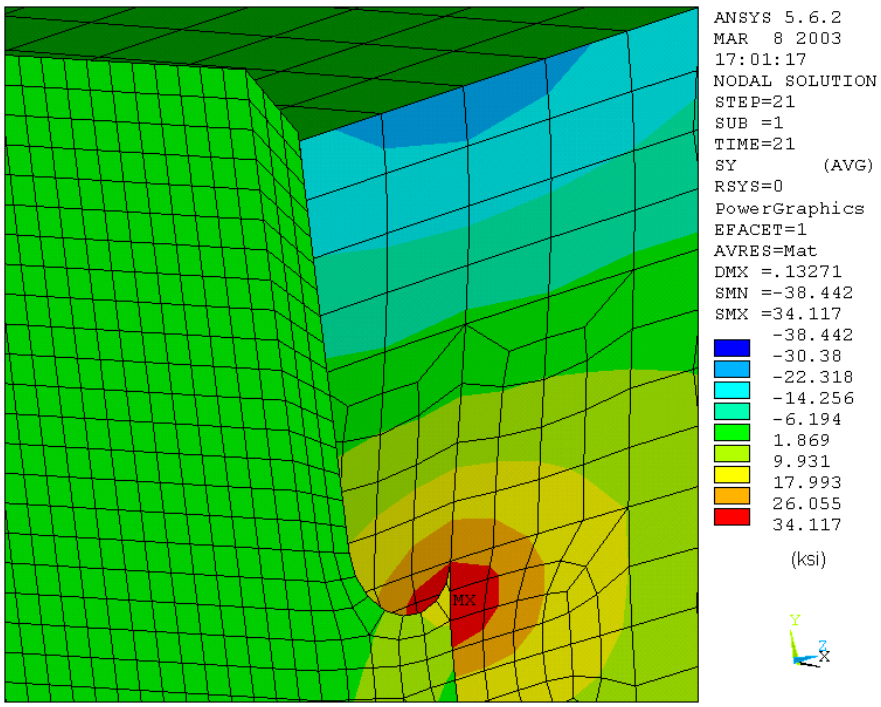

Figure B-3 Submodel of Web-Gap Region (4.5 in. Slot Repair)

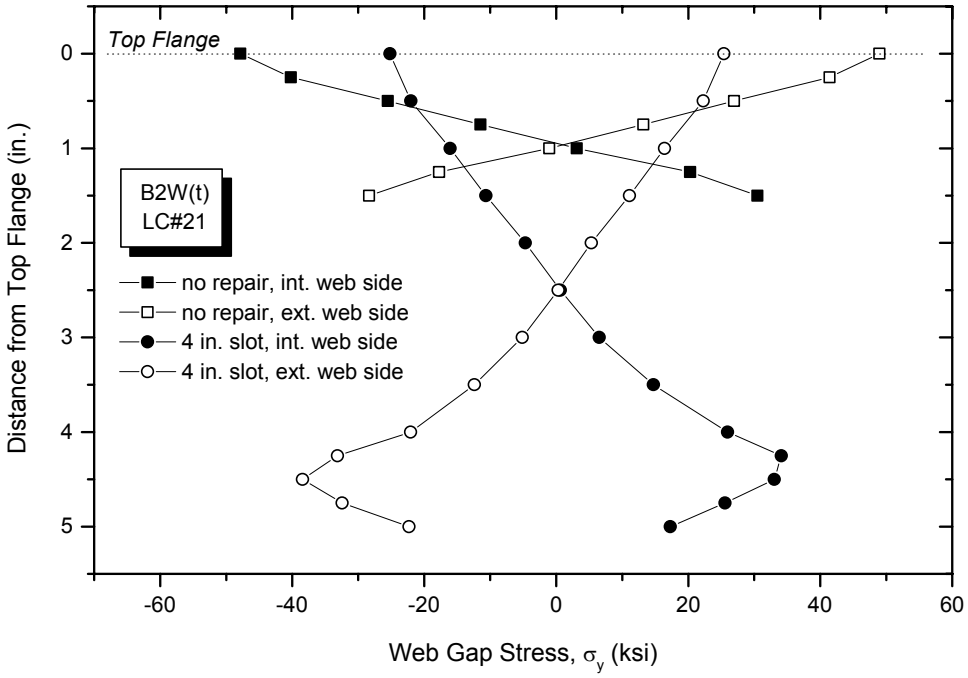

Figure B-4 Upper Web-Gap Stress Distribution (4.5 in. Slot Repair)

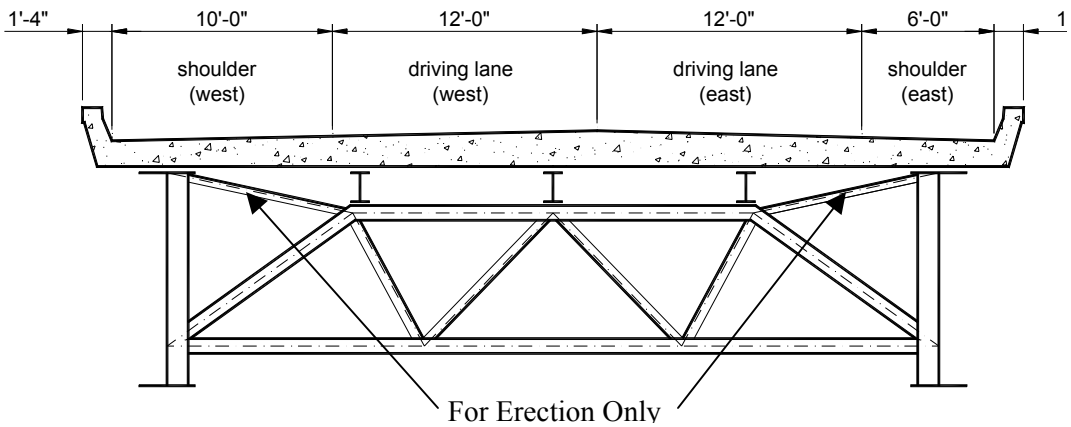

Figure B-5 Cross section of the Westgate Bridge

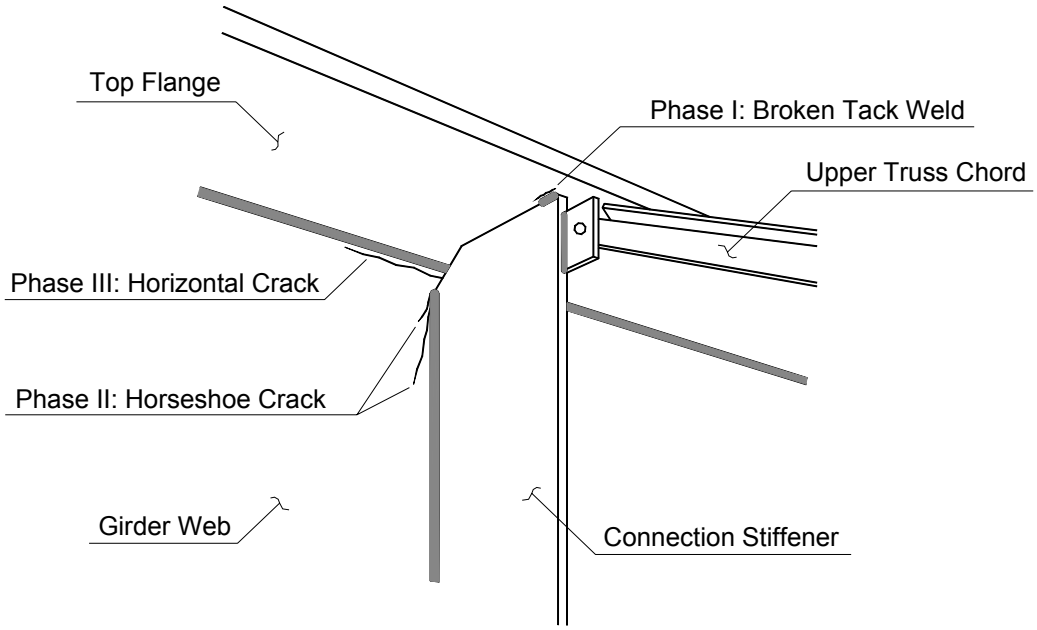

Figure B-6 Crack Growth in the Westgate Bridge

APPENDIX C INSTRUMENTATION PROCEDURE

C.1 Gage Installation

Even after utilizing time-reducing procedures, gage installation still took the majority of the instrument installation time. All the gage installation materials were placed into small boxes for easy transportation. The boxes were placed into plastic totes fastened to each of the snooper's buckets. Faster gage installation was accomplished by squeezing two individuals into one side of the bucket, while the snooper operator stood in the second bucket. Although uncomfortable, having two individuals simultaneously working made the task go much more quickly. Figure C-1 shows the snooper basket with plastic totes.

C.1.1 Gages

In addition to one, 2 element, stacked 90° rosette, twenty-one single-element gages were utilized for this test. The single element gages, designated CEA-06-250UW-350, were purchased from Micro Measurements, Inc. The 90° rosette, specified as CEA-06-250WQ-350, was also purchased from M&M, Inc. A resistance of 350±0.3% ohms, instead of 120 ohms, was chosen to reduce the amount of heat build-up of the electrical resistance gages. The gages had enlarged soldering tabs, which was essential when soldering in a windy environment.

C.1.2 Grinding

The first step in installation was the removal of the paint from the area for gaging. This task was accomplished by using a braided, wire wheel mounted on a grinder. A generator on the snooper powered all electrical equipment. Paint, rust, and grime were easily removed with the heavy-duty wire wheel. Grinding continued until the base metal was clearly visible. A patch approximately four inches long by three inches wide was created for each gage location. The ground surface appeared gray and dull. Grinding was performed for all locations prior to further surface

preparation since grinding could easily contaminate other gage locations. Dust masks and eye protection were used since the paint was lead-based. After removing the paint, each gage location was labeled on the bridge using a permanent marker.

C.1.3 Surface Preparation

In addition to grinding, additional surface preparation was required. The locations were first sprayed with degreaser and wiped clean with gauze pads. M-Prep Conditioner A was liberally sprayed on the surface. Both the conditioner and neutralizer solutions were transferred from their regular containers into window-cleaner sprayers for easy application. 320-grit sandpaper was used to smooth the surface. The surface was kept moist with the conditioner while sanding to prevent clogging of the sandpaper. After sufficient sanding, the surface was scrubbed using cotton swabs. Conditioner was continually sprayed on the surface during scrubbing. Scrubbing continued until the swabs showed no discoloration due to surface grime. Finally, the surface was wiped clean using cotton gauze pads. Care was taken to prevent wiping from outside the cleansed surface, which would bring contaminates into the conditioned environment. Sanding/ conditioning procedures were repeated using 400-grit sandpaper. M-Prep Neutralizer was then sprayed on the surface. The area was scrubbed with the cotton swabs and gauze pads using the same procedure as the conditioner. Gage alignment marks were placed on the bonding surface with a permanent marker.

C.1.4 Gage Placement

After accomplishing an adequate bonding surface, the gages were taped onto the surface using PCT-2A cellophane tape. Prior to installation, the gages were adhered to the tape in the lab. After ensuring the tape strips was aligned parallel with the gage, the gage and tape strip were placed onto a rigid, plastic sheet for easy transporting. After carefully removing the tape from the plastic sheet, the gages were positioned by lining up the gage alignment marks with the permanent marks on the bridge. After adhering the taped gage to the surface, the tape was slowly folded back

onto itself, revealing the entire gage surface. Approximately 1.5 in. of the tape was left adhered to the steel to maintain the proper alignment. Peeling the tape back was performed at a low angle relative to the steel to prevent bending the gage. The gage surface then was brushed with M-Bond 200 catalyst. The brush, which is provided with the catalyst, was wiped ten times on the bottle lip prior to application. After the small amount of catalyst was allowed to dry for one minute, M-Bond 200 adhesive was placed on the gage surface. The tape was pulled back to a shallow angle with the bonding surface. A small drop of adhesive was placed at the fold of the tape and the bonding surface, just outside the gage surface. The tape was slowly lowered into contact with the bonding surface. The adhesive was distributed over the gages by stroking the tape with a gauze pad. Firm pressure was kept on the gauze pad for one minute.

C.1.5 Soldering

After adhering a gage to the bridge, another gage was worked on while the other set up. This method allowed the gage to dry sufficiently before soldering. After the gage was sufficiently bonded to the girder, the cellophane tape was removed from the gage. The tape was peeled back directly over itself, which prevented any upward tugging on the gage. Drafting tape was placed on the metal surface next to the soldering tabs. The drafting tape prevented any short-circuiting of the gage wires. A drop of soldering flux was placed onto a cotton swab and wiped upon the soldering tabs. The shielded portion of the gage wire was duct taped next to the soldering tabs. The soldering iron was first cleaned on a damp sponge. The tip was tinned with a small amount of solder, which was specified as 0.032 in. diameter, light-duty, rosin core solder. With one hand, the exposed wires were held down to the soldering tab by a small dental pick. The other hand dabbed the soldering iron onto the tabs, leaving a small mound encasing the exposed wires. For consistency, the white/black wire was placed on the left-hand soldering tab, while the red wire was placed on the right. The two wires were then bent into an arch to prevent any short-circuiting.

Installed gages without moisture protection are shown in Figure C-2. M-Coat A Polyurethane was brushed onto the strain gage surface and on the exposed wires. The polyurethane offered moisture protection and prevented short-circuiting. M-Coat B, a rubber-based coating, was placed on the gage and exposed wire after the polyurethane had dried for 15 minutes. After the M-Coat B was allowed to dry for one minute, marine goop, a contact adhesive and sealant, was liberally placed over the entire gage.

C.2 Wire Preparation

Shielded wiring, specified by Belden Electronics as 326DFV, was purchased from Newark InOne, connected the data acquisition system to the gages. Shielded wire was used to reduce background electrical noise in the data. Also, the shielding prevented any damage to the wires by handling. The wire should be able to be reused for the post-retrofit test. A larger wire gage was used to reduce heat build-up along the length of the wire.

The wire was previously cut to length in the lab. Spade terminals were soldered onto one end of each of the wires. Two inches of the wire shielding was removed using a knife. The three wire strands were stripped 0.5 in. from the ends. The spade terminals were slipped over the exposed wire. Solder was placed on the top portion of the spade terminal, locking the exposed wire to the terminal.

The wire shielding of the other end of the wire was stripped approximately two inches. The braded wires contained within the shielded covering were each stripped 1.5 in. One individual wire was taken from the white strand and left straight. The rest of the strand was wound around the bottom of the straight wire. The entire black strand was also wound around the bottom of the single white wire in much the same fashion as the white wires. A single red wire was also left straight, while the rest of the red wires were rapped around the only straight one. The entire wire wrapping, for both the white/black wire and red wire, was bound with electrical tape. The electrical tape wrap extended from the shielded covering to approximately one

inch from the end of the single wire. The inch of exposed wire provided room for soldering. To ensure adequate protection of the wires, duct tape was wrapped around the electrical tape.

C.3 Data Acquisition System

The data acquisition system used for testing was a Waveform Data Acquisition and Analysis Module. This wavebook, shown in Figure C-3 was connected to a Dell laptop computer, which stored the data collected. The wavebook, specified as a WB516, interchanged with three WBK16/SSH modules. Waveview acquisition software interfaced with the data acquisition equipment. Three power converters were used to power the workbooks. These three modules connected to the terminal strips of each gage with a cable. The 23 terminal strips, configured in a quarter-bridge, were mounted on plywood to prevent tangling. The spade terminals simply screwed into the terminal strips, as shown in Figure C-4. The terminal strips were appropriately labeled to prevent any mix-ups.

Since the roadway was composed of two narrow lanes and small shoulders, the data acquisition system setup could not safely be setup upon the bridge deck. The testing vehicle and ambient traffic would have created a hazard for the data collector. One option would have been to place the data acquisition system at the bridge abutment. This setup would have worked adequately, but the expense of the added length of wiring created a desire for a different approach. The setup chosen was the placement of the data acquisition system upon pier 29. The large pier had more than enough room to allow an individual to collect data. A wooden table, as seen in Figure C-5, was constructed to safely hold the data acquisition system and laptop. The table clamped onto the girder flange and effectively held the data acquisition equipment. All the strain gage wires were run to this location. The wires were secured using zip ties and duct tape.

Prior to testing, all equipment was tested for accuracy and precision. By using a small beam in the lab, each channel for the data acquisition system was checked.

Strain gages were placed onto the beam. In addition to testing the data acquisition system, gaging the beam provided valuable practice for actual gage installation. After loading the beam with a known weight, the recorded strains were compared with calculated values. All channels were deemed acceptable for testing. After checking the data acquisition system, an amp meter was used to check all wiring to ensure adequate current flow.

C.4 Accelerometer Installation

Four accelerometers were placed on the structure to measure the vibrations induced by the truck. The instruments, produced by Endevco, were specified as Isotron Modal 61A-500 piezoelectric accelerometers. The accelerometers were connected to the WBK512. This wavebook was connected to the rest of the data acquisition system and utilized the same Waveview software. Plastic connectors, provided by the accelerometer manufacture, allowed easy installation of the instruments. The accelerometers simply slid into the plastic connectors. The connectors were mounted onto 3 in. x 2.25 in. sheet metal plates using silicon adhesive. The steel plates were adhered to the surface of the girder by using silicon caulking, as seen in Figure C-6.

The silicon caulking used to adhere the accelerometers was found to reduce high-frequency vibrations in lab studies. Different dampers were used under the accelerometers in an effort to reduce high frequency vibrations. Each accelerometer was mounted on the same beam used to test the strain gages. Free vibration was induced in the beam, and the accelerations were recorded. The frequency of the vibrating beam was measured by the accelerometers and was compared with the theoretical natural frequency. All accelerometers were shown to have comparable accelerations and frequencies. The instruments were deemed acceptable for testing.

Figure C-1 Snooper Basket

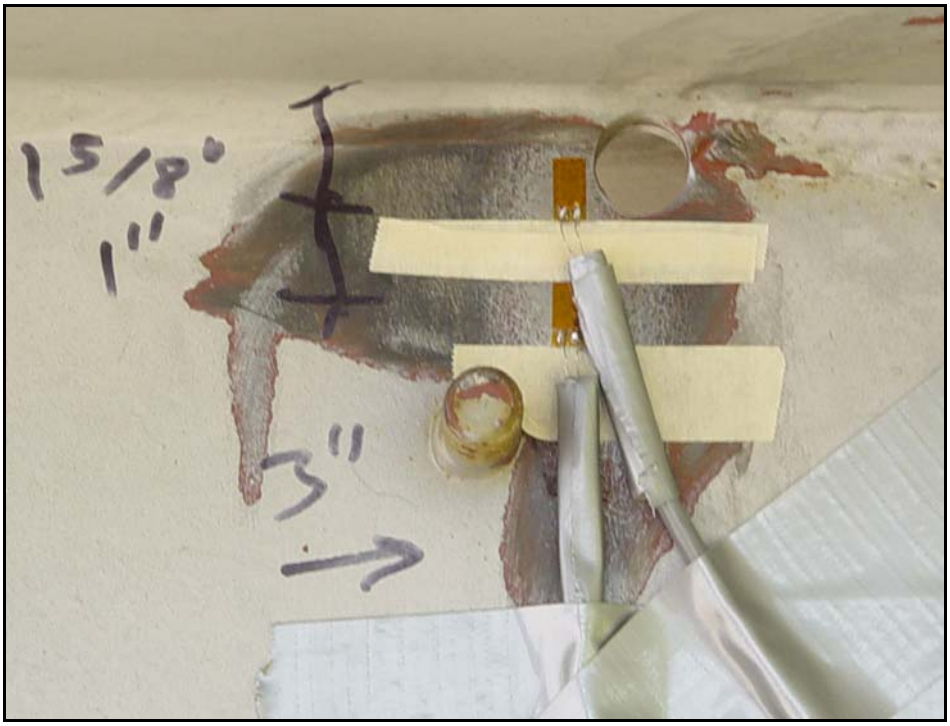

Figure C-2 Installed Gage (Prior to Environmental Protection)

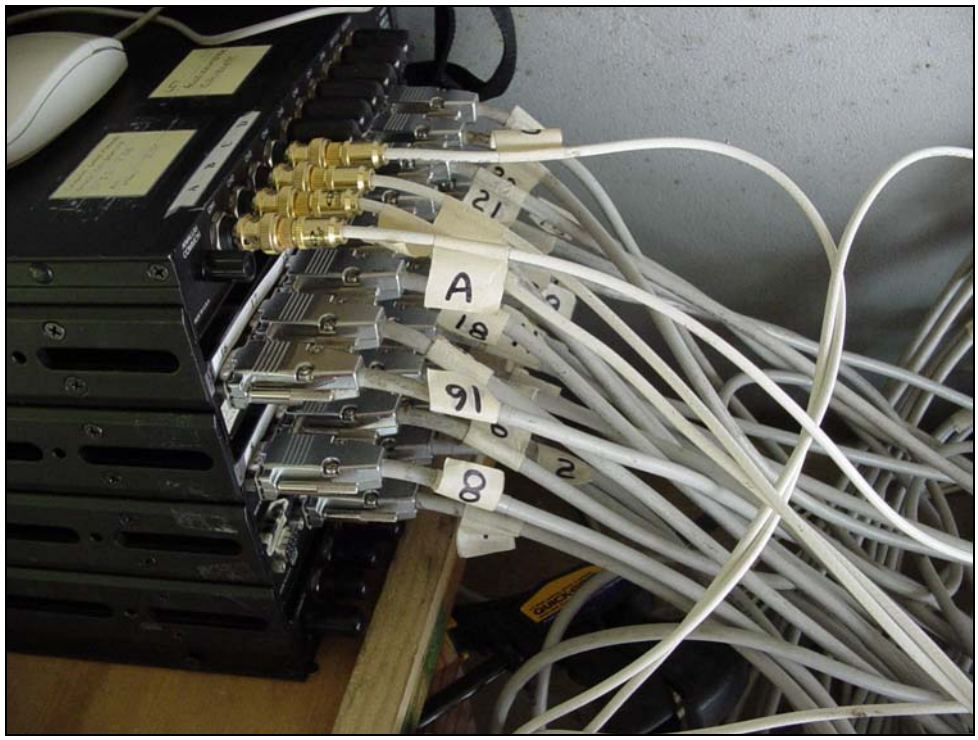

Figure C-3 Data Acquisition System

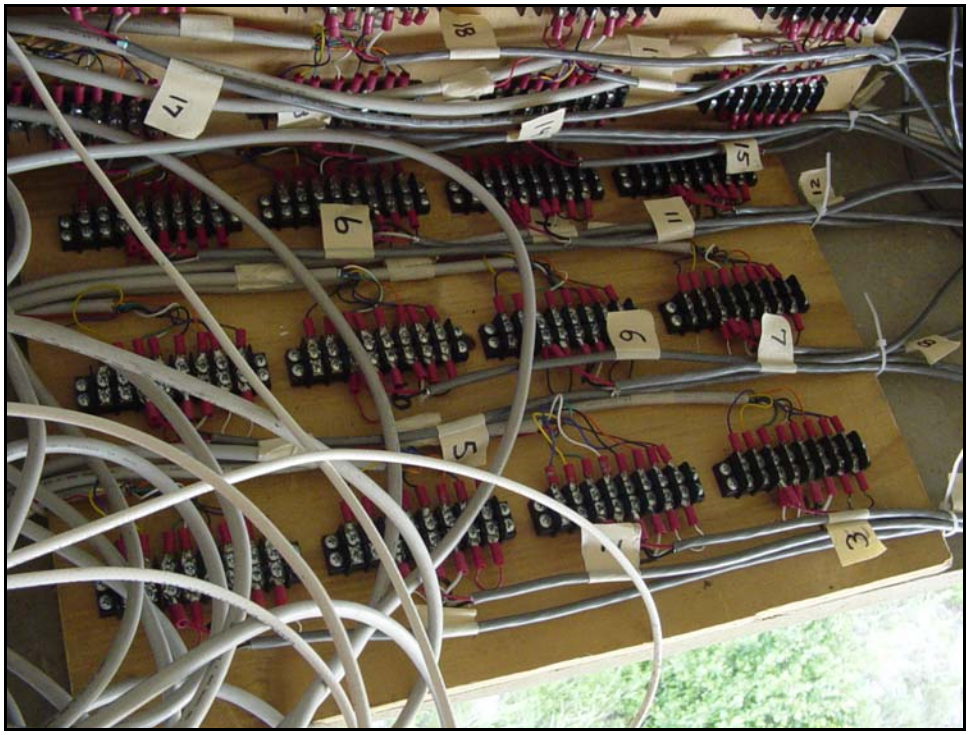

Figure C-4 Terminal Strips

Figure C-5 Data Collection Station

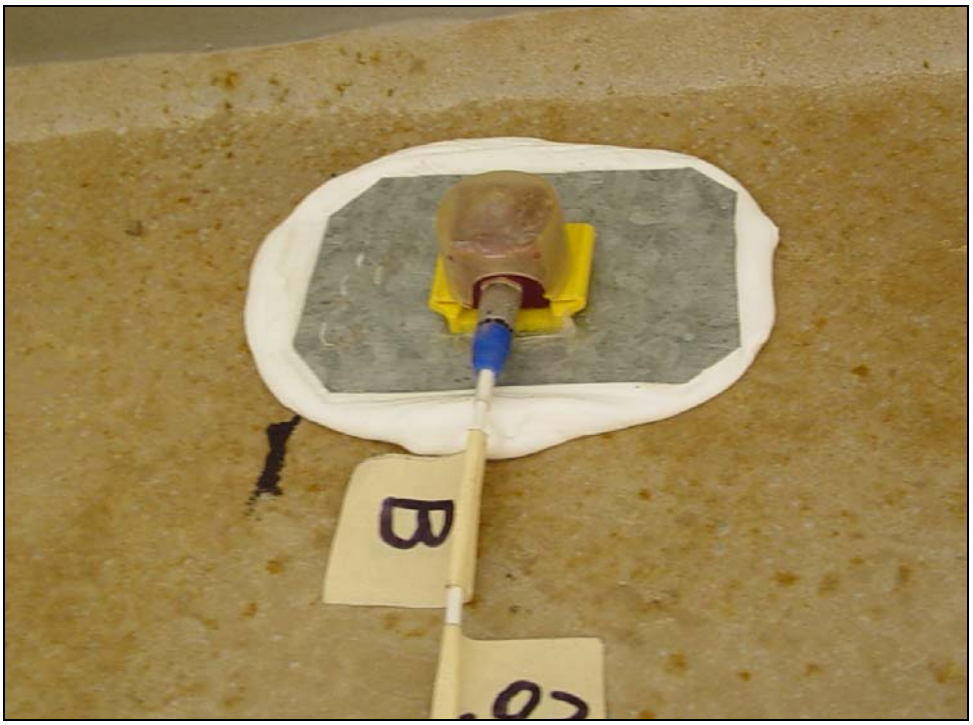

Figure C-6 Installed Accelerometer

APPENDIX D DYNAMIC BEHAVIOR

Along with studying the stresses within the structure, the dynamic behavior of the bridge also was examined. Studying the dynamic behavior of the bridge, such as the dynamic amplification factor and vibration frequencies at points along a span, should assist in creating a more accurate finite element model.

The dynamic amplification factor, a ratio of the dynamic effect versus the static effect, was found from the strain gage readings. Since the loadings from the truck were performed at varying speeds, any variations in stresses due to truck speed could be easily determined. Also, accelerometers were placed at four positions on the bridge. The accelerometers measured vibration frequencies induced by the bridge. These frequencies would be helpful when modifying finite element models.

D.1 Dynamic Amplification (Strain Gages)

A moving vehicle should theoretically apply larger stress magnitudes than the same vehicle idling. The ratio of these stresses is defined as the dynamic amplification factor. AASHTO design manuals require engineers to apply a dynamic amplification factor of 15% to all fatigue calculations (AASHTO LRFD 1994). This amplification is due to imperfections of the bridge deck that may cause bouncing of the vehicle. In Zhao's finite element model, she used a 10% increase in load due to impact. The span gaged was located near the abutment, which had a noticeable bumpy transition from the pavement to the bridge deck. A sizeable increase in stress was expected for vehicles traveling at higher speeds.

For this experiment, however, a comparison of the stresses of the gages did not indicate much difference at varying speeds. The vehicle's speed did not significantly alter the stress produced within the bridge. Examples of this low variance are displayed with a gage-stress history in Figure D-1. The data indicates that the use of a dynamic amplification factor may be conservative when calculating theoretical stresses in the bridge. A slight difference can be observed when the

moving average is used. This difference, however, is not due to the varying speeds. The moving average flattens out the higher speeds more since it has fewer data points within the peaks. Therefore, the 65 mph stress would appear lower than the 5 mph stress when using a moving average, but they are actually relatively the same value prior to using the moving average. Based on the results from this test, future finite element models should use a dynamic amplification factor of one for true accuracy.

D.2 Accelerometers

Accelerometers were helpful in understanding the dynamic behavior of the bridge. The goal for the accelerometers was to measure vibration frequencies of the bridge. These natural frequencies can be utilized to improve future finite element models. Models can be improved by adjusting structural variables, such as stiffness, to produce the measured frequencies. Another reason for studying the dynamic properties of the bridge is the possibility of resonance. If the forces induced by the live load approached the natural frequency, the bridge would be excited. Excitation would cause an increase in girder deflections. Since the fatigue cracking for this bridge is caused by distortion, any additional deflection due to vibration would be detrimental. Therefore, studying the frequencies of the bridge may assist in preventing further fatigue damage.

D.2.1 Instrument Locations

Four accelerometers were used to measure dynamic properties of the bridge. Figure D-2 displays the positions of the accelerometers. Details of installation of the accelerometers can be found in Appendix C. Accelerometer readings were taken in addition to the strain gage tests. Six additional truck passes were performed with only data collected from the accelerometers. The data was recorded and brought back to the University of Kansas for analysis.

D.2.2 Accelerometer Analysis

All accelerometers calculations were performed in *MathCAD* with the add-on package, *Signal Processing.* The data was exported into *MathCAD* from the original *NotePad* files. The accelerometer readings were integrated twice to determine the deflection of the girders. A moving average was incorporated to reduce the high frequency noise, as shown in Figure D-3. The *Signal Processing* add-on was utilized to determine the modes of vibration. A Fast Fourier Transform, which is a *Signal Processing* function, was used to measure the frequency distribution of the acceleration data. An example of a frequency distribution graph is displayed in Figure D-4. The FFT window was only on the acceleration data after the peak acceleration. This data window was assumed to be during free-vibration, which makes the frequency distribution much less noisy than during forced vibration.

In order to visualize the data collected, an animation of the displacements was created in MathCAD. All four displacement readings were placed on a 3D graph. After a time variable was set, MathCAD cycled through all the data and created an animation. The 3D model effectively demonstrated the movement of half the span under truck loading. Figure D-5 displays the 3D motion of the bridge under loading. Twisting of the bridge can be observed in the model.

D.2.3 Results

Results of the accelerometers clearly indicated that the bridge is vibrating at particular natural frequencies. This report does not speculate on the mode shapes associated with these natural frequencies due to uncertainties about the torsional frequencies. The most noticeable frequencies for each loading are presented in Table D-1. The two most abundant frequencies occur at approximately 2.4 and 3.6 Hertz. These frequencies are comparable with the theoretical frequency of 3.2 Hz for a four-span, continuous beam. The measured frequencies can be compared with the finite element models. The data collected can also be evaluated with the frequencies measured after the retrofit. Since the retrofit should stiffen the structure, the repair

should alter the frequencies. An increase of the natural frequency of the bridge would be expected after the retrofit.

Eastbound

	Midspan	Quarterspan
65 mph	1.45	1.45
	2.27	2.27
	3.64	3.64
45 mph	2.06	-
	3.67	-
	-	-
25 mph	2.35	2.35
	3.66	3.66
	-	-

Westbound

	Midspan	Quarterspan
65 mph	1.45	2.55
	2.55	3.10
	3.64	3.64
45 mph	2.40	2.40
	3.64	3.11
	4.22	3.64
25 mph	1.61	2.26
	2.26	2.99
	3.64	3.64

Table D-1 Measured Frequencies (Hz)

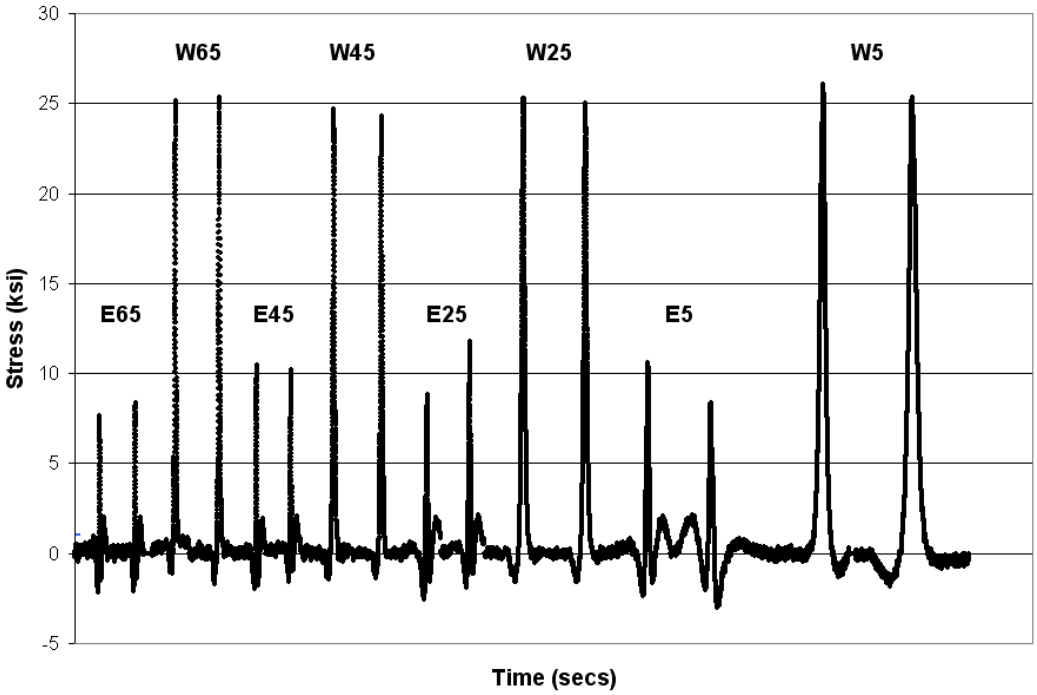

Figure D-1 Strain History (Gage 3)

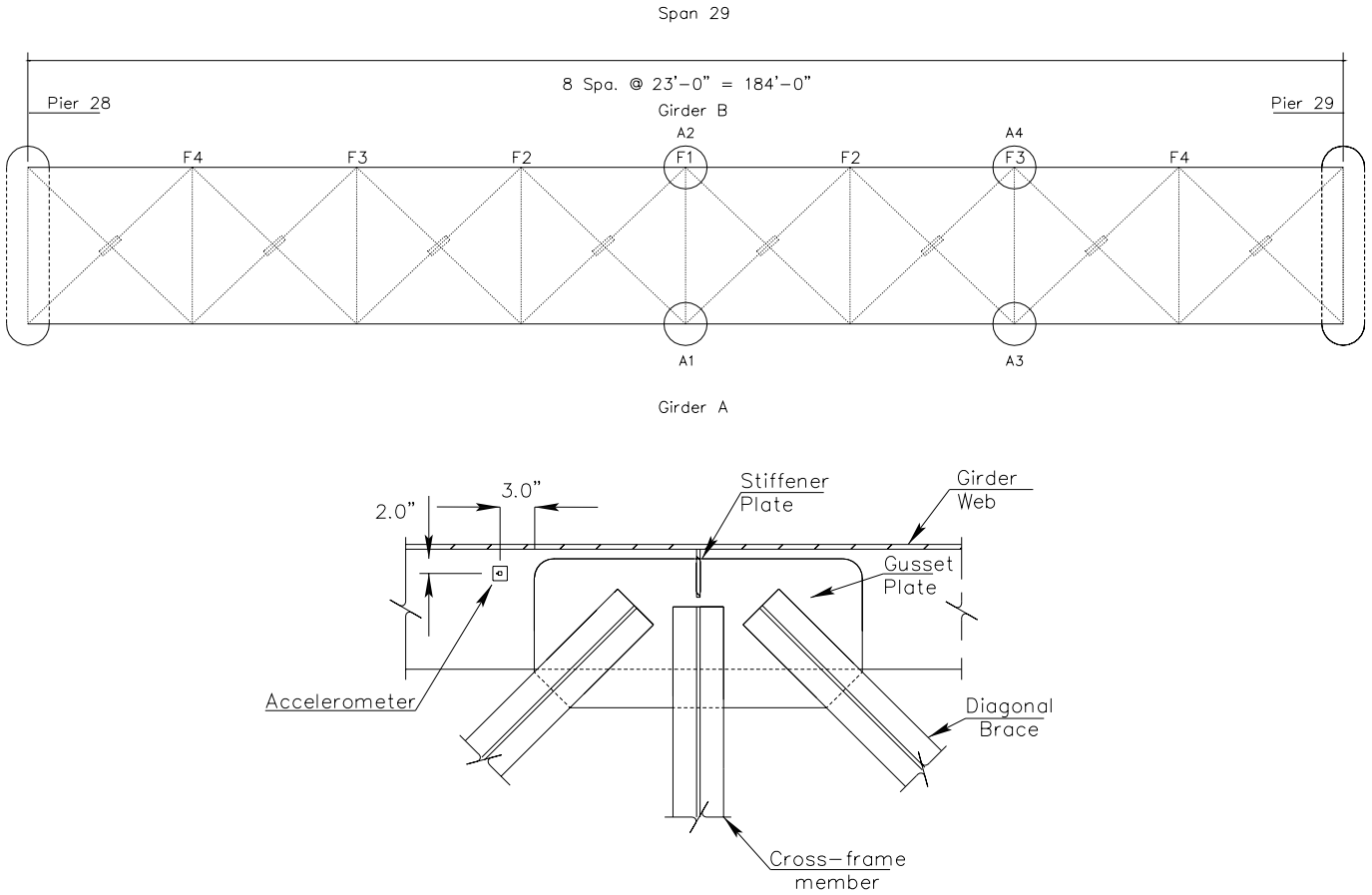

Figure D-2 Accelerometer Locations

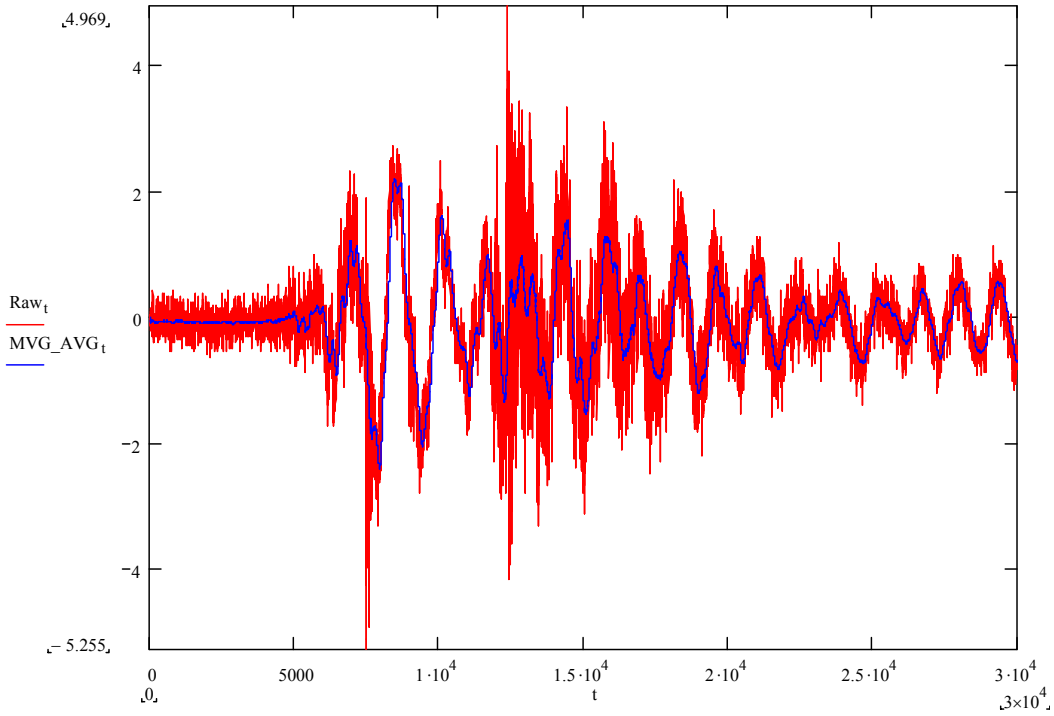

Figure D-3 Bridge Vibration

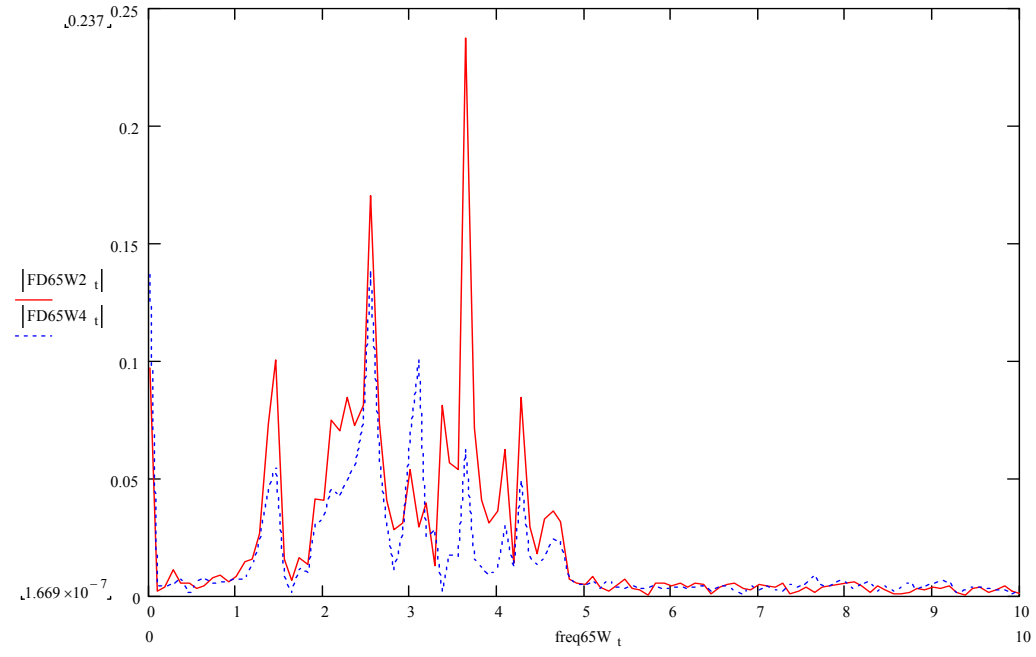

Figure D-4 Frequency Domain

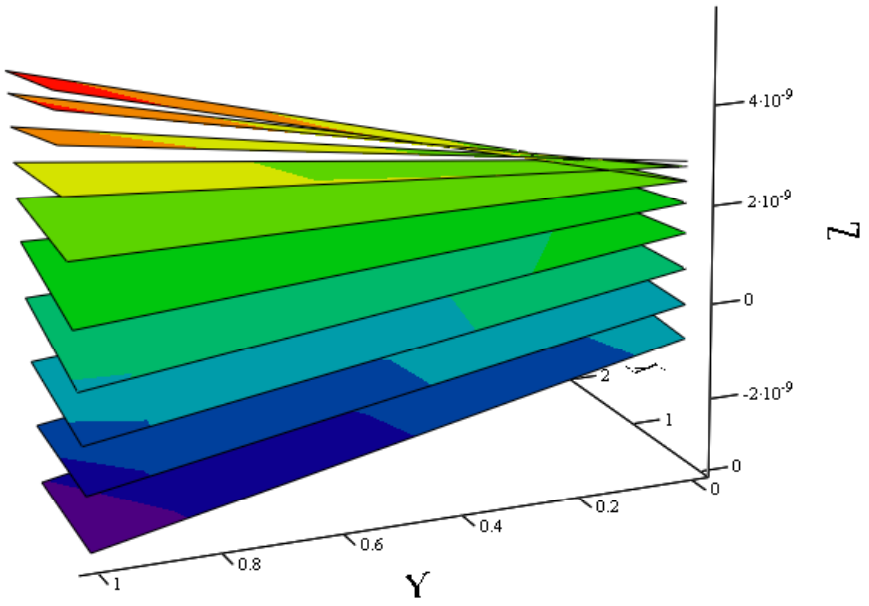

Figure D-5 3D Model from Acceleration Data

APPENDIX E
RECOMMENDATIONS FOR POST-RETROFIT TESTING

Retrofitting of the Tuttle Creek Bridge is scheduled for the summers of 2005 and 2006. A post-retrofit test will be conducted after the repairs have been performed. The test results from this test will be compared with those values obtained during the pre-retrofit test. After researching different methods of testing, some suggestions are presented to assist the future tester of the bridge. Although this test was successful, improvements can always be made to simplify testing and to acquire more insightful data.

E.1 Bridge Monitoring

Many bridge testing projects utilized ambient traffic to load the structure. For this test, only a pre-weighed truck was used. Previous testers of bridges have configured their data acquisition systems to record only stresses imposed by truck traffic. A similar system could be setup on the bridge and left for several months. Ambient traffic would give a designer a better idea of the stress levels a structure is actually undergoing.

Of particular interest is the daily truck traffic on this bridge. The bridge is not a large highway crossing where truck weights can be easily enforced. The Tuttle Creek Bridge is located in a region of farming; thus overloaded, farming trucks may be crossing the bridge. These vehicles would create a much higher stress range than what an H15 vehicle would theoretically. An interesting comparison would be to compare the stresses created by a standard H15 truck with the most common stress level measured under ambient traffic. If many overloads are occurring, the stress differences could be significant.

E.2 Gage Locations

Post-retrofit testing should be used to determine the effectiveness of the retrofit. Some of the gage locations used in the pre-retrofit test should be reused to demonstrate the stress reduction created by the repair. Gages placed in the web-gap regions should be reused in order to measure the reduction of stress created by the positive attachment of the connection stiffener to the girder flanges. The gage placed near the longitudinal stiffener should also be reused to quantify the effectiveness of the repair.

Many gage locations will not need to be used again. Gages placed on the braces were used to assist the future finite element modeling. The information gathered from these gages should not change much before and after the retrofit. Gages placed on the upper and lower flanges, which were used to measure composite action, do not need to be reused. The rosette placed on the gusset plate could be reused, but the bolts being placed through the plate may inhibit placement at the same location.

For this test, 23 gages was a proper amount to gather information about the structure. If more than 23 gages need to be installed for the next test, the data acquisition system will be overloaded. One solution to this dilemma is to leave the extra gages disconnected and swap them in and out during each truck pass. Installation and load testing will take longer, but more information about the structure can be obtained.

E.3 Background Noise Reduction

During the testing, an abundance of noise was noticed in gages with low stress ranges. For gages with higher stresses, the noise was unnoticeable due to their large magnitude. Although applying a moving average smoothes out the data, researching types of noise reduction measures may be beneficial.

To solve this problem, the source of the noise must be identified. For the pre-retrofit test, the particular source of the noise was not easily determined. Since the data acquisition system was positioned high above the ground, perhaps improper grounding of the system is a cause of the noise. The wind on the bridge may have created the noise. Testing was performed on a relatively calm day for Central Kansas, however the wind was gusting at times. Obviously, there is no solution for this noise, but it could be a source.

Another possibility for the noise is the generator used for power. The generator was required to power the data acquisition system and the laptop. The generator was positioned on the abutment as far as possible from the gages. Vibrations from the generator could have created background noise. Using a car battery and an inverter could be another method of powering the system.

E.4 Data Collection Time

Data collection time for the Tuttle Creek Bridge testing should have been extended to capture more loadings of the structure. The peak stresses were captured, however, the data collecting was not always ended at zero strain. This prevented permanent strain from being observed. Loading distance was from the abutment to the first hinge, a total of 552 feet. Increasing the loading distance until the second hinge is recommended.

APPENDIX F CALCULATIONS

This chapter includes details of the analysis procedures used for this test. Since so much data was collected, an easier method of analyzing was used to expedite the process. By using macros, the data was much more organized and easier to interpret.

F.1 Strain Gage Analysis

After acquiring the data, the strain gage data was transferred from Notepad to Microsoft Excel files. Visual Basic programming, an Excel tool, was used to analyze the data much quicker than normal spreadsheet analysis. Macros were produced which duplicated commands for each file. Instead of altering each file individually, one file change could be recorded as a macro. The recorded macro could be used to reproduce the same commands on the other files. Visual Basic code was written to produce graphs by simply selecting the data of interest. Userforms were also added with the code to improve the user interface. Userforms are boxes that appear on screen that have controls to interface with Microsoft Excel and execute Visual Basic code. An example of a userform used during analysis is shown in Figure F-1.

The use of userforms allowed data to be sorted very simply. By selecting from the easy-to-use userforms, particular files of interest could be opened. Also, the selection of figures inside a userform could be used to alter calculations performed by Visual Basic. A common choice for the userforms is the selection of a range for the moving average. Other calculations performed by Visual Basic included the conversion from strain to stress, the zeroing of data, and outputting maximum and minimum points.

Userforms were designed as branch system. Each selection would create another userform to appear based on what selected in the prior userform. This procedure would continue until the desired graph was produced. The first userform allowed the user to pick whether to view a particular load case, a single gage history,

or accelerometer readings. The "load case" branch allowed users to choose a particular load case. By selecting from a list of the gages, any of the gage readings from this load case could be accessed. After selecting a single gage or a multitude of gages, a graph would be instantly produced displaying the desired data. Visual Basic allowed graphs of different gages to be shown simultaneously to compare and contrast values for easy interpretation.

The "gage history" branch allowed users to choose a particular gage to view. A graph displaying the entire stress history of a gage or a single truck event could be produced. Toggle buttons were added to the userform to allow a user to choose between eastbound or westbound stress histories.

F.2 Moving Average

Data collection always has elements of noise that obstruct the data of interest. High frequency noise, created by electrical static, is the most common form of scatter in field-testing. For this project, vibrations induced by the truck engine and electric generator also created scatter. For high strain values, such as in the web-gap regions, this noise is less noticeable. However, for most of the other gages, the scatter interfered with the data of interest. Because of this interference, a moving average was incorporated in the analysis of the data. Figure F-2 displays the benefit of the moving average in the analysis of the data.

A moving average simply replaces a data point with the average of a specified range of points following it. The moving average formula is shown below.

$$A_{t+1} = \frac{1}{n}\sum_{i-n}^{n} s_{t-i+1} \quad \text{(F-1)}$$

Where:

A_{t+1} = Moving average data point

s_{t-i+1} = Recorded data point

n = Number of preceding data points specified

F.3 Fatigue Calculations

Current AASHTO LRFD Specifications place steel bridge details into eight categories of fatigue resistance. The empirical-based categories relate the number of cycles a detail can endure at a particular stress cycle without crack initiation, as shown in Figure F-3. For the field test, a typical truck was used to induce stress cycles. If the amount of truck traffic is known, the fatigue life of the design detail can be estimated. A detail's fatigue resistance is based on the constant amplitude fatigue threshold, CAFT, which is the stress range that the detail can withstand 2 x 10^6 cycles. If the detail's stress cycles are below ½ CAFT, the design life of the detail is considered to be infinite.

$$N\gamma = \frac{A}{365 \cdot (\Delta\sigma)^3 (ADTT)_{SL}} \qquad \text{(F-2)}$$

N_γ = Fatigue Life
A = Fatigue Category Constant
$\Delta\sigma$ = stress range (ksi)
ADTT = Average daily truck traffic

(AASHTO 2000)

When designing a fatigue-resistant detail, engineers load the structure with an HS15 truck with a gross weight of 54 kips. The vehicle models an eighteen-wheeler with 30 feet between the two rear wheel axles. Yuan Zhao's finite element model utilized an HS15 truck. This design truck differed slightly from the truck used to load the structure during the field test. The vehicle used for the testing was a three-axle dump truck, also with a weight of 54 kips, but with a rear-axle spacing of approximately 4.5 feet. Theoretically, the dump truck used should create higher stress cycles, since the weight is more concentrated upon the bridge. This assumption makes the calculated fatigue life conservative.

Three separate details were of interest in the Tuttle Creek Bridge: the web-gap region, the gusset plate connection, and the longitudinal stiffener. Fatigue calculations were performed on the details to estimate the fatigue life. After the retrofit, the recorded stresses will be used to determine the new fatigue life. Hopefully, the retrofits performed will significantly extend the fatigue lives of the details.

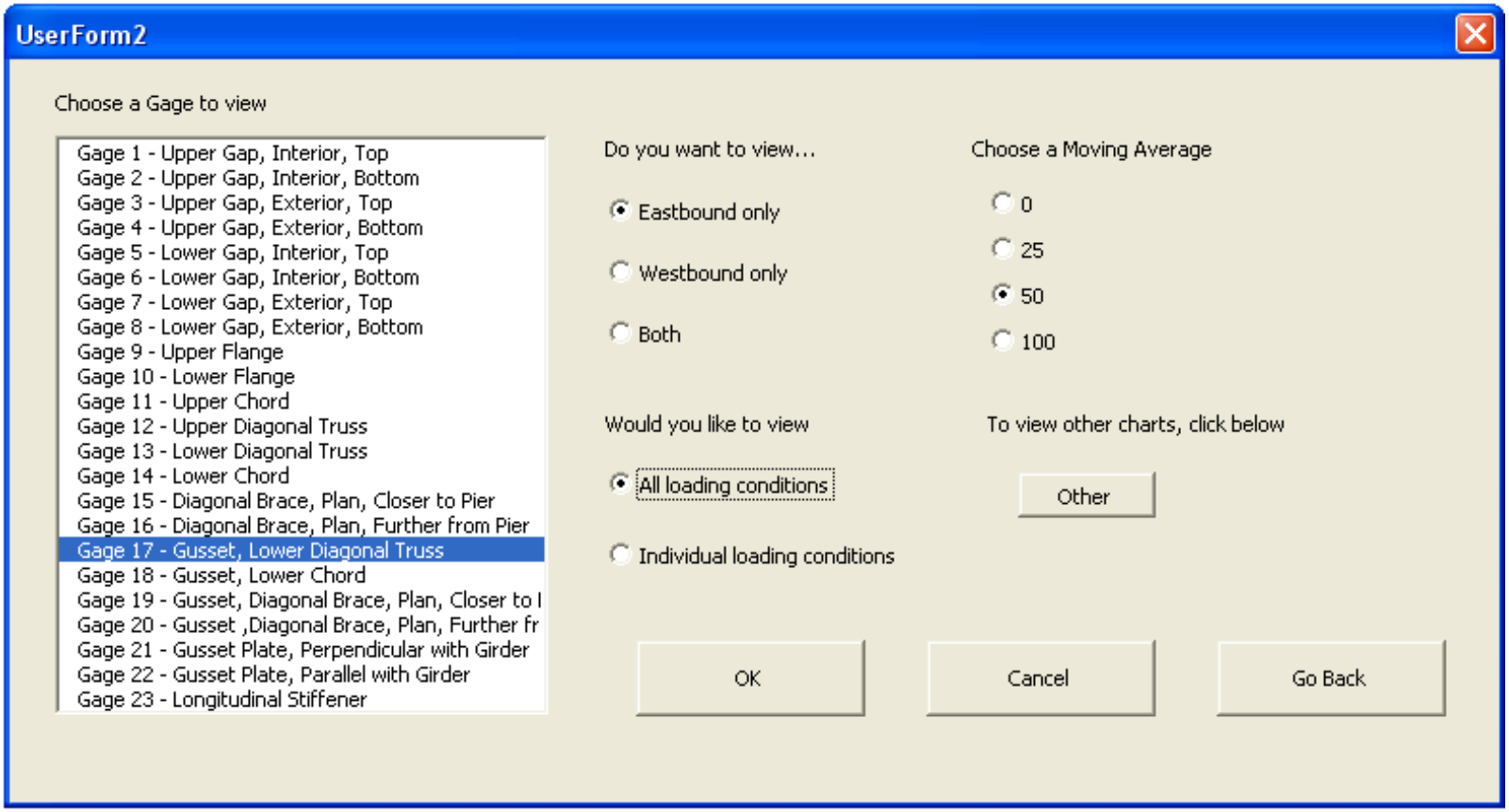

Figure F-1 Userform

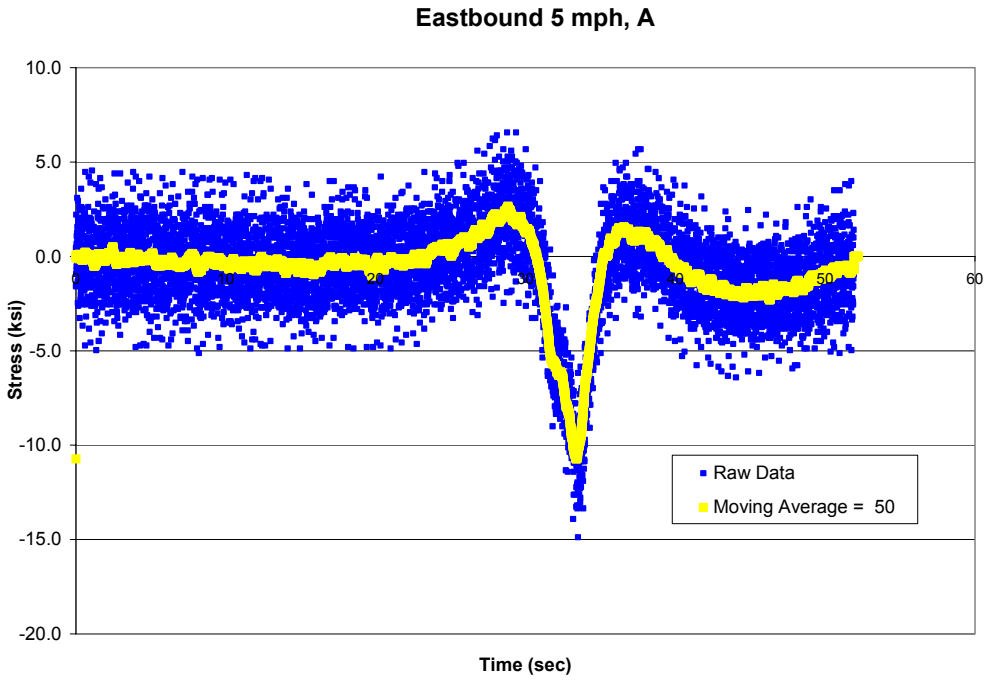

Figure F-2 Moving Average Graph

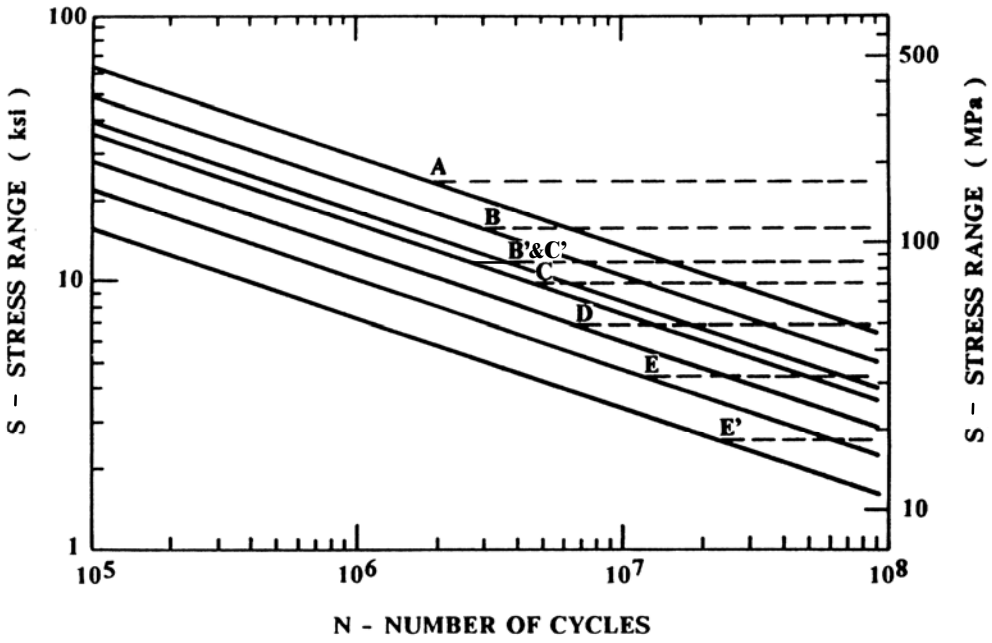

Figure F-3 AASHTO Fatigue Detail Categories